Assessment of Stable Tearing on Fatigue Fracture Surfaces in Aluminium Alloy

A thesis submitted in fulfillment of the requirement for the degree of Doctor of Philosophy

Mohd Fairuz Ab Rahman

B.E., M.Sc.

School of Aerospace, Manufacturing & Mechanical Engineering

RMIT University

January 2012

Author's Declaration

I hereby declare that except where due acknowledgement has been made, the work is that of the author alone; the work has not been submitted previously, in whole or in part, to qualify for any other academic award; the content of this thesis is the result of work which has been carried out since the official commencement date of the approved research program; and, any editorial work, paid or unpaid, carried out by a third party is acknowledged.

…….

Mohd Fairuz Ab Rahman

January 2012

Abstract

Fractographic analysis of fatigue fracture surfaces is used extensively in aircraft accident investigation to correlate various progression markings, associated with the crack front position, with the load cycle history which was experienced by the failed component in service. This analysis is vital to estimate the crack growth history in the critical component. Matching the results of this analysis to the predicted fatigue crack growth, however, is often complicated by stable tearing crack growth. Bands of stable tearing are often observed on fracture surfaces in a range of structural metals but their growth is not incorporated in fatigue predictive models. As a result, the presence of large stable tearing bands can greatly complicate the derivation of a crack growth history, especially in cases where the load history record is poor. Therefore, the key challenge in fracture surface analysis is to relate the multiple tears, of different lengths, to the loads present in the load history. The main objective of this research is to develop improved analytical and prognostic models for predicting the stable tearing jump length Δa in aluminium alloys. This research involved a series of tests which produced stable tearing in 7075 aircraft aluminium alloy under constant amplitude (CA) and variable amplitude (VA) loading.

Macroscopic and microscopic characteristics of CA and VA tearing were studied and the main conclusion relates to the notable differences between tearing under CA and VA loading. Tearing under VA conditions usually appears to be duller than under CA tearing, but both types of tearing have similar fracture mechanism and are also comparable to the face of the final unstable failure. This study revealed that the stress intensity factor was one of the key controlling parameters in tearing onset and arrest. The CA and VA tearing can be characterized by the first onset stress intensity factor

$K_{2D}(a_i)$ at which these two tearing conditions occur. The magnitude of $K_{2D}(a_i)$ for VA tearing is found to be equivalent to the material's plane strain fracture toughness, K_{Ic}, but is slightly lower than the initiation K-value for CA tearing. The loading conditions also have been observed to impose different effects on the size of tearing. This study suggests that for similar K, the CA tearing at initiation has smaller tearing crack jump length Δa, than the VA tearing, but as the crack progresses, the size of Δa under VA conditions is markedly larger than that sustainable under CA conditions. The CA condition seems to confer apparent resistance to tearing, which results in smaller tearing crack jumps, than in VA loading conditions. This study also shows that stable tearing crack jump length Δa under CA and VA conditions can be associated with the plastic zone size, but their correlations with the plastic zone size differ between the two loading conditions.

The static tearing curve is developed based on the standard K_R curve test method. This study shows that the K-value at which the static tearing commences is approximately equivalent to the first onset stress intensity factor for VA tearing. This result supports the notion that the onset of stable tearing occurs at a K-level of magnitude that is comparable with the static plane strain fracture toughness K_{Ic}. The K_R (K-value with plastic zone correction) is plotted against the change in effective crack length Δa_e and the fatigue tearing data from these tests are found to agree very well with the static R-curve. This result shows that the R-curve method can be used to estimate the Δa of both CA and VA tearing during fractographic analysis, but this technique requires the R-curve to be developed for particular configurations.

The complex crack front curvatures observed at tearing arrest distort simple estimates of stress intensity factor and hence a three-dimensional (3D) finite element

(FE) analysis has been undertaken to estimate the through thickness stress intensity factor K_{3D} variation. Generally, the K-value at mid-thickness region reduces, while the K-values at the sides of the specimen increase as the crack-front becomes more curved. Based on the parametric finite element analysis of the stress-intensity factor K_{3D} at the mid-thickness of three VA tearing, this study presents a new validated stable tearing model for predicting the crack jump length Δa during stable tearing. The main features of this new model are that the tongue-shaped region of stable tearing is idealised as a trapezoidal shape and the average of areal ratio of tearing is approximately constant. Comparisons between the model predictions and experimental results indicate that this new model produces satisfactory prediction of stable tearing crack jump length Δa in aluminium alloys of different cross-sectional thickness.

The study provides advanced knowledge in predicting the stable tearing behaviour under fatigue conditions and improves the modelling capability for the phenomenon of stable tearing in aluminium alloys structural metals. The results of this study help in establishing confident and accurate durability assessment of aircraft structure, notably in assisting quantitative fractography during accident investigation and assessing physical validation to the fatigue crack growth prediction model. The usefulness of the knowledge can also be applied and extended to other engineering materials and structures.

Acknowledgements

I would like to express my gratitude to my supervisors, Professor Chun H. Wang, Professor Graham Clark, Dr Adrian Orifici and Dr Reza D. Mohammed of the School of Aerospace, Manufacturing & Mechanical Engineering in RMIT University for their patient guidance during my PhD candidature.

I would like to thank the Public Services Department of the Malaysian Government for providing my scholarship and the Department of Occupational Safety and Health, Ministry of Human Resources, Government of Malaysia for giving me an opportunity to pursue this study.

And finally, special thanks to my wife, Dr. Aini Afifah Abdul Karim for unyielding support, our two boys; Fauzan Azeem and Umair for continuing entertainment, our family and friends in Australia and Malaysia.

Table of Contents

List of Figures

List of Tables

List of Publications

Journal paper

i. Ab Rahman, M.F., Mohammed, R.D., Yu, X., Liu, Q., Clark, G. 2010. Assessment of stable tearing on fatigue fracture surfaces. *Engineering Failure Analysis* 17(6): 1313-1327.

ii. Ab Rahman, M.F., Mohammed, R.D., Yu, X., Liu, Q. & Clark, G. 2010. Prediction of stable tearing in fatigue crack growth. *Procedia Engineering* 2(1): 1515-1521.

Conference paper

i. Ab Rahman, M.F., Mohammed, R.D., Yu, X., Liu, Q., Clark, G. 2010. Prediction of stable tearing in fatigue crack growth. In *Proceedings of the 10th International Fatigue Congress*. Prague, Czech Republic.

ii. Ab Rahman, M.F., Mohammed, R.D., Yu, X., Liu, Q., Clark, G. 2010. Stable tearing in aircraft materials. In *Proceedings of the 27th International Congress of the Aeronautical Science*s. Nice, France.

iii. Ab Rahman, M.F., Mohammed, R.D. & Clark, G. 2010a. The influence of plastic zone size in stable tearing. In *Proceedings of the 21st Australasian Conference on the Mechanics of Structures and Materials*. Melbourne, Australia.

Others

i. Ab Rahman MF, Mohammed RD, Clark G. 2011. The influence of plastic zone size in stable tearing. In S. Fragomeni, S. Venkatesan, N.T.K. Lam, S. Setunge, (eds), *Incorporating sustainable practice in mechanics of structures and materials*: 679-684. Leiden: CRC Press.

ii. Ab Rahman MF, Mohammed RD, Wang C, Yu X, Liu Q, Clark G. 2011. Stable tearing in fatigue crack growth. In P. Jackson, C. Trasteli, (eds), *A review of Australian and New Zealand investigations on aeronautical fatigue during the period April 2009 to March 2011*: 2-4. DSTO-TN-09931.

Nomenclature

a crack length

a_e effective crack length in K_R curve test

a_i initial crack length at the end of fatigue pre-cracking in fatigue tests

a_o crack length at the end of fatigue pre-cracking in K_R curve test

a_p crack length measured in K_R curve test

Δa stable tearing crack jump length

Δa_e the change in effective crack length in K_R curve test

Δc the fatigue crack growth increment prior to the tearing jump

Δn the interval numbers of load cycles prior to the tearing jump

A_c stable tearing area

A_l ligament area

b width of flat crack front at stable tearing arrest

C crack front curvature correction factor

D depth of shear lip

K stress intensity factor

$K_{2D}(a_i)$ the first onset stress intensity factor

K_{3D} the through thickness stress intensity factor

K_G the applied driving force in resistance curve

K_{Ic} plane strain fracture toughness

K_{plat} the plateau level of the K_R curve

K_R the stress intensity factor resistance curve

l	crack front line length
P	remote tensile force
$r_{y,R}$	plastic zone size
R	cyclic load ratio (= P_{min}/P_{max})
s	distance along the crack front line length
ζ	a factor that accounts for the local ductility at the transition between fatigue crack and tearing
σ	stress
σ_U	ultimate strength
σ_Y	yield strength
t	specimen thickness
U	displacement
υ	Poisson's ratio
W	specimen width
z	the actual stable tearing crack front

Abbreviations

CA constant amplitude fatigue loading

CT compact tension specimen

FE finite element

LEFM linear-elastic fracture mechanics

VA variable amplitude fatigue loading

Chapter 1. Introduction

1.1. Background of metal fatigue in aircraft structures

1.2. Background of current study

1.3. Motivations of current study

1.4. Objectives of current study

1.5. Outline of thesis

This chapter introduces metal fatigue in aircraft structures and presents the background, motivations and objectives of this study. The presence of stable tearing complicates fatigue fracture surface analysis and current prediction models do not incorporate stable tearing model. The main objective of the current study was to develop a predictive model for stable tearing behaviour in an aerospace aluminium alloy.

1.1. Background of metal fatigue in aircraft structures

Fatigue of engineering metals has been scientifically studied for almost two centuries (Mann, 1983; Schutz, 1996) and perhaps one of the key findings was made by August Wohler in 1870 who realised that the repetition of loads, all of which are nominally lower than the material's static strength, may eventually cause a complete failure. While a variety of definitions of the term *metal fatigue* have been suggested, this author prefers to use the definition encapsulated in ASTM E 1823 (2009), which refers it to as a sequential process of gradual, localised and irreversible metallurgical damages (by plastic deformation) of a component subjected to cyclic loads that are nominally lower than its static strength, and repetition of these loads over time may cause complete failure of the component. The fatigue failure of metallic structures had been regarded as a mysterious phenomenon, possibly due to a lack of apparent indicators of imminent failure, but now is generally well-known and acknowledged as a significant engineering problem.

Fatigue has been a major threat to aircraft metallic structures for many years. It has been highlighted by Bland and Sandorff (1943), while reviewing the design

methodology used at that time and still remains a difficult technical issue affecting the design and service life assessment of aircraft (Finlay and Harrison, 2002). Fatigue failure has been acknowledged (Lancaster, 1997; Stephens *et al*., 2001) as the leading cause of accident in most engineering structures, and estimated to be the cause of about 50% of mechanical failures (Stephens *et al*., 2001). A survey by Lancaster (1997) has shown that fatigue is the most common failure mechanism in various engineering designs such as aircraft, petrochemical plant, boiler and pressure vessel.

Many aircraft accidents have occurred, which have significantly changed the design and safety landscapes of the aviation industry (Schijve, 1994, 2009a; Schutz, 1996; Blom, 2001; McEvily, 2002; Wanhill, 2002). One good example was the accident involving two de Havilland Comet I aircraft in 1954, caused by fuselage decompression failure at high altitude, where multiple fatigue cracks were observed to initiate from the bolt or rivet holes near several windows. The main reason was that various important design and manufacturing issues were unknown at that time (Withey, 1997). Table 1 summarises some major catastrophic accidents, and also lists some of the knowledge learned from such misfortunes.

From a technical point of view, designing an aircraft structure against fatigue is truly a formidable task because an aircraft consists of a complicated assembly of materials that are exposed to complex loading spectra (Hoeppner, 1996; Schijve, 2009a). Various aircraft components are also known to be susceptible to fatigue failures (Campbell, 1981; Campbell and Lahey, 1984; Lancaster, 1997; Bhaumik *et al*., 2008), especially those with holes, corners or joints. Surveys such as that conducted by Campbell and Lahey (1984) have listed various aircraft components that are prone to fatigue failure and identified two main fatigue crack initiation sites, namely holes

(threaded or smooth) and notches. Debate continues regarding the best strategies for designing and maintaining an aircraft structure (Toor, 1973; Hardrath, 1973; Wood, 1975; Goranson, 1997; Swift, 1999; Stephens *et al.*, 2001; Eastin, 2003) and one issue that has grown in importance is the capability to accurately predict the fatigue life and crack growth in critical components of aircraft (Schijve, 2009a).

Table 1. Survey of often cited major aircraft fatigue-related accidents, adopted from Schijve (1994), McEvily (2002) and Wanhill (2002).

Year	Aircraft type (description of failure)	Lessons learned
1948	Martin 202 (fatigue crack in a joint of the wing spar)	Material selection, joints
1954	de Havilland Comet (fatigue crack at a window in a fuselage)	Full-scale fatigue test with realistic flight loading
1969	F-111 (fatigue initiated from undetected material flaw)	Introduction of damage tolerance concept and assumption of initial flaw
1976	Hawker Siddeley 748 (fatigue crack in lower wing skin)	Use of more realistic load spectra during full-scale fatigue test
1977	Boeing 707 (fatigue crack in the upper spar of the stabiliser)	Ineffectiveness of fail-safe design, fatigue issues in ageing aircraft
1979	DC-10-10 (fatigue cracking of the aft bulkhead of the pylon)	Correct maintenance procedures
1988	Boeing 737 (multiple cracks fuselage skin)	Multiple-site damage and corrosion at joints in ageing aircraft
2000	Concorde	Ineffectiveness of fail-safe design

Predictive models of fatigue crack growth; especially under variable amplitude loading spectra are numerous (Pelloux, 1969; Paris and Erdogan, 1969; Schutz, 1979; Fatemi and Yang, 1998). One major criticism of these models is their lack of general validity and reliability (Zheng, 2001; Pook, 2007; Schijve, 2009b). For instance, Vasudevan *et al*. (2001) pointed out the absence of a unified fatigue damage processes predictive model, which deals with the crack initiation stage to micro- and macro-cracks growth to final failure, Daneshpour *et al*. (2009) emphasised the limitation of prediction model in welded panels and Bao and Zhang (2010) highlighted the inadequacy of current prediction models to predict crack branching. Zhao *et al*. (2008) mentioned an inaccurate interpretation of cyclic plasticity behaviour in a plasticity-based fatigue prediction model, in addition to its incapability to account for the complex mechanism immediately after the overload, and Goldsmith *et al*. (1996) stressed the deficiency of the existing prediction model in accommodating the presence of stable tearing bands.

Furthermore, the accuracy and reliability of fatigue crack growth prediction models, especially for variable amplitude load excursions, are usually limited to certain practical cases (Beden *et al*., 2009). One of the most significant issues is load interaction effects (Schijve, 1979), whereby substantial retardation of crack growth rate can occur in the subsequent load excursions. It signifies that an increment of crack length a in each cycle of load history is no longer directly related to the characteristic stress intensity factor K. Skorupa (1998) noted that similar type of variable amplitude load sequences can result in either acceleration or retardation in subsequent load cycles. It should also be noted that some types of variable amplitude

load history may have negligible prior loading effects (Vardar and Yildirim, 1990; Dougherty *et al*., 1992; Schijve, 1996).

Despite the above-discussed limitations, the existing prediction models enable fairly satisfactory (or rather conservative) estimation of fatigue crack growth that is considered to be sufficient from an engineering standpoint (Schijve, 2009b). Schijve (1991), however, pointed out that a good prediction model should be able to predict both the crack growth rates and cycle-by-cycle crack length increments. This implies that the predicted crack growth rates should also match the progression markings as observed on a fracture surface, namely the prediction model should corroborate with the physical observation. To this end, it is becoming increasingly difficult to ignore the presence of stable tearing on fatigue fracture surfaces, which has been established to complicate the accuracy and reliability of fatigue life and crack growth prediction models (Frost, 1962; Hudson and Hardrath, 1963; Wanhill *et al*., 1979; Partl and Schijve, 1990; Barter *et al*., 1993; Goldsmith *et al*., 1996; Clark *et al*., 1997; Newman Jr., 1997).

1.2. Background of current study

An accident involving an RAAF Aermacchi MB326H trainer jet, which lost one of its wings during a simulated air combat operation in 1990, was due to the fatigue failure of the lower aluminium wing spar. The recovered section of the spar is shown in Figure 1. The fatigue crack initiated at the conical section of the blind rivet fastener hole that had a severe machining flaw, as indicated by an arrow in Figure 1 (Barter *et al*., 1993). The crash of the trainer was unexpected because its service life was

substantially lower (about 70%) than the predicted safe-life. The accident prompted immediate suspension of use to the remaining aircraft in the RAAF fleet and triggered extensive investigations to guarantee the continued airworthiness of the remaining fleets (Goldsmith *et al*., 1996).

Figure 1. The recovered section of the crashed Aermacchi trainer jet, showing multiple large tearing bands which appear as dull crescent-shaped regions (Clark *et al*., 1997). Arrow indicates location of a severe machining flaw.

One of the main undertakings was to develop a crack growth model for this critical component, which involved examining the fatigue fracture surface (Goldsmith *et al*., 1996). The challenge in this fracture surface analysis was to relate the rather

uncertain load history to a sequence of markings, and this process was made difficult by the presence of multiple large tearing bands (Goldsmith *et al*., 1996), visible in Figure 1 as dull crescent-shaped regions in contrast to the "bright" background fatigue surface. It was not understandable how the extent of each tearing band could be linked to the service loads.

This complexity led to considerable interest in understanding the occurrence of stable tearing crack growth during fatigue in aircraft materials. Extensive experimental works have been carried out to analyse stable tearing in aluminium alloys, especially by Clark and co-workers (Goldsmith and Clark, 1989, 1990; Barter *et al*., 1993, 1997; Goldsmith *et al*., 1996; Clark *et al*., 1997; Byrnes *et al*., 1998, 2000; Liu *et al*., 2005) at the Defence Science and Technology Organisation (DSTO), Australia. Several key findings from these studies are:

- The presence of substantial bands of stable tearing crack growth on a fatigue fracture surface complicates the process of determining the in-service fatigue crack growth rate of the failed part and can cause some difficulties in safety management of aircraft (Goldsmith *et al*., 1996);
- Multiple tear bands are observed on several un-failed spars, and these bands resulted from high in-service loads (Barter *et al*., 1993). In most cases, the fracture by stable tearing dominates the overall fatigue fracture surface;
- Two key models (Vlasveld and Schijve, 1979; Bowen and Forsyth, 1981) have been employed for analysing stable tearing, but both of the models inherit one major limitation in that both are only intended for post-failure analysis (Byrnes *et al*., 2000). Application of both models requires some

measurements of tearing geometrical parameters to be carried out on the fracture surface;

- None of the existing fatigue crack growth prediction models incorporates these existing stable tearing models (Byrnes *et al*., 1998);
- Numerical results have shown that the curved crack front has a U-shaped stress intensity factor *K* distribution (Liu *et al*., 2005). The *K*-value is lowest at the mid-thickness region and highest at free surfaces; and
- The numerical modelling of stable tearing phenomenon is complicated by the lack of suitable failure criterion to represent the onset and arrest of tearing, the change in crack front shape and the effect of plasticity (Liu *et al*., 2005).

1.3. Motivations of current study

Stable tearing adds complexity to fracture surface analysis, especially in determining the in-service crack growth model. The in-service crack growth model is a more realistic representation of the cracking behaviour of the critical component and is essentially used to derive the safe management standard of the remaining fleet. The two existing stable tearing models (Vlasveld and Schijve, 1979; Bowen and Forsyth, 1981) have been shown to be capable of interpreting some of the tearing characteristics, and have assisted in fractographic analysis of fatigue fracture surfaces. So far, however, there has been little discussion about the prospect of developing these models further as an in-service predictive tool.

The two existing models have been derived from the fractographic analysis of stable tearing that has occurred under variable load amplitude (VA) (Vlasveld and Schijve, 1979) and constant load amplitude (CA) (Bowen and Forsyth, 1981) fatigue. The research to date has tended to focus on the application of the CA model (Bowen and Forsyth, 1981) in VA tearing, and no research has been found that applies the VA model (Vlasveld and Schijve, 1979) in CA tearing. In addition, no comparative study has been carried out to compare the occurrence of stable tearing under CA and VA load excursions especially in terms of their macroscopic and microscopic characteristics.

The occurrence of stable tearing is not yet incorporated in fatigue predictive models, and thus the prediction of the onset and arrest of tearing in fatigue crack growth is still not possible. Several empirical models (Vlasveld and Schijve, 1979; Bowen and Forsyth, 1981) have been formulated, but one major drawback of these models is that they are only valid for post-failure analysis. More importantly, complexities arise when an attempt is made to utilise these models in predicting the individual jump in crack length Δa.

Another notable problem with stable tearing is that significant crack front curvature may cause the inaccurate assessment of the service life of a component, as the crack length increment is normally obscured and difficult to detect using methods which rely on surface inspection. It further implies that determination of crack length during in-service inspections may become complicated, and hence the predictive capability of stable tearing behaviour during fatigue loading is vital in order to establish a more accurate fatigue crack growth model.

1.4. Objectives of current study

The main objective of the current study is to develop a predictive model for stable tearing behaviour in an aerospace aluminium alloy. The objective of the current study was achieved by investigating the following research questions:

(a) Does stable tearing occur under both CA and VA fatigue conditions in a 7075 aluminium alloy compact tension (CT) specimen?

(b) Is there any difference between the macroscopic and microscopic characteristics of CA and VA tearing?

(c) Is it possible to develop the existing post-failure models as a useful tearing-prediction tool?

(d) What are the main parameters that control the onset and arrest of tearing, and are there any other factors, which may influence the extent of each tear?

(e) Is it possible to use finite element (FE) software to study the effect of crack front curvature on stress intensity factors at the onset and arrest of tearing?

(f) Can the study help in further understanding stable tearing and establishing the potential usage in durability assessment and damage tolerance evaluation of an aircraft structure?

The study provides advanced knowledge in fatigue crack growth, which helps in establishing confident and accurate durability assessment of aircraft structure. There are two engineering aspects that can be most benefited by the results of this study, namely in assessing physical validation to the fatigue crack growth prediction model

and assisting quantitative fractography during accident investigation. The knowledge can also be applied to other engineering structures.

1.5. Outline of thesis

In Chapter 1, the background, motivations and objectives of this study are presented after a brief overview of metal fatigue in aircraft structures. The presence of stable tearing complicates fatigue fracture surface analysis and the current prediction models do not incorporate stable tearing model. The main objective of the current study is to develop a predictive model for stable tearing behaviour in an aerospace aluminium alloy.

Chapter 2 of this thesis critically reviews various aspects of stable tearing from the literature. Several characteristics of stable tearing are discussed, starting with the occurrence of stable tearing in a range of engineering alloys and under various loading conditions. The significance of stable tearing is discussed in detail in terms of its implication to fractographic analysis of fatigue fracture surface and fatigue crack growth prediction model. Current crack growth prediction models are lacking in physical validity, which means that the current models predict the cycle-by-cycle crack length increment, but this result is not always matched with the fracture surface morphology. Several theoretical approaches and existing models for analysing stable tearing are critically analysed. The main conclusion is that the prediction of stable tearing jump length Δa is still not possible especially in aluminium alloy.

Chapter 3 describes the experimental methods used to study the parameters controlling the onset of stable tearing, and the factors that affect the size of tearing in aircraft 7075-T651 aluminium alloy CT specimens. In view of uncertainties about the

controlling parameters for CA and VA tearing, comparative tests are conducted. Multiple stable tearing bands are produced under CA and VA fatigue conditions, whereby the VA tearing is achieved by inserting overloads into a background of CA fatigue. The resistance curve for this particular material (7075-T651) and thickness (6.5 mm) was determined according to the standard test method, by using specimen of identical design and size to the fatigue tests. The results of the experimental testing are presented in Chapter 4. A total of 56 tears were produced from this study and various parameters of these tears were quantified. In addition to that, multiple tears, in a range of aluminium alloys and thicknesses, reported in the literature are also quantified and summarised at the end of this chapter.

Chapter 5 evaluates the significance of various measured tearing parameters, and assesses the effectiveness of the existing empirical models. These analyses provide some insight into the influence of the stress intensity factor K on the CA and VA tearing crack jump length Δa. The CA and VA tearing crack jump lengths Δa are compared to the theoretical plastic zone size and the static resistance curve plot is compared with the stable tearing crack jump length Δa. The multiple stable tears generated in this study and experimental data from the literature were utilised to develop a new alternative predictive model, which idealises the shape of tearing and incorporates some of the key parameters of stable tearing.

The new predictive model is supported by a combination of experimental testing and computational simulation. This model relates the stress intensity factor parameters at stable tearing onset and arrest to the stable tearing crack jump length and the curved geometry of the crack front. A new semi-analytical equation for stable tearing is proposed and its functional relationship is determined using the FE method. This

chapter also elaborates the FE analysis, in which the parametric solution of the stress intensity factor at the front of the trapezoidal crack front is obtained. This chapter ends with comparisons between the model predictions and the experimental results, which show excellent agreement.

Chapter 6 presents the extended Forsyth and Schijve models, which use the idealised shape of tearing in the new model to provide alternative methods for predicting stable tearing jump length. Each of these extended models is validated by using various empirical results from literature, and shows good agreement between the prediction and measured stable tearing crack jump length. The advantages and disadvantages of each model are presented and discussed.

Finally, the conclusions of the current study are presented in Chapter 7, with recommendations for future work. A new prediction model is proposed for estimating the extent of stable tearing jump crack jump length Δa under CA and VA fatigue conditions and the existing empirical models are further developed as useful tearing-prediction tools. These models are empirically validated with various results in the literature. This study highlights the significance of fatigue fracture surface analysis in interpreting the fracture behaviour of metal under fatigue loading conditions and provides advanced knowledge in stable tearing crack growth prediction during quantitative fractographic analysis, which helps in establishing confident and accurate fatigue life and crack growth predictions.

Chapter 2. Critical Literature Review

2.1. Stable tearing crack growth mechanisms

2.2. Observation of stable tearing on fatigue fracture surfaces

2.3. Implications of stable tearing on fractographic analyses

2.4. Implications of stable tearing on fatigue crack growth rates prediction

2.5. Thickness effect on stable tearing

2.6. Theoretical analyses for stable tearing

2.7. Empirical analyses for stable tearing

2.7.1. Forsyth model (CA tearing in aluminium alloy)

2.7.2. Schijve model (VA tearing in aluminium alloy)

2.7.3. Resistance curve approach

2.7.4. Troshchenko model (CA tearing in steels at very low temperature)

2.8. Summary of literature review

This chapter critically reviews various aspects of stable tearing from the literature. Several characteristics of stable tearing are discussed, starting with the occurrence of stable tearing in a range of engineering alloys and under various loading conditions. The significance of stable tearing is discussed in detail in terms of its implications for fractographic analysis of fatigue fracture surfaces and fatigue crack growth prediction models. Current crack growth prediction models are lacking in physical validity, which means that the current models predict the cycle-by-cycle crack length increment, but this result is not always matched with the fracture surface morphology. Several theoretical approaches and existing models for analysing stable tearing are critically analysed. The main conclusion is that the prediction of stable tearing jump length Δa is still not possible especially in aluminium alloy.

2.1. Stable tearing crack growth mechanisms

The fatigue fracture surface usually exhibits distinctive macroscopic markings, which represent a succession of crack fronts during crack growth periods (Laird, 1967). These progression markings are often referred to in the literature as beach markings, tide markings, conchoidal markings, oyster-shell markings or clamshell markings (Forsyth and Ryder, 1960; Mann, 1967). Over the past decades there has been a dramatic interest in the study of the fatigue fracture surface, since the work of Zapffe and Worden (1949), who applied a high magnification technique to study fracture surfaces; and fracture surface analysis has been employed extensively in engineering failure analysis (Ryder *et al*., 1987; Lynch and Moutsos, 2006), especially during aircraft accident investigation (Goldsmith and Clark, 1989, 1990).

The fatigue fracture surface of a range of structural metallic materials that were used in aircraft components, sometimes exhibits stable tearing bands, visible as dull crescent- or tongue-shaped regions in contrast to the "bright" background fatigue surface (Forsyth and Ryder, 1961). Such tearing is commonly visible at the central cross-section of the component while the crack fronts that appear on the free surface are lagging behind. Some examples of tearing on the fracture surfaces of laboratory test coupons and in-service failure of aircraft spars are depicted in Figure 2. Multiple stable tear bands, shown in Figure 2a, have been produced under CA fatigue conditions (increasing ΔK), while Figure 2b-d show the tear bands that are produced under VA fatigue conditions.

Throughout this thesis, the term stable tearing will refer to the tear bands of the kind shown in Figure 2, although other terms have been used to describe this phenomenon in aluminium alloys, such as brittle crack growth (Hudson and Hardrath, 1963), tensile crack jumping (Forsyth, 1976, 1978), quasi-cleavage (Bathias and Vancon, 1978), tongue-shaped crack extension (Vlasveld and Schijve, 1979, 1980; Partl and Schijve, 1990), ductile tearing rupture (Vlasveld and Schijve, 1979, 1980) and mixed fatigue-tensile crack growth (Forsyth, 1976, 1978; Bowen and Forsyth, 1981). Other terms have also been used for similar occurrence in steels such as crack jump-wise (Bolotin, 1999a, 1999b), jump-like crack propagation (Troshchenko, 2009) or self-similar crack growth (Ivanova, 1982b).

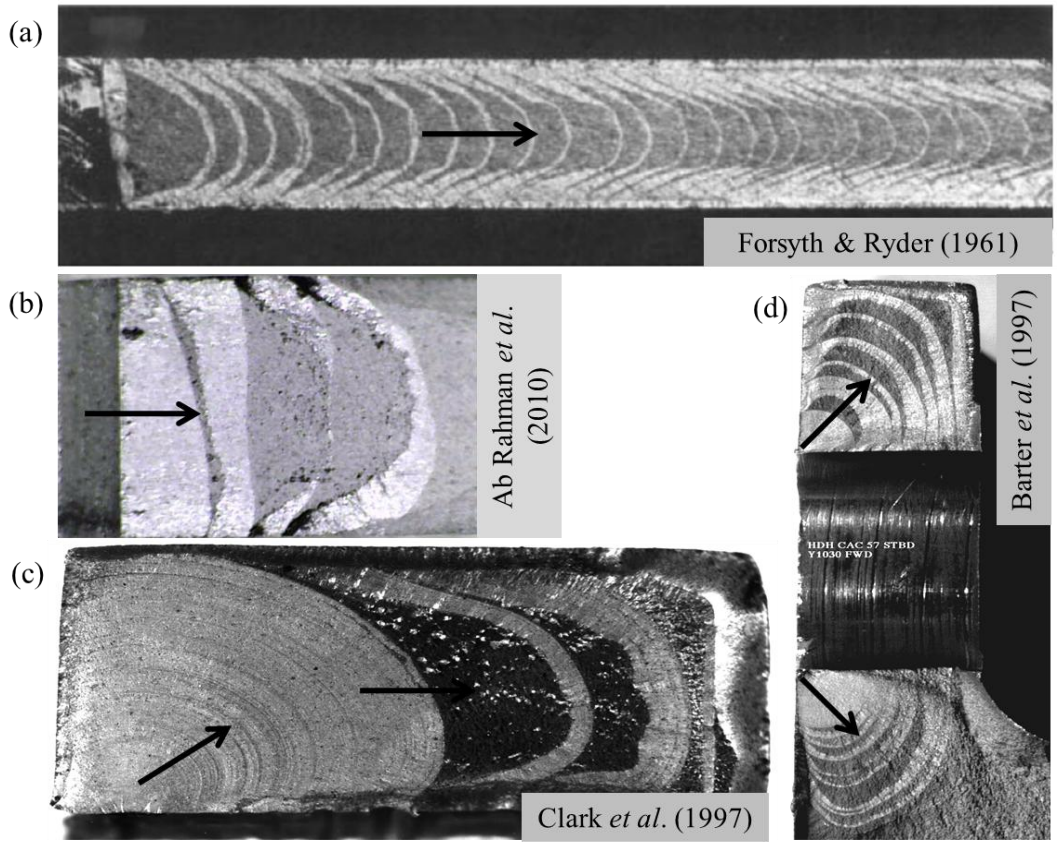

Figure 2. Examples of stable tearing bands on fatigue fracture surfaces: (a), (b) laboratory coupons of aluminium alloys (Forsyth and Ryder, 1961; Ab Rahman *et al*., 2010a), and (c), (d) fracture surfaces from wing spars in RAAF aircraft (Clark *et al*., 1997; Barter *et al*., 1997). Arrows indicate the direction of crack growth.

Essentially, stable tearing can be associated with the middle part of the crack front becomes unstable during fatigue crack growth, jumps ahead and causes two apparently unfractured ligaments near the surface. It implies that the critical conditions for fracture are only achieved at the middle cross-section of the crack front (Forsyth and Ryder, 1961), which further suggests that there could be two differing fracture conditions that govern the cracking condition at mid-thickness and near

surface regions. These unfractured ligaments effectively restrain further tearing jumps, and are proposed to deform plastically (Vlasveld and Schijve, 1979, 1980). This proposal is supported by experimental evidence of the butterfly-shaped deformations around the crack tip on the free surface (Bathias and Vancon, 1978; Daneshpour *et al*., 2009). After a quick burst of crack jumping, the crack growth reverts back to being fatigue-driven, with the more usual slow fatigue crack growth pattern occurring mainly in the unfractured ligaments.

A noteworthy macroscopic characteristic of the crack growth by the fatigue-tearing-fatigue process is the continuing changes in crack front shape from straight to curved and straight again (Forsyth and Ryder, 1961). The onset of tearing usually occurs at a slightly curved crack front, and the fatigue crack growth that ensues subsequent to tearing appears to re-straighten the crack front, after it has been severely curved by tearing. Forsyth (1976, 1978) has shown that the lengths of crack front lines at tearing onset and arrest are critical during the occurrence of stable tearing and this finding further implies that the other related macroscopic tearing parameters such as shape and size (area) could also be key parameters in controlling the onset and arrest of tearing, as well as the tearing crack jump length.

The tearing usually occurs and recurs at a suitably high load in VA conditions (Hudson and Hardrath, 1963), while in CA sequences, its occurrence is usually observed in regions of high fatigue crack growth rates (Troshchenko, 2009). This implies that multiple tearing bands may ensue prior to the final unstable separation. Substantial crack growth in each tear band is produced within a single fatigue cycle, whereby the process of tearing growth should occur in the period before K_{max} is reached (Vlasveld and Schijve, 1979). In some cases, stable tearing has been observed

to occur relatively early in the fatigue cracking process (Forsyth, 1978; Goldsmith *et al*., 1996), and hence the accumulated tearing areas may even make up a very large fraction of the overall fracture surface.

The generalisability of much published research on the microscopic characteristics of stable tearing is problematic. Several studies have reported that tearing growth can be categorised as brittle or cleavage fracture (Frost, 1961; Hudson and Hardrath, 1963; Pearson, 1968; McIntyre, 1975), with typical morphological features such as ridge pattern (McIntyre, 1975) and transgranular growth (Schijve and de Rijk, 1965). In contrast, a number of researchers, such as Forsyth and Ryder (1961), Schijve *et al*., (1976), Bathias and Vancon (1978) and Vlasveld and Schijve (1979), suggest that the tearing area is predominated by a dimpled pattern, which is a typical attribute of ductile failure and similar to the tensile failure of the final fracture (Forsyth and Ryder, 1961).

However, it should be noted that these observations are made on different alloys, and therefore it is most likely that in some materials cleavage fracture is dominant, while in others the fracture surface of stable tearing is mainly made up of ductile fracture. Forsyth (1978) suggested that the microscopic appearance of stable tearing can be related to the strength of the material, namely stronger material (low toughness) is more likely to produce cleavage fracture, while in material of low tensile strength (high toughness), the stable tearing surface will be predominated by ductile fracture.

2.2. Observation of stable tearing on fatigue fracture surface

There is a large volume of published studies relating to the observation of stable tearing bands on fatigue fracture surfaces of various engineering metals, subjected to a

range of loading conditions. For instance, this phenomenon has been observed on many fatigue fracture surfaces of various aluminium alloys which are often used in aircraft components (Vlasveld and Schijve, 1979, 1980; Bowen and Forsyth, 1981; Byrnes *et al*., 2000; Liu *et al*., 2005). Stable tearing can also be evident on the fracture surfaces of other aircraft structural metallic materials such as steels and titanium alloys (Liu *et al*., 2005; Pearson, 1968; Powell, 1995). Particularly, stable tearing has been reported on many fracture surfaces of in-service failures of various aluminium alloys components such as wing spars (Hudson and Hardrath, 1963; Mann, 1967; Barter *et al*., 1993, 1997; Goldsmith *et al*., 1996; Clark *et al*., 1997; Vlasveld and Schijve, 1979, 1980; Hersman and Higgins, 2007), fuselage skins (Forsyth, 1978; Ciesielski *et al*., 2009), piston engine components (Turan and Karci, 2009; Molent, 2010) and others (Liu *et al*., 2005; Molent, 2010).

Stable tearing has also been observed on fracture surfaces of various steels used in other engineering structures, such as pressure vessels (Troshchenko *et al*., 1980c, 1992; Yasnii, 1981; Kitsunai, 1986), compressor blades (Limar, 1987; Limar *et al*., 1989; Troshchenko, 2003a; Botvina *et al*., 1981b), rails (Glinka *et al*., 1984; Vander Voort, 1992; Rungta *et al*., 1985) and many others (Torres *et al*., 2010; Wanhill, 2003; McIntyre, 1975; Wei, 2010). One noteworthy fact is that some of these structures were operated either at extremely low or high temperatures. Moreover, stable tearing can also occur under a range of fatigue cracking conditions such as creep (Christensen, 1961; Ivanova *et al*., 1972), stress corrosion (Forsyth and Ryder, 1961; Schijve and de Rijk, 1965; Schijve *et al*., 1976; Ivanova *et al*., 1972), dynamic loading (Ivanova *et al*., 1972; Johnson and Radon, 1976) and hydrogen embrittlement (Ivanova *et al*., 1972). It has conclusively been demonstrated that stable tearing is similar to the pop-in

behaviour usually seen during fracture toughness testing (Bowen and Forsyth, 1981), and tearing-like growth can be observed on many fracture surfaces of specimens exposed to quasi-static loading conditions (Ivanova *et al.*, 1972; Neale, 1978; Torres *et al.*, 2010).

From the preceding paragraphs, it can be concluded that the occurrence of stable tearing is wide-ranging, namely it occurs in many engineering materials and structures, exposed to a range of loading conditions. It also indicates that many critical components are susceptible to the stable tearing crack growth mechanism, which further accentuates its significance and the need for better understanding of the fatigue crack growth. Besides, it has been established in the previous section that stable tearing may occur during fatigue crack growth under either CA or VA fatigue conditions.

Stable tearing under CA fatigue cycles usually occurs in region III of the double log plot of fatigue crack growth rates da/dN versus the stress intensity factor range ΔK (Troshchenko and Pokrovskii, 1980a), as shown in Figure 3. It should be noted that Schijve (2009) also named region III of fatigue crack growth rates plot as the stable tearing region, because patches of localised ductile tearing are sometimes observed between the periods of fatigue striations. The onset of CA tearing occurs for a ΔK cycle with the K_{max} equal to a certain critical value of stress intensity factor K_i. In 7178 aluminium alloy, the K_i is equivalent to the plane strain fracture toughness K_{Ic} (Bowen and Forsyth, 1981), but for many steels at low temperature the K_i is appreciably lower than the K_{Ic} determined under similar conditions (Troshchenko, 2009).

Stable tearing under VA fatigue cycles is generally observed when high loads are applied against a background of lower CA fatigue cycles. Experimental evidence has shown that stable tearing can also be produced on fracture surfaces of various aluminium alloy specimens exposed to flight simulation loading conditions (Wanhill *et al*., 1979; Liu *et al*., 2005). Similar to the CA tearing, the onset of VA tearing also occurs at K_c that is apparently equivalent to the K_{Ic} (Vlasveld and Schijve, 1979, 1980). This implies that the VA tearing is more likely to occur in region II (Paris region) of the fatigue crack growth curve. This condition should be expected because an application of a ΔK with $K_{max} = K_{Ic}$ in region III will theoretically cause the final unstable fracture of the specimen.

It implies that the conditions for the onset of CA and VA tears are equivalent, but this critical state ($K_{max} \geq K_{Ic}$) is achieved through two different conditions, namely by having longer crack length a in CA fatigue, while in VA fatigue the onset is mainly due to the overload. The occurrence of CA tearing in region III and VA tearing in region II of fatigue crack growth rate plot has substantial consequences on fatigue crack growth predictions, and this issue is discussed in detail in section 2.4. It is noteworthy that the fatigue crack growth rates plot is preceded by a threshold region (region I) and the comprehensive description and significance of each region can be sought from major textbooks on metal fatigue, such as Suresh (1998), Stephens *et al*. (2001), Pook (2007) and Schijve (2009).

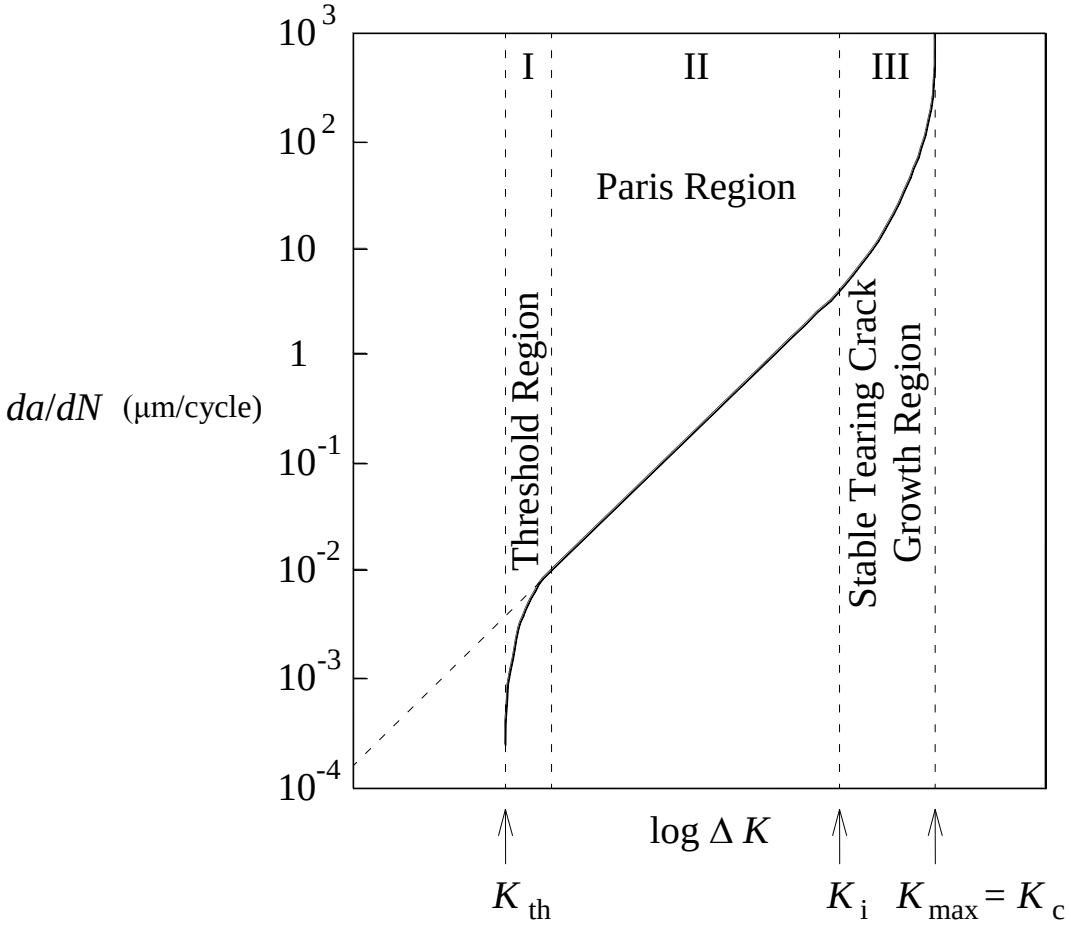

Figure 3. The three regions of fatigue crack growth under CA fatigue cycle. The onset of CA tearing usually occurs in region III when the condition of $K_{max} \geq K_i$ is attained by virtue of having longer crack length, while the onset of VA tearing takes place in region II as the overload cycle can induce the $K_{max} \geq K_i$ condition. Adapted from Schijve (2009).

2.3. Implications of stable tearing on fractographic analyses

From macroscopic observation, it can be concluded that the crack advance by tearing is analogous to the final unstable fracture of the component (Bowen and

Forsyth, 1981; Ab Rahman *et al*., 2010b), but with the distinct difference that the tearing is stable. The final unstable fracture occurs when the remaining cross-section can no longer sustain the applied load, whilst in tearing; the crack growth is arrested after a certain distance of crack front advancement and then resumed by further fatigue crack growth. Macroscopic evidence has also shown that multiple stable tearing bands, separated by regions created by fatigue crack growth, may be visible on a single fracture surface (Ab Rahman *et al*., 2010a, 2010c, 2010d), to the extent that they may even make up the majority of the fatigue fracture surface (Goldsmith *et al*., 1996).

The challenge in fracture surface analysis – known as quantitative fractography (Forsyth and Ryder, 1960; Goldsmith and Clark, 1989, 1990; Lynch and Wanhill, 2004) – is usually to relate a sequence of flight loads to a sequence of markings, revealing relationships between the crack front progression markings on the crack surface and the loading history of the component. Quantitative fractography is crucial in developing a crack growth history against flights, to assess the structural integrity of the (grounded) fleet and plan the periodic inspections for fatigue cracks. Such analysis could provide vital crack growth history for the failed part, and in this case, the extensive stable tearing made the process difficult, since it was not obvious how the extent of each tear could be linked to loads.

One particular surface that provides a good example is given in Figure 4, which shows the fracture surface of an aluminium alloy wing spar that failed during flight (Clark *et al*., 1997; Barter *et al*., 1997). The fracture surface shows many large tear bands, visible in Figure 4 as dark crescents, and notably large proportions of the fracture surface consist of tearing. Figure 5 shows part of the spar fracture surface, including flight numbers in which various markings occurred. The inset in Figure 5

highlights the differences between some very small increments in crack length or changes in surface topography, appearing as progression marks in a fatigue region, and two large neighbouring stable tear bands (each of which occurred during a single flight load cycle).

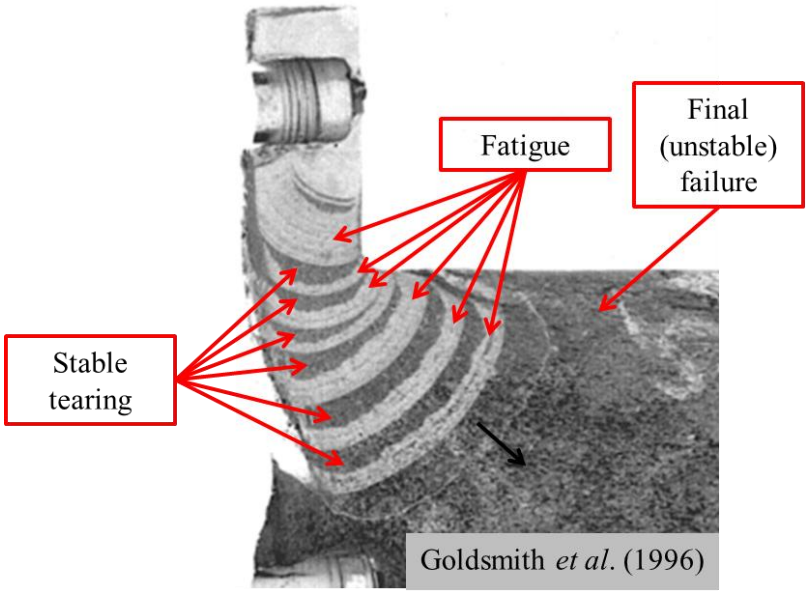

Figure 4. Fracture surface appearance of 7075 aluminium alloy lower wing spar from an Aermacchi MB326H (Goldsmith *et al*., 1996), showing evidence of brighter regions of in-service fatigue crack growth, with progression markings, interrupted by dull bands of stable tearing. An arrow indicates the crack growth direction prior to final unstable failure.

In the absence of a valid stable tearing model, fracture surface analysis demands extensive effort to devise ways to match up some of the large tears to the loads present in the (rather uncertain) load history (Goldsmith *et al*., 1996). Several attempts have been made to relate the size of each tear to the applied load, notably by Hudson and

Hardrath (1963) in an aluminium alloy specimen, but have been unsuccessful. In few steels, empirical evidence shows that the size of each tear can be related to the plastic zone size (Troshchenko and Pokrovskii, 1983a; Kitsunai, 1986), but the correlation is only specific to a certain type of steels and there is no generic solution.

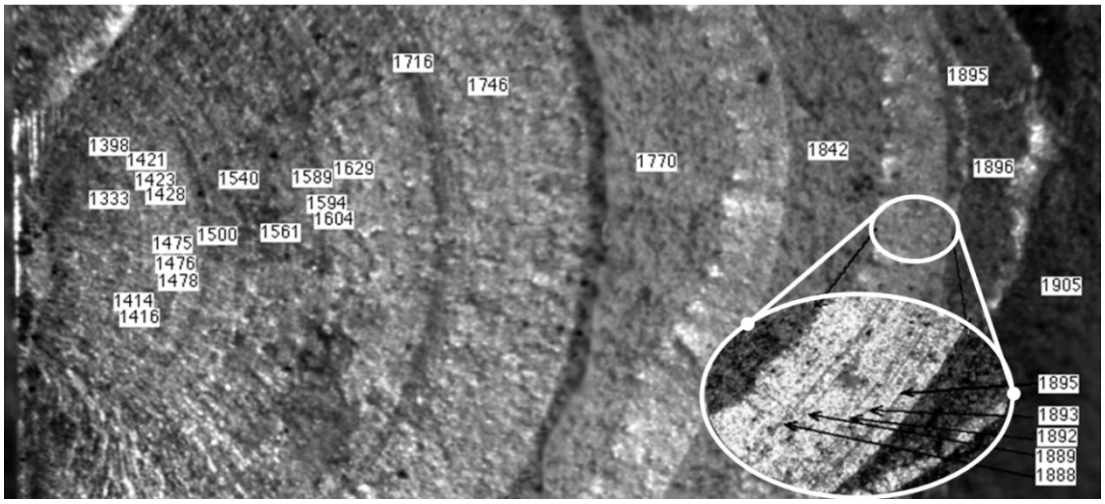

Figure 5. Part of the fracture surface of the failed spar of an Aermacchi MB326H, with the flight numbers in which specific markings occurred are shown (Barter *et al*., 1993). Several large tears are evident.

2.4. Implications of stable tearing on fatigue crack growth rates prediction

The first serious discussions and analyses of stable tearing in fatigue crack growth emerged in 1961, when the first report was put forward by Forsyth and Ryder (1961), who observed stable tearing in a thin sheet of aluminium alloy specimen (thickness t = 4.5 mm). They presented a theoretical analysis for stable tearing based on the work of Cottrell (1958). In the same year, other researchers had reported

similar observations during the proceedings of the Crack Propagation Symposium in Cranfield (Christensen, 1961; Hardrath and McEvily, 1961; Frost *et al*., 1961). For instance, Christensen (1961) demonstrated that stable tearing occurs under fatigue-creep conditions and highlighted the importance of plastic deformation at the ligaments in arresting the crack growth. Like Forsyth and Ryder (1961), he also noted the importance of shape and contour of the crack front in controlling the fatigue crack growth rate.

Fundamentally, stable tearing can be regarded as a departure from steady fatigue cracking, featuring a rapid "jump" of crack length in one loading cycle, after which fatigue resumes. Vlasveld and Schijve (1979) noted that each tearing jump cannot be detected on the surface of the specimen but showed conclusively that the growth of each tear takes place continuously during an increasing load in a single fatigue cycle on the potential drop records. They also noticed that this process is much faster than normal fatigue crack growth and the crack front advance in much greater, whilst Frost (1962) and McIntyre (1975) concluded that the overall fatigue crack growth with bands of tearing actually consists of periods of slow fatigue crack growth interspersed with periods of fast stable fracture by tearing.

Stable tearing has been recognised as a major issue affecting accurate and reliable predictions of fatigue life and fatigue crack growth (Frost, 1962; Hudson and Hardrath, 1963; Wanhill *et al*., 1979; Partl and Schijve, 1990; Barter *et al*., 1993; Goldsmith *et al*., 1996; Clark *et al*., 1997; Newman Jr., 1997). For CA conditions, Schijve (2009) mentioned several empirical relationships to account for the fatigue crack growth rate in region III, and concluded that none of these functions has physical validity. The erratic nature of fatigue crack growth in this region suggests that it is

more practical to discard components when the calculated K_{max} reaches K_{Ic}, namely at the first onset of tearing, and implies that the predicted overall crack growth life is rather conservative. However, in many engineering metals, multiple tear bands between fatigue crack growth periods can occur, notably as shown by the test results of Forsyth and Ryder (1961) and Frost (1962), and hence the addition of fatigue-tearing crack growth life can have significant effect on the predicted overall crack growth life.

In VA loading sequences, a stable tearing band usually forms upon the application of a ΔK with $K_{max} = K_{Ic}$, and most likely occurs during the increasing tensile loading cycle of the high load cycles (Vlasveld and Schijve, 1979, 1980). This means that a single high load cycle (overload) can produce significant increase in crack length in addition to retardation in subsequent fatigue crack growth. Newman Jr. (1997) indicated that the presence of stable tearing will cause the plasticity-induced crack closure model to underestimate the crack growth rate after an overload, whilst Vardar and Yildirim (1990) observed that the large tearing jump length can cause the actual crack growth rate to deviate from the Paris relationship.

It is worthwhile to note that a considerable amount of literature has been published on the retardation (or sometimes acceleration) effect of an overload (Geary, 1992; Singh *et al*., 2011). In 7075 aluminium alloy, several fatigue crack growth retardation mechanisms have been proposed, such as crack tip branching and plasticity-induced crack closure (Bucci *et al*., 1980). Numerous studies have also been conducted to develop crack growth prediction models that account for such a retardation effect in 7075 aluminium alloy, for example Vardar (1988), Yildirim and Vardar (1990) and Celik *et al*. (2004). It should be noted that Vardar (1988) ignored the correlation between the retardation mechanisms (stable tearing) and the delayed

period. Yildirim and Vardar's analysis, however, did not take into account the presence of tearing jump, nor did they examine the relationship between the tearing jump and the retardation periods.

A practical question is whether prediction models for stable tearing will improve the reliability and validity of the overall fatigue life and crack growth prediction models. It has been emphasised that the presence of tearing bands can generally be regarded as reflecting incipient failure, namely the K_{max} at the crack tip is approaching the critical condition K_{Ic}. However, tearing can start very early during fatigue life (within 30% of the fatigue crack growth life (Forsyth, 1978)) and therefore is most likely to dominate the fatigue crack growth region. The overall fatigue crack growth prediction model up to the final unstable failure is limited to steels operating at very low temperatures and is not yet available for aluminium alloys.

The studies on crack growth prediction models for VA loading usually neglect the occurrence of stable tearing (Bathias and Vancon, 1978; Vardar and Yildirim, 1990), partly because its occurrence is only observed under certain conditions. For example, test results of the two aluminium alloys, 2024-T3 and 7075-T6 with 4 mm thick specimens showed that stable tearing was only observed on 7075-T6 alloy (Schijve, 1974). A similar observation has been reported by Bathias and Vancon (1978) in other series of aluminium alloys. Other possibilities are that many previous fatigue crack growth studies are often limited to measuring the crack length over fatigue load cycles, without comparison being made to the fracture surface (Zhao *et al*., 2008) or the application of overload has an insignificant effect on the overall fatigue crack growth curve (Barter *et al*., 2005). Zhao *et al*. (2008) noted the limitation of the Wheeler's model in describing the complex phenomena immediately subsequent

to overloading, such as crack acceleration and arrest. A similar conclusion has been suggested by Bathias and Vancon (1978) for Willenborg model.

Schijve (2009) and Pook (2007) noted that the empirical verification of the fatigue crack growth prediction models under VA loading is rather limited. One way to accomplish this is by matching the crack growth prediction model with the striation spacing on fatigue fracture surface (Schijve, 2009). Such comparative analyses, sometimes referred to as fatigue crack growth reconstitution (Kunz *et al*., 2010), have been conducted (Siegl *et al*., 1991, 2009), but are found to be complicated by the presence of other fracture mechanisms such as stable tearing (Siegl *et al*., 2009). Lauschmann *et al*. (2006) argued that the conventional definition of fatigue crack growth rate, which is based on the crack length increment over number of loading cycles, is only suitable for CA loading.

However, under VA load excursions, the crack growth rate is not directly related to the striation spacing, as an overload cycle (high load cycle) can cause a substantial increase in crack length, but in the subsequent low fatigue cycles, no noticeable crack growth marks appear on fracture surface due to the effect of retardation. Better correlation between the crack growth prediction models with the fracture surface morphology will definitely improve the accuracy of predicting fatigue crack growth (Schijve, 1999).

2.5. Thickness effect on stable tearing

The observation of greater crack advance at the mid-thickness region of a component or specimen has prompted several researchers to believe that stable tearing usually occurs in materials of intermediate thickness whereby regions of plane strain

and plane stress coexist (Hardrath and McEvily, 1961; Dixon, 1966; Vlasveld and Schijve, 1979, 1980; Lynch, 2007). The survey in Table 2 indicates that stable tearing has mostly occurred in materials of intermediate thickness. It has been established in section 2.2 that the critical condition for the occurrence of stable tearing in aluminium alloys is the attainment of $K_{max} = K_{Ic}$. This is possible only if a fraction of the crack front is under plane strain condition. It should also be noted that tear bands can also occur in fairly thin or thick materials, where fully-developed plane stress or strain conditions respectively, are expected. For example, stable tearing can occur in alloys 2024, 7050, 7075 and 7178 of thickness 2 to 3 mm, while the occurrence of stable tearing in a very thick specimen is reported only in 7075 alloy of 25 mm thick.

It should be noted, however, that the test results of Byrnes *et al*. (2000) suggest that tearing in a very thick specimen is not quite stable, as a slight increase in K_{max} can cause the final unstable fracture. In their test, three relatively thin tearing bands were produced by applying overload of K_{max} slightly less than the material's fracture toughness. This is only possible for 7075 alloy, while two 7050 specimens were failed when tested under similar condition, namely K_{max} is slightly less than K_{Ic}. This implies that the crack growth life after the first onset of tearing in a relatively thick specimen is very short, and as a consequence, the engineering application of a stable tearing prediction model in this range of thicknesses is very limited.

Table 2. Surveys of experimental studies of stable tearing in various aluminium alloys and thicknesses.

Alloy	*t* (mm)	Researchers
2024-T3	2	Schijve *et al*. (1976), Partl and Schijve (1990)
	3	Yasnii and Pyndus (2002)
	4.9	Shanyavsky *et al*. (1995)
	10	Schijve *et al*. (1976)
2024-T4	10	Bathias and Vancon (1978)
	19.1	Hudson and Hardrath (1963), Hardrath and McEvily (1961)
2618	10	Bathias and Vancon (1978)
7050-T7451	3	Liu *et al*. (2005)
	6, 12	Byrnes *et al*. (2000)
7075-T6	2	Schijve and de Rijk (1965), Schijve *et al*. (1976)
	4	Schijve (1974)
	10	Schijve *et al*. (1976)
	25	Byrnes *et al*. (2000)
7075-T651	6.4, 12.7	Vlasveld and Schijve (1979, 1980)
7075-T7	6.4	Vlasveld and Schijve (1979, 1980)
7178-T6	2.5, 3.3	Frost *et al*. (1961), Frost (1962)
	4.5	Forsyth and Ryder (1961)
7178-T651	3	Bowen and Forsyth (1981)

Experimental evidence in several studies has suggested that the occurrence of stable tearing in material of thin and intermediate thicknesses under CA conditions can be associated with the transition of a fatigue crack from a tensile mode (flat fracture surface) to the shear mode (slant fracture surface), in which the crack front becomes more curved during the process (Frost, 1962; Bowen and Forsyth, 1981; Rhodes *et al*., 1980; Limar *et al*., 1989). For example, Limar *et al*. (1989) reported this condition in a thin titanium alloys specimen of thickness 3.5 mm. This suggests that in a range of metals, the occurrence of stable tearing expedites this transition, and this condition is found to be the case especially at the high *K* region (Frost, 1962).

The fracture mode transition is mainly caused by an increase in the plastic zone size as the crack progresses (Broek, 1986), as depicted in Figure 6. In the early stages of cracking, the plastic zone size is small, promoting plane strain conditions. As the crack and its plastic zone enlarge, fracture can occur on the slanted boundary of the growing region of plane stress. One of the limitations of this explanation is that if the specimen is very thin, the final unstable fracture will usually be caused by net section yielding, which implies that the use of the *K*-criterion may be invalid. Therefore, it suggests that the occurrence of CA tearing is related to the size of the plastic zone, and this suggestion is supported by some empirical evidence, especially in steels at very low temperatures (Kitsunai, 1985, 1986; Troshchenko and Pokrovskii, 1983a; Troshchenko *et al*., 1978).

The occurrence of stable tearing in a thick material is not very well understood, but for aluminium alloy, it has only been reported (Hudson and Hardrath, 1963; Bathias and Vancon, 1978; Byrnes *et al*., 2000) as occurring under VA loading, where one or more tensile peak loads are applied against a background of less severe load

cycling. The occurrence of CA tearing in thick materials has been reported in various steels at very low (Troshchenko *et al*., 1980b) or high (Pearson, 1968) temperatures. In these conditions, the onset of tearing is observed to occur at *K*–level that is appreciably lower than its equivalent temperature plane strain fracture toughness K_{Ic} (Pearson, 1968), as will be discussed in section 2.7.4.

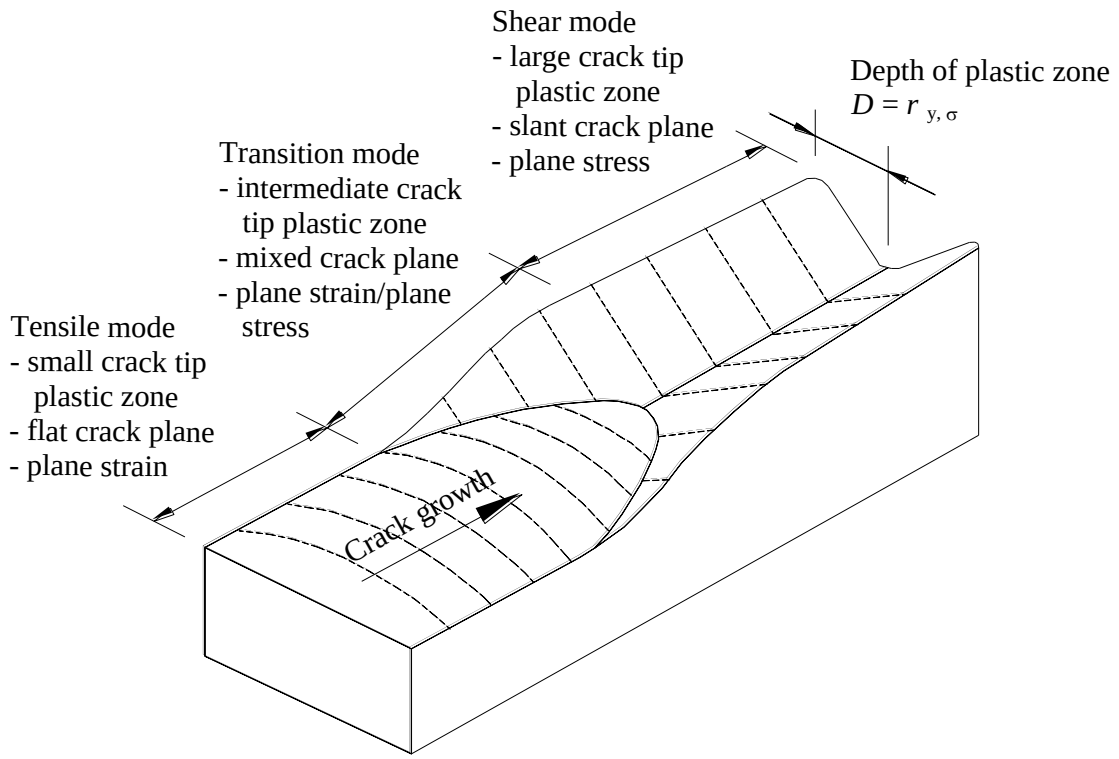

Figure 6. Fatigue crack growth transition from tensile mode to shear mode (adapted from (Broek, 1986). The depth of shear lip *D* from the side of the specimen is approximately equal to the plane stress plastic zone size (Hertzberg, 1996).

The application of a high tensile peak load or overload under VA fatigue conditions can induce material in the central portion of the specimens (which is predominantly under plane strain) to reach critical conditions ($K_{max} \geq K_{Ic}$), causing the

crack front to jump. This implies that the critical conditions of tearing are only achieved and maintained at the central part of the crack front during tear growth. The occurrence of VA tearing in thick material is also similar to the pop-in phenomenon during plane strain fracture toughness test (Brown and Srawley, 1966), but unlike the static test, in VA conditions, transitory stability returns once the overload cycle is replaced by a less severe fatigue cycle.

The arrest of tearing have been associated with other mechanisms that occur in the surrounding material, such as retardation by residual compressive stress caused by the overload at the mid-thickness region (Hardrath and McEvily, 1961; Hudson and Hardrath, 1963; Bathias and Vancon, 1978), the restraining effect of uncracked ligaments at the edges (Vlasveld and Schijve, 1979, 1980) and an increase in the length of the crack front (Bowen and Forsyth, 1977, 1978, 1981) (especially in a CA fatigue condition). It should also be noted that, since the tearing under VA conditions occurs as a result of an overload, other fracture retardation mechanisms are also possible such as crack deflection, strain hardening, plastic blunting/re-sharpening, depending on the types of material (Ward-Close *et al*., 1989), except for plasticity-induced crack closure. The effect of crack closure is only possible when the crack is about to open or close, when the fracture surfaces are in contact with each other (Elber, 1970), whilst the tearing advancement process occurs progressively during loading to K_{max}.

Therefore, it can be concluded that although stable tearing may occur in very thick metals, its occurrence is more significant in metal of intermediate and thin thicknesses because the crack growth life after the first onset of tearing may be substantial. The occurrence of tearing in a relatively thick metal is rather unstable. Stable tearing in relatively thin and intermediate thicknesses materials under CA

conditions can be associated with the transition of fatigue crack modes, as the crack front becomes more curved, and thus can be related to the plastic zone size.

2.6. Theoretical analyses for stable tearing

A number of theoretical analyses for stable tearing have been put forward. Sih (1981) postulated that the crack growth condition of stable tearing is similar to the total of critical strain energy density and its process is assumed to be similar to the ductile fracture under static loading. According to this theory, the stable tearing process is governed by the release of dilatational energy ahead of the crack front, and this energy is concentrated more in the mid-thickness region, while material near the surface can deform. The fatigue growth that follows each tear is then dominated by distortion in the material at the trailing edge near the free surface, which is associated with more energy stored at the free surface than at the central zone.

The occurrence of stable tearing therefore can be predicted by counting the hysteresis energy density during each loading cycle, and the onset of stable tearing is assumed to occur when the total hysteresis strain energy density $\left(\frac{\Delta W}{\Delta V}\right)_{\text{average}}$ achieves a critical value,

$$\left(\frac{\Delta W}{\Delta V}\right)_{\text{average}} \times \Delta n = M \qquad (1)$$

where M is a material constant, which has to be determined by experimentation or numerical analysis, Δn is the interval between numbers of cycles and $\frac{\Delta W}{\Delta V}$ is the strain energy density function (ΔW is the strain energy and ΔV is the volume). Detailed description of this failure criterion can be found in Gdoutos (2005). Sih (1981) described a few methods by which this failure criterion can be developed, but none of these are supported empirically. The criterion emphasises the importance of the shape of the crack front and the fracture surface area as some of the controlling parameters.

Bolotin (1999a) presented a theoretical framework for analysing stable tearing (or jump-wise) based on the thin plastic zone model derived from the work of Leonov, Panasyuk and Dugdale. The main parameter of this approach is the plastic zone size, in which the damage process occurs. Bolotin (1999a) suggested that the tearing crack jump length Δa can be estimated by the extent of the cyclic plastic zone size. However, similar to the critical strain energy density criterion, this approach lacks an experimental validation.

Ivanova (1982b) used the similarity theory in combination with linear fracture mechanics approaches to determine various fundamental properties related to the occurrence of stable tearing. In her work, stable tearing has been referred to as self-similar fatigue crack growth or jump-wise propagation of fatigue cracks. This theory is based on the assumptions that the density of plastic deformation energy remains constant as the crack grows and the stress state at the crack tip can be represented by a single parameter of stress intensity factor (plane strain condition).

According to this theory, the onset of tearing occurs when the crack acquires sufficient energy for a jump. This energy is required to create a sizeable plastic zone

size in front of the crack tip and the resultant temporary state of instability is referred to as plastic instability. The extent of the first jump of crack length Δa can be estimated by the following relationship,

$$\Delta a = \frac{1}{\pi}\left[\frac{K^{\mathrm{R}}{}_{\max}}{\zeta \times \sigma_{\mathrm{Y}}}\right]^2 \tag{2}$$

where $K_{\max}$ represents the maximum stress intensity factor, ζ is a factor that accounts for the local ductility at the transition between fatigue crack and tearing and σ_{Y} is the material's tensile strength. She proposed various other empirical relationships based on the similarity conditions, detail of which can be obtained from Ivanova (1982b). Ivanova's model, however, has been subjected to considerable criticism by Barenblatt (Barenblatt, 1982a, 1982b; Ivanova, 1982a, 1982c) especially on the theoretical foundation of her model. Perhaps the most serious disadvantage of this approach is that many of the terms must be determined by laborious experimental methods.

Finally, Margolin and Shvetsova (1991) proposed an analytical model that uses the critical brittle failure stress S_{c} as a limiting parameter for the onset of the first stable tear. The validity of the model has been substantiated by using steel (Ni-Cr-Mo-V). One limitation of this model is that it only predicts the onset of the first stable tear. Another limitation of this model is that its empirical formula involves various parameters, which have to be determined experimentally. Moreover, no attempt has been made to predict the length of the tearing jump length nor does it explain why the tearing stops.

2.7. Empirical analyses for stable tearing

Several empirical models have been proposed in the literature (Troshchenko *et al*., 1982; Ab Rahman *et al*., 2010b) for analysing stable tearing on fatigue fracture surfaces, which are all based on the two-dimensional analysis of the crack front and use stress intensity factor *K* as the main parameter. For aluminium alloys, three principal studies, by Forsyth (Forsyth, 1976, 1978; Bowen and Forsyth, 1981), Schijve (Vlasveld and Schijve, 1979, 1980) and Clark (Byrnes *et al*., 1998, 2000; Liu *et al*., 2005), have attempted to produce models which allow tearing characteristics to be assessed from fracture surfaces, by relating the observed shapes to the crack front line length *l*, to a stress intensity factor modified by the size of the uncracked fracture surface ligament, and to the material's resistance curve. Details of these models are presented in Section 2.7.1, 2.7.2 and 2.7.3.

Several alternative empirical methods have been proposed in the literature to account for specific applications (Glinka *et al*., 1984; Troshchenko, 2009). For example, Glinka *et al*. (1984) studied stable tearing in an elliptical crack in three types of steels rails. Due to the three-dimensional nature of an elliptical crack, the stress intensity factor *K* was only determined at the deepest point of the crack (at the end of the short axis) and given by the following relationship,

$$K_{2D}(a) = K(\sigma_{max}) + K(\sigma_r) \tag{3}$$

where $K(\sigma_{max})$ and $K(\sigma_r)$ represent the *K* (in MPa$\sqrt{m}$) due to the maximum applied stress and the residual stress, respectively.

Glinka *et al*. (1984) carried out all the tests using CA loading, and multiple tear bands were observed on all three types of steels. The main conclusion was that the onset and arrest of tearing occurred due to variation of the *K*-value at the deepest point of the crack front. Similar to the empirical evidence reported by Forsyth (Forsyth, 1978; Bowen and Forsyth, 1981) and Schijve (Vlasveld and Schijve, 1979, 1980), the onset of stable tearing in these steels was observed at $K_{max} = K_{Ic}$. The arrest of tearing was attributed to the change in crack front shape, by being more curved at arrest, and hence resulted in reduction of the *K*. As mentioned before, the proposed method applies only for stable tearing in an elliptical crack, and therefore the effect of residual stresses is very significant. Other than that, observations in this study are fundamentally similar to that of Forsyth (Forsyth, 1978; Bowen and Forsyth, 1981) and Schijve (Vlasveld and Schijve, 1979, 1980).

Kitsunai (1985) presented some empirical observations of stable tearing in welded structural steel at low temperature, Pearson (1968) studied the occurrence of stable tearing in turbine disc steel at high temperature, but perhaps, the most extensive investigations of stable tearing in steels have been conducted by Troshchenko and co-workers (Troshchenko, 2003, 2009; Troshchenko and Pokrovskii, 1980, 1983a, 1983b, 2003a, 2003b; Troshchenko *et al*., 1978, 1079, 1980a, 1980b, 1982, 1985, 1987, 1988, 1992, 1994). Most of these studies were carried out on steels at very low temperature ranges. Details of his work are presented in section 2.7.4.

2.7.1. Forsyth model (CA tearing in aluminium alloy)

Forsyth and Ryder (1961) examined CA fatigue cracking in 4.5 mm thick 7178-T6 aluminium alloy specimens, in which fatigue crack growth was interrupted by periods of stable tearing. They investigated changes in the crack front line length l and noted that for each tear the length was always greater at tearing arrest, denoted as $l(a_i + \Delta a)$, than at the onset of tearing $l(a_i)$. Later, Forsyth (1976) hypothesised that CA tearing was halted, despite having longer maximum crack length and hence greater nominal stress intensity factor, because the $l(a_i + \Delta a)$ was longer. Measurement of pairs of maximum crack length and crack front line length data for the onset and arrest of CA tearing enabled Forsyth (1976) to suggest that the ratio of the square root of crack length to the crack front line length was approximately constant at onset and arrest of tearing, as represented by Eq. (4), although the value at onset was marginally higher than the arrest as indicated in Eq. (5).

$$\frac{\sqrt{a_i}}{l(a_i)} = \frac{\sqrt{a_i + \Delta a}}{l(a_i + \Delta a)} \approx \text{constant} \tag{4}$$

$$\frac{\sqrt{a_i}}{l(a_i)} > \frac{\sqrt{a_i + \Delta a}}{l(a_i + \Delta a)} \tag{5}$$

Eq. (4) implies that the onset of tearing occurs when the fracture condition is attained along the crack front, while Eq. (5) suggests that this critical fracture condition for tearing is always higher than for the resumption of fatigue (Forsyth, 1978).

Forsyth (1978) argued that the lengthening and shortening of crack front during tearing and fatigue, respectively, occurred because the crack front attempts to retain the minimum-energy curvature, and by doing this the $\frac{\sqrt{a}}{l}$ ratio either at onset or arrest of tearing would be affected by various parameters; he nominated the specimen thickness t, maximum applied stress σ_{max} and fracture toughness K_{Ic}, as follows:

$$\frac{\sqrt{a}}{l} = \frac{K_{Ic}}{C_w \times t \times \sigma_{max}\sqrt{\pi}} \tag{6}$$

where C_w is the correction factor to account for finite width, but excluding any correction factor for the curved crack front.

Bowen and Forsyth (1981) proposed that each CA tear commences when the maximum stress intensity factor K_{max} in the fatigue cycle reaches the fracture toughness of the material K_{Ic}. As the crack front line length l increases during tearing, they argued that stability can only be maintained if the K_{max} is reduced by a ratio $\frac{t}{l}$. In effect, they proposed that the conditions for the onset and arrest of tearing are maintained throughout the tearing process with line length changing to maintain the stability (Wanhill *et al*., 1982). As illustrated in Figure 7, the Forsyth model assumes that the tearing initiates from a rectilinear crack front, namely $l(a_i) = t$ and the cessation occurs with a curved crack front and by modifying Eq. (6), the maximum stress intensity factor $K_{2D}(a_i + \Delta a)$ at each tearing can be estimated by the following equation.

$$K_{2D}(a_i + \Delta a) = K_{Ic} \times \frac{l(a_i + \Delta a)}{t} \qquad (7)$$

Bowen and Forsyth (1981) further suggested that CA tearing occurs under predominantly plane strain conditions and the stable tearing crack jump length is controlled by an energy density or line tension along the crack front length. They argued that the constancy of Eq. (4) is only possible for CA tearing, while VA tearing has been shown to produce scattered values.

The finding of Forsyth and Ryder instigated more research being done on the stable tearing phenomenon or referred to as Forsyth-Ryder mechanism (Plumbridge and Ryder, 1969), particularly by Troshchenko and co-workers at Pisarenko Institute for Problems of Strength in the Ukraine. Eq. (6) was applied by Botvina *et al*. (1981) to study stable tearing in a compressor blade titanium alloy, while Vlasveld and Schijve (1979, 1980) used Eq. (7) to validate their VA tearing empirical model. A similar approach in compensating the effect to crack front curvature, as in Eq. (6), was used by Neale (1976, 1978) to approximate the stress intensity factor for a thumbnail crack in fracture toughness testing. The Forsyth concept had also been used by various authors to explain some fatigue-related phenomena, for example in crack growth retardation (Ward-Close *et al*., 1989; Bowen and Forsyth, 1977; Forsyth and Bowen, 1981; Forsyth, 1983) and an apparent discontinuity in fatigue crack growth curves (Barenblatt and Botvina, 1993). Botvina and Limar (1985) also emphasised the usefulness of the crack front line length during quantitative fractography.

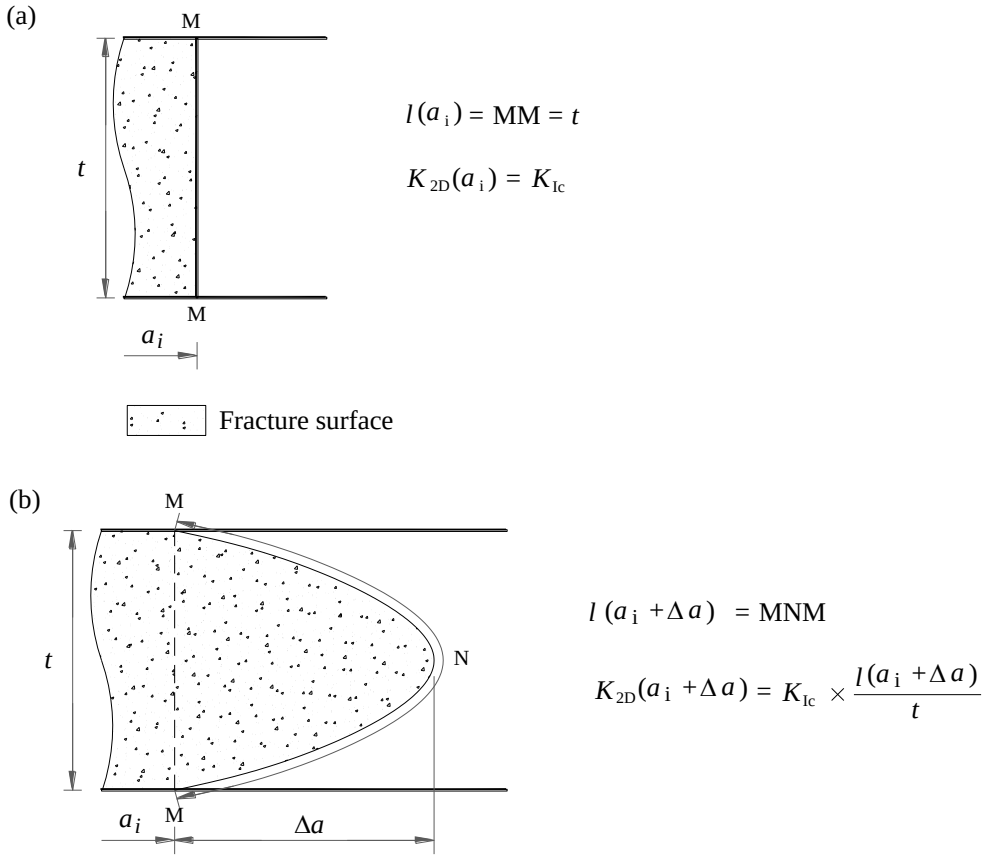

Figure 7. Schematic representation of the Forsyth model: (a) at tearing onset and (b) at tearing arrest.

2.7.2. Schijve model (VA tearing in aluminium alloy)

Tearing under VA loading had been reported by Schijve and co-workers (Schijve and de Rijk, 1965; Schijve, 1974; Schijve *et al*., 1976, 2004; Vlasveld and Schijve, 1979, 1980; Partl and Schijve, 1990), though the first fractographic study on VA tearing may be credited to Hardrath and McEvily (1961). Unlike the Forsyth model, which proposed that the plane strain conditions prevailed in CA tearing, Vlasveld and Schijve (1980) recognised the potential for through-thickness constraint – plane strain

and plane stress conditions – to play a role in VA tearing. They introduced the key concept of a change in the stress intensity factor (denoted as K_l) due to the restraining ligaments, which prevent unstable fracture occurring, with the stress intensity factor at tearing arrest is given by

$$K_{2D}(a_i + \Delta a) = K_{Ic} + K_l \tag{8}$$

where K_l is derived based on the assumptions that the restraining ligament is plastically deformed under plane stress conditions and its size increases linearly with the crack jump length Δa. It is defined as

$$K_l = -\frac{4\sigma_Y}{t}\sqrt{\frac{a_i + \Delta a}{\pi}}\left[\frac{1}{\pi}\left(\frac{K_{Ic}}{\sigma_Y}\right)^2 + \alpha \cdot \Delta a\right]\left[\sqrt{1+\frac{2a_i}{\Delta a}} - \frac{a_i}{\Delta a}\arccos\left(\frac{a_i}{a_i + \Delta a}\right)\right] \tag{9}$$

where α is the slope factor that accounts for the depth of plane stress penetration and is defined as

$$\alpha = \beta - \frac{1}{\pi.\Delta a}\left(\frac{K_{Ic}}{\sigma_Y}\right)^2 \tag{10}$$

where β is the angle between the tearing boundary to the free edge of the specimen in radians, as depicted in Figure 8. Based on the measurement of tearing on 12.7 mm thick specimens, Vlasveld and Schijve (1980) used α = 0.24 and assumed that this value was a constant.

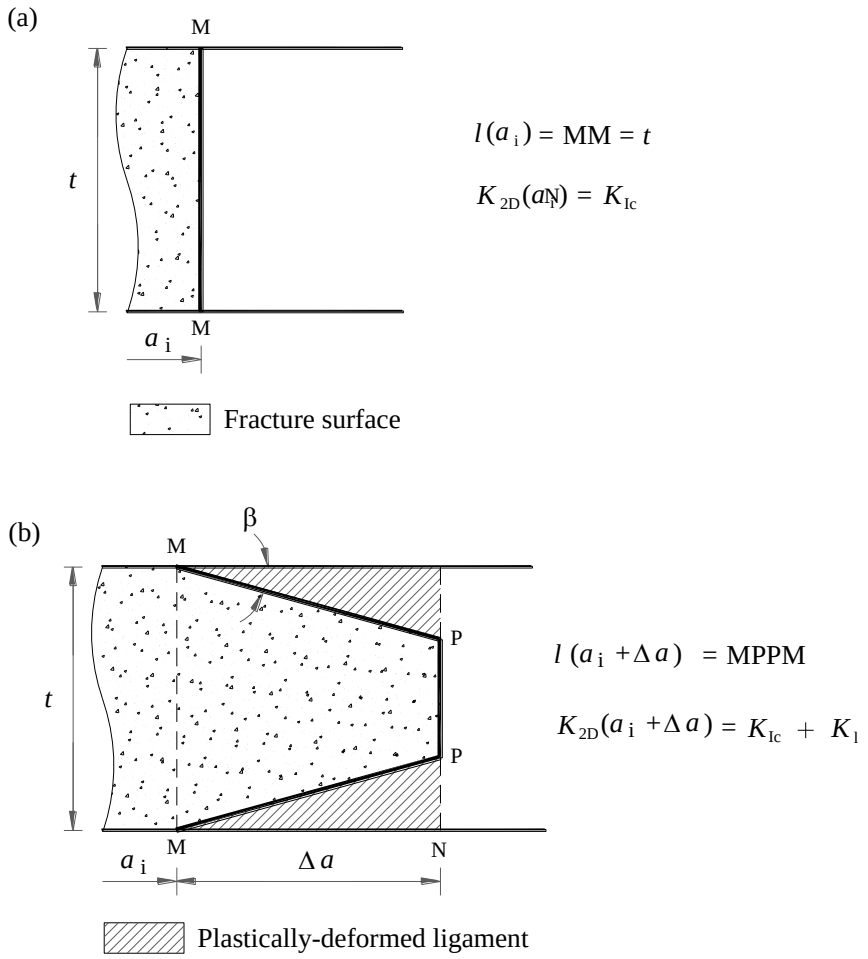

Figure 8. Schematic representation of the Schijve model: (a) at tearing onset and (b) at tearing arrest.

Like Forsyth (Forsyth, 1976, 1978; Bowen and Forsyth, 1981), Vlasveld and Schijve (1979, 1980) also believed that stable tearing will commence when the stress intensity factor reaches the fracture toughness K_{Ic}, and assumed a straight crack front at the start of tearing. Since tearing has been suggested to occur predominantly under plane strain conditions, where triaxial crack tip stress predominates (σ_x, σ_y and $\sigma_z \neq 0$) (Dixon, 1966), they argued that the stress intensity factor at the flat crack front (namely $a = a_i + \Delta a$) will equal K_{Ic}. In essence, their model implies that the stress intensity factor at arrest of tearing $K_{2D}(a_i + \Delta a)$ is not the stress intensity factor

calculated on the maximum crack length, but is lowered by an amount reflecting the effect of the restraining ligaments K_l.

Vlasveld and Schijve (1979, 1980) stressed that this model is very sensitive to Δa, which implies that a high level of measuring accuracy must be employed. They also acknowledged the legitimacy of using α as a constant for a particular aluminium alloy, and further noted that the α-value should be affected by the specimen thickness. Due to these constraints, Eq. (9) was validated by using substantially large tears, namely $\Delta a > 3$ mm, in 12.7 mm thick specimens and shown to give a good prediction result. Byrnes *et al*. (2000) also highlighted a practical complication in determining the α-value especially for skewed tearing. Another limitation of this model is that it does perform very well for tearing in a very thick or very thin specimen, as the conditions of plane strain and plane stress are expected to predominate, respectively. This notion is verified by Byrnes *et al*. (2000), who concluded that the model works very well, relatively poorly and not at all for predicting the theoretical K at tearing arrest in 7050 aluminium alloy specimen thickness of 12.0 mm, 6.0 mm and 24.0 mm, respectively. This indicates that the Schijve model is only suitable for intermediate thickness material.

2.7.3. Resistance curve approach

The resistance curve (or K_R curve) represents the toughness development in materials during a period of slow stable crack extension (ASTM E 561, 2009), which sometimes precedes unstable failure and can be used to characterise the ductile tearing resistance of crack extension under plane stress conditions (Brocks *et al*., 2010). This

steady fracture mechanism is often observed when loading a metal of relatively thin section containing a crack, in which the stressing state is either full or predominantly plane stress conditions. In this stress state, the crack often grows by ductile fracture and exhibits a tunnelling effect (the crack grows more at the centre of the specimen) in addition to a change in curvature of crack front contour as the crack progresses (Anderson, 2005).

The conceptual foundation of the K_R curve has been hypothesised by Krafft *et al*. (1961), and its physical meaning is confirmed by several studies. For instances, Knott (1973) presented experimental verification, Heyer and McCabe (1972) experimentally confirmed that the K_R curve is an intrinsic property of a material for a given thickness and Janssen *et al*. (2006) provided justification for K_R independence on initial crack length.

Several practical applications of this method have been proposed in the literature (Heyer, 1973; Vlieger, 1988). For example, Vlieger (1988) used the *R*-curve to predict the crack growth behaviour in the thin stiffened-skin of aircraft specimens. Since the region under plane stress (near the specimen edge) plays a major role in developing ligaments and controlling the extent of tearing (Vlasveld and Schijve, 1979, 1980), it is interesting to investigate the usefulness of the *R*-curve in estimating the Δa at a specific applied stress intensity factor $K_{2D}(a_i)$.

The rising K_R curve can be divided into two parts, as shown in Figure 9. The first part is a vertical segment A-B, which corresponds to no crack growth at low applied stress intensity factor K_G (represented by line K_{G1} in Figure 9). In reality, even if there is any crack growth, its amount is almost undetectable because the crack tip is

usually obscured by plastic deformation at the free surface. Observable stable crack extension (segment B-C) starts when the applied driving force K_G is greater than the K-value at which ductile tearing commences, denoted as K_i in Figure 9. For instance, at K_{G2}, the crack extends for Δa_e from its initial crack length and the crack growth during this condition is stable by the fact that the K_G curve remains below the K_R curve after they intersect. The state of stability is maintained until the K_G exceeds the critical K-value at K_c. The point of instability at K_c has two characteristics (Sanford, 2003): the crack driving force curve is higher than the resistance curve, ($K_G > K_R$); and the point between the K_G and K_R curves must also meet the tangency condition of $\partial K_G/\partial a > \partial K_R/\partial a$.

K_i in Figure 9 is analogous to the plane strain fracture toughness, K_{Ic} and can be regarded as a lower limit of the K_{Ic} (Schwalbe, 1977, 1979). Schwalbe (1979) found that K_i is independent of the main dimensions of the specimen (namely width, thickness and crack length) and that each material has a unique K_i-value. It is therefore sensible to assume that even in a relatively thin section, the onset of crack growth takes place inside the plane strain enclave, which can then be used to explain the constancy of the K_i value. In contrast, the K_c values are dependent on the section thickness. Further explanations of this term and K_{plat} can be sought from Jenssen *et al*. (2006) and Schwalbe (1979).

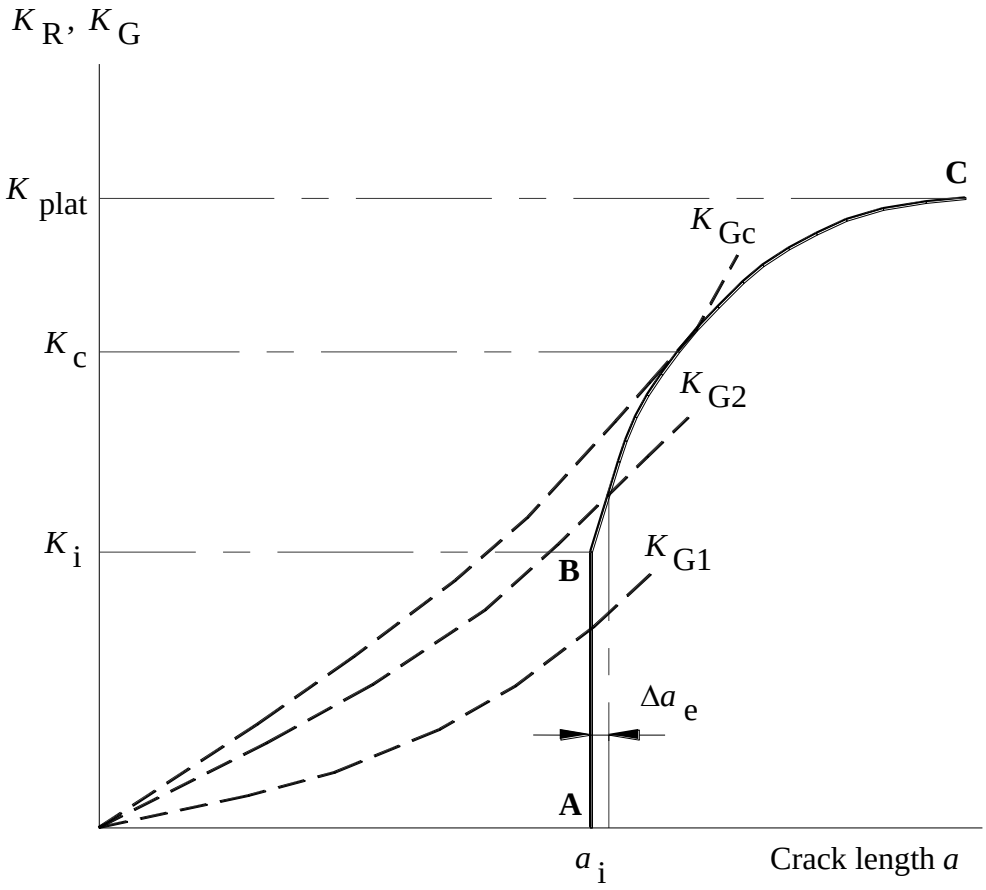

Figure 9. The resistance curve in terms of stress intensity factor or K_R curve and K_G. K_{plat} is the plateau level of the K_R curve (Janssen *et al*., 2006).

The resistance curve (*R*-curve) approach in analysing stable tearing has been proposed by Byrnes *et al*. (2000), who noted that this method could become an alternative predictive model to the Forsyth and Schijve models. It should also be recognised that the theoretical model by Bolotin (1999a) is fundamentally similar to the *R*-curve concept. This idea has been further investigated by Liu *et al*. (2005), who proposed that the stable tearing jump length Δa can be related to the static (ductile tearing) Δa_e by the following Eq. (11),

$$\Delta a_{\mathrm{e}} = \Delta a + r_{\mathrm{y}} \tag{11}$$

where r_{y} is the plane stress Irwin's correction factor determined by the following equation,

$$r_{\mathrm{y}} = \frac{1}{2\pi}\left(\frac{K_{2\mathrm{D}}(a_{\mathrm{e}})}{\frac{\sigma_{\mathrm{Y}} + \sigma_{\mathrm{U}}}{2}}\right)^2. \tag{12}$$

where $K_{2\mathrm{D}}(a_{\mathrm{e}})$ is the stress intensity factor at effective crack length a_{e}, σ_{Y} and σ_{U} are the yield and ultimate strengths of the material.

They concluded that the *R*-curve method gives good prediction of the *K*-value at the final unstable failure, but is unreliable in predicting the size of a stable tearing crack jump Δa, especially for thick specimens. Some of the drawbacks of this method are that it requires some regression analyses and multiple correction factors to estimate parameters such as *K* and Δa, whilst its application is limited to post-failure analysis. One of the proposed correction factors is to account for the effect of crack front curvature, which can be significant in stable tearing but is assumed to be non-existent in the static *R*-curve approach. Liu *et al*. (2005) proposed an equivalent area concept, which means that the Δa of stable tearing is actually longer than the static Δa_{e} of the *R*-curve for an equal fracture surface area. However, the study of Liu *et al*. (2005) did not actually develop the characteristic *R*-curve for a specific thickness of material, and no explanation was given on the specific criteria for the onset and arrest of tearing.

2.7.4. Troshchenko model (CA tearing in steels at very low temperature)

An empirical model has been developed by Troshchenko and co-workers (Troshchenko, 2003, 2009; Troshchenko and Pokrovskii, 1980, 1983a, 1983b, 2003a, 2003b; Troshchenko *et al*., 1978, 1079, 1980a, 1980b, 1982, 1985, 1987, 1988, 1992, 1994), for stable tearing jumps that occurred in various structural steels, such as 15Kh2MFA (Cr-Mo-V), 15Kh2NMFA (Ni-Cr-Mo-V), 15G2AFDps (Cr-Mn-V), which are often used in the boilers and pressure vessels of nuclear reactors and the compressor blades of marine gas turbines. The specimen thickness was varied from 7.5 to 150 mm, while the testing temperatures were in the ranges from 77 to 623 K. The Troshchenko model is based on the assumption that cyclic loading causes the material at the crack tip to weaken, and thus decreases its fracture toughness (Troshchenko and Pokrovskii, 2003b; Troshchenko *et al*., 1978). The typical crack growth curve at 183 K is shown in Figure 10, which clearly can be distinguished by the present of eight tearing jumps, where the final jump leads to final unstable fracture.

The experimental methods were laborious, and thereby extensive empirical results were reported. Therefore, only several noteworthy experimental findings are mentioned as follows:

(i) The tearing jump occurs at $K_{2D}(a_i) < K_{Ic}$, whereby both stress intensity factors were determined under similar conditions (Troshchenko, 2009). Troshchenko and Pokrovskii (1983a) noted that aluminium alloys can be categorised as cyclically stable materials, which implies that its $K_{2D}(a_i)$ is approximately equal to K_{Ic};

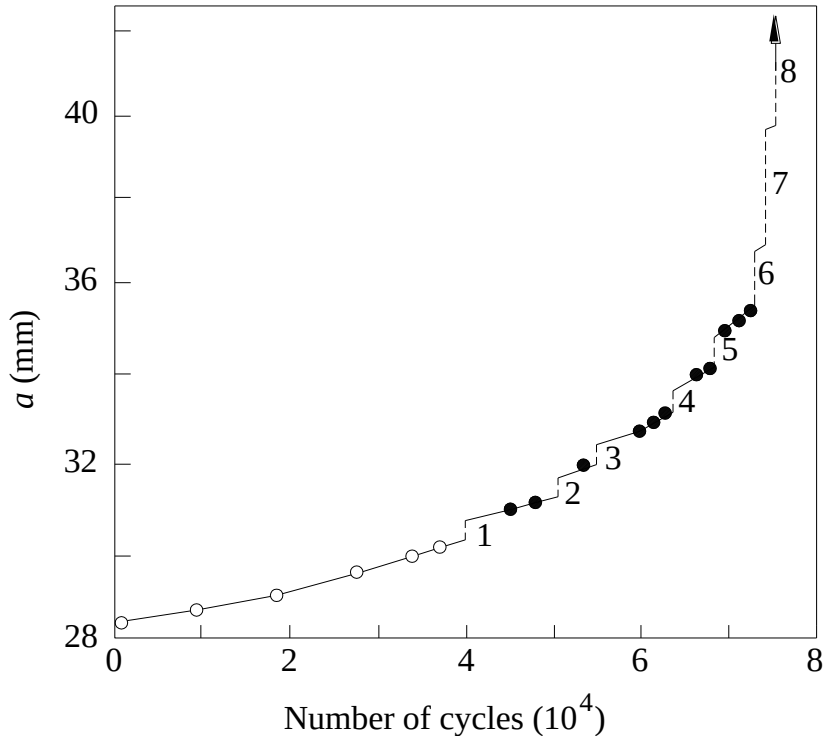

Figure 10. The fatigue crack growth curve for Cr-Mo-V steel at 183 K (Troshchenko *et al*., 1980a). The solid line represents slow fatigue cracking, the vertical dash line corresponds to tearing jumps and 1 to 8 indicates serial numbers of the tearing jumps. The empty and full circles represent the fatigue crack growth in Region II and III (as in Figure 3), respectively.

(ii) Stable tearing can take place even in the threshold region (region I as in Figure 3) of fatigue crack growth rate curve, which corresponds to a crack growth of just 1 mm in about 10^7 cycles (Troshchenko *et al*., 1985);

(iii) The tearing crack jump length Δa is usually larger than the theoretical plastic zone size at the start of tearing and the tearing arrest occurs in the undamaged material ahead of the crack tip. This implies that the extent of

each tear may be controlled by the size of the damaged zone (generated by the previous cycle) at the tip of the crack front (Troshchenko *et al*., 1982);

(iv) The tearing crack jump length Δa increases with an increase in crack length, which implies that an increment of tearing jump can be associated with an increase in the stress intensity factor (Troshchenko *et al*., 1980a);

(v) The occurrence of stable tearing in these particular steels is controlled by various factors: (i) the critical stress intensity factors at the onset of the first and the final tearing jumps, denoted as $K_{2D}(a_i)$ and $K_{2D}(a_f)$ respectively; (ii) the tearing crack jump length Δa; (iii) the interval number of load cycles prior to the tearing jump Δn; and (iv) the fatigue crack growth increment prior to the tearing jump Δc (Troshchenko *et al*., 1992);

(vi) The crack growth rate curve in between the two tearing jumps follows the stable crack growth rate curve (region II) prior to the first onset of a tearing jump, as illustrated in Figure 11 (Troshchenko *et al*., 1980a). Figure 11 also denotes that the crack growth rate in between tearing jumps can be described by the Paris equation, namely similar values of C and the exponent m can be used to describe the crack growth behaviour.

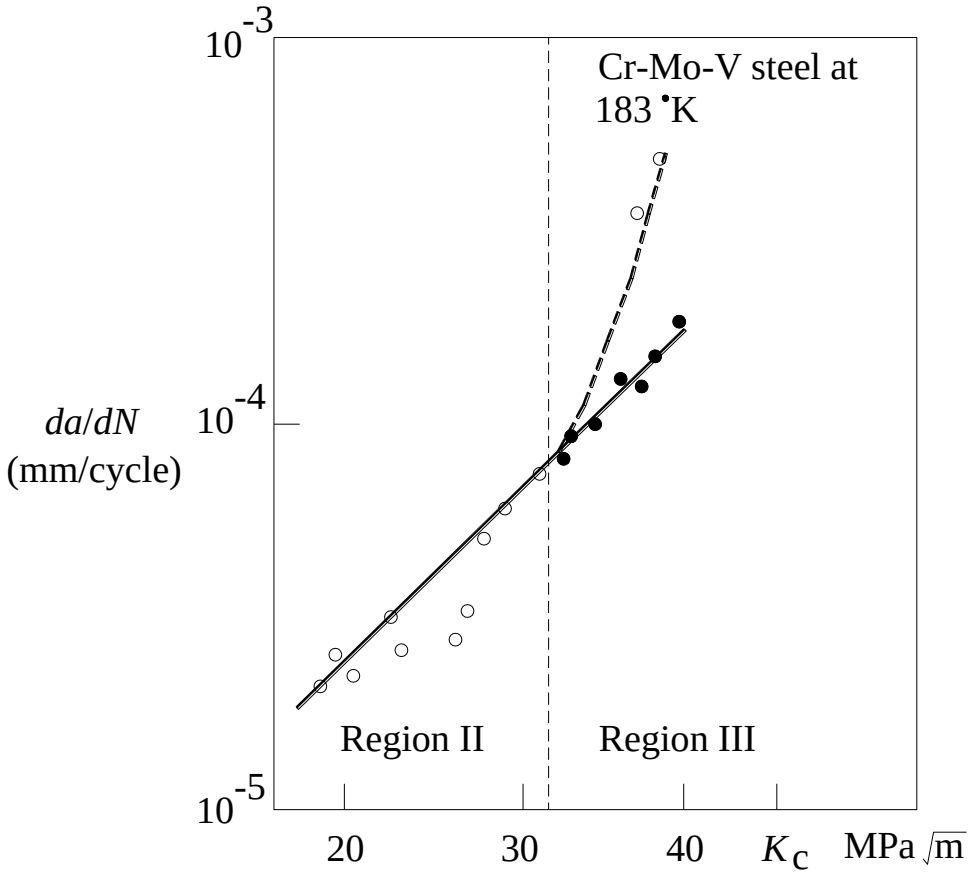

Figure 11. The fatigue crack growth rate curve for Cr-Mo-V steel at 183 °K (Troshchenko *et al*., 1980a). In region III, the empty circles represent the crack growth rate curve with jumps, while the full circles correspond to crack growth rate curve without jumps.

Troshchenko *et al*. (1982) proposed an empirical relationship between the cyclic stress intensity factor $K_{2D}(a_i)$ with the number of loading cycles interspersed in between two successive tearing jumps Δn as

$$\Delta n = \chi\left[(1-R)K_{2D}(a_i)\right]^e \tag{13}$$

where R is the load ratio, and χ and e are material's constants. It has been shown that Eq. (13) is independent of initial crack length a_i, thickness of the specimen t and the stress intensity factor at pre-cracking. This implies that as the serial number of tearing jump increases, the Δn decreases. A similar trend is also reported by Yasnii (1981) for other steels.

The increase in tearing jump length Δa has been associated with an increase in the plastic zone size (Troshchenko *et al*., 1978) and the nominal stress intensity factor $K_{2D}(a_i)$ (Yasnii, 1981), and thus Δa can be approximated by the following correlation (for cyclically softening steels) (Troshchenko and Pokrovskii, 1983a):

$$\Delta a = \frac{1}{3\pi}\left(\frac{K_{2D}(a_i)}{\sigma_p^c}\right)^2 \tag{14}$$

where $\sigma_p{}^c$ is the cyclic proportionality limit, determined experimentally from the stress-strain curves. Some scatter was observed, and the reason put forward was that tearing jumps at the beginning of stable tearing did not extend to the full thickness of the specimen (Troshchenko and Pokrovskii, 1983b). Other empirical relationships have been proposed in the literature (Kitsunai, 1986; Troshchenko *et al*., 1987, 1982; Yasnii *et al*., 1983), all of which are based on trends observed in test results. It should be understood that none of the formulae can claim a physical background, which implies that their engineering significance is limited to the type of material and loading conditions. It is also noteworthy that the empirical verification of this model shows

that the model allows prediction of fatigue-tearing growth up to the final unstable fracture.

2.7.5. Summary of literature review

The face of the fatigue fracture surface in a range of structural metals that were used in aircraft components, sometimes exhibits stable tearing bands, visible as dull crescent- or tongue-shaped regions in contrast to the "bright" background fatigue surface. Such tearing is commonly visible at the central cross-section of the component while the crack fronts that appear on the free surface are lagging behind. After a quick burst of crack jumping, the crack growth reverts back to being fatigue-driven, with the more usual slow fatigue crack growth pattern, which occurs mainly at the unfractured ligaments. The occurrence of stable tearing is wide-ranging, namely it occurs in many engineering materials and structures, being exposed to a range of loading conditions. It has also been established that stable tearing may occur during fatigue crack growth under either CA or VA fatigue cycles.

Stable tearing under CA and VA fatigue cycles usually occurs in region III and II, respectively, of the double log plot of fatigue crack growth rates da/dN versus the stress intensity factor range ΔK. The critical conditions for the onset of CA and VA tears are equivalent, but this critical condition ($K_{max} \geq K_{Ic}$) is achieved through two differing means, namely by having longer crack length in CA fatigue, while in VA fatigue the onset is mainly due to the overload. Stable tearing crack growth mainly complicates the fracture surface analysis during fatigue failure investigation and during crack growth reconstitution for providing physical validity of prediction models. The

development of crack growth prediction models usually neglects the occurrence of stable tearing, and hence a stable tearing crack growth model is not included in the existing fatigue crack growth prediction models. Moreover, in the absence of a valid stable tearing crack growth model for predicting the extent of crack jump, quantitative fractography demands extensive effort to devise ways to match up tears to the loads present in the load history.

This literature survey indicates that stable tearing mostly occurs in materials of intermediate thickness. Stable tearing crack growth in a very thick specimen is not quite stable, as a slight increase in K_{max} can cause the final unstable fracture. This implies that the crack growth life after the first onset of tearing in a relatively thick specimen is very short, and as a consequence, the engineering application of a stable tearing prediction model in this range of thicknesses is very limited. Experimental evidence in several studies has suggested that the occurrence of stable tearing in material of thin and intermediate thicknesses under CA conditions can be associated with the transition of a fatigue crack from a tensile mode (flat fracture surface) to the shear mode (slant fracture surface), in which the crack front becomes more curved during the process.

The arrest of tearing have been associated with other mechanisms that occur in the surrounding material, such as retardation by residual compressive stress caused by the overload at the mid-thickness region, the restraining effect of uncracked ligaments at the edges and an increase in the length of the crack front (especially in a CA fatigue condition). It should also be noted that, since the tearing under VA conditions occurs as a result of an overload, other fracture retardation mechanisms are also possible such

as crack deflection, strain hardening, plastic blunting/re-sharpening, depending on the types of material, except for plasticity-induced crack closure.

A number of theoretical analyses for stable tearing have been put forward. A notable weakness of these theoretical analyses is that they are not provided with sufficient experimental validation. The Sih (1981) and Bolotin (1999a) proposals would have been more interesting if the authors had recommended any experimental technique for engineering practical purposes. The foundation of Ivanova's similarity theory has been devastatingly critiqued, despite the fact that her approach is supported by some experimental results. The proposed experimental technique is however complicated and time-consuming, whilst its empirical formulae involve a range of parameters. Similar criticisms can also be deduced to the experimental approach and empirical formulae that are proposed by Margolin and Shvetsova (1991) for their critical brittle failure stress approach. These theoretical analyses, however, have highlighted several aspects of stable tearing prediction and these parameters that may be useful in order to develop a more generic analytical stable tearing model.

Several empirical models for analysing stable tearing crack growth have been proposed. The Troshchenko model is the most comprehensive but its application is limited to steels at very low temperatures, in which the onset of tearing jump occurs at $K_{2D}(a_i) < K_{Ic}$ (both K values are determined under similar conditions). In aluminium alloys, these empirical models establish that the first onset of stable tearing under either CA or VA fatigue loading occurs when the K_{max} of the ΔK cycle equals the material's plane strain fracture toughness K_{Ic}. It should be noted that these aluminium alloys are mainly in the intermediate range of thickness. For a very thick aluminium

alloy, the K_{max} must be slightly lower than K_{Ic}, in order to produce a thin strip of quasi-stable tearing.

A comment should be made on the validity of using the stress intensity factor K to characterise the condition for the onset of tearing. Experimental evidence has shown that the crack front shape at the initiation of the first stable tearing is usually fairly straight. As such the use of K to describe the severity of stresses at the vicinity of the crack front is valid, whereby the straightness of the crack front can be assessed according to conditions given in ASTM E 399 (2009). The cracking condition at stable tearing arrest, however, is more complicated due to significant curvature of the crack front; indeed the curvature is clearly one of the possible contributors to the arrest of the tearing.

Noting this, both the Schijve (Vlasveld and Schijve, 1979, 1980) and Forsyth (Forsyth, 1976, 1978; Bowen and Forsyth, 1981) models proposed that the effective K must be reduced, and the extent of K-reduction depends on several characteristic dimensions, which need to be measured from the fracture surface. Therefore, these models provide support as post-failure analysis tools, especially in identifying the loading cycle that caused the stable tearing (Byrnes *et al*., 2000). However, these existing models do not make it possible to predict the stable tearing jump length in terms of the material's fracture properties and the applied loads.

Chapter 3. Experimental Testing

3.1. Material

3.2. Specimen design

3.3. General experimental procedure

3.3.1. CA fatigue test

3.3.2. VA fatigue test

3.3.3. K_R test

3.4. Fracture surface examination and measurement

3.5. Determination of stress intensity factor K

3.6. Definition of areal and width ratios

This chapter describes used experimental methods to study the parameters controlling the onset of stable tearing, and factors that affect the size of tearing in aircraft 7075 aluminium alloy compact tension (CT) specimens. In view of the uncertainties about the parameters for CA and VA tearing, comparative tests are conducted. Multiple stable tearing bands are produced under CA and VA fatigue conditions, whereby the VA tearing is achieved by inserting overloads into a background of CA fatigue. The resistance curve for this particular material and thickness is determined according to the standard test method, by using specimen of identical design and dimension to the fatigue tests.

3.1. Material

Aluminium alloys are widely used in aircraft structures due to their strength (Dorward and Pritchett, 1988; Immarigeon *et al*., 1995; Starke Jr. and Staley, 1996; Heinz *et al*., 2000) and have been the primary material for aero-structure components since the 1930s (Froes, 1989; Hoff, 1985; Jakab, 1999; Paul and Pratt, 2004; Williams and Starke Jr., 2003). The aluminium alloy 7075-T651 was used in this study to represent the 7XXX series, which is commonly used in aircraft structures such as stringers and spars (Starke Jr. and Staley, 1996; Williams and Starke Jr., 2003). This alloy is known for its strength, but very poor resistance to corrosion (Dorward and Pritchett, 1988; Starke Jr. and Staley, 1996). Typical static mechanical properties in the rolling direction (at room temperature) and the alloy's chemical composition (Dowling, 2007) are shown in Table 3. It should be noted that although the thickness of the material used in this study can be categorised as being intermediate, the value

K_{Ic} in Table 3 is still valid, as supported by the empirical results of Weitzmann and Finnie (1972).

Table 3. Typical mechanical properties and chemical composition of 7075-T651 aluminium alloy (Dowling, 2007).

σ_Y (MPa)	σ_U (MPa)	ε_f (%)	K_{Ic} (MPa$\sqrt{m}$)
505	570	11	29

Principal alloying element	Zn	Cu	Cr	Mg
Typical % by weight	5.6	1.6	0.23	2.5

3.2. Specimen design

The CT configuration, shown in Figure 12, was adopted for three main reasons: (i) economical of materials (Kaufman, 1970; Anderson, 2005), (ii) standardised configuration (and thus a *K*-solution is readily available) (Schijve, 2009) and (iii) proven ability to replicate CA and VA tearing (Bathias and Vancon, 1978; Byrnes *et al.*, 2000). Schijve (2009) stated two other advantages of the CT specimen: it is comparatively small in size and only a relatively low load is required to generate a high *K*-value. The latter advantage is very important especially in replicating CA tearing, which has been shown to occur in the high K_{max} region (region III) in fatigue crack growth rates plot. Schijve (1998) noted that a drawback of this configuration could be related to the effect of bending moment during an opening of the crack, which generally does not occur in real structures.

The specimens were designed according to ASTM E 651 (2009), so that identical specimen of identical dimensions could be used for both tearing replication and *R*-curve development. The specimens had an average width *W* of 40.00 ± 0.05 mm and thickness *t* of 6.50 ± 0.01 mm, as shown in Figure 12. The width *W* was measured from the plane of the centre of the loading hole to the specimen edge, and the average thickness of the specimens was measured at three spots in the plane of the notch between the notch tip and the specimen edge.

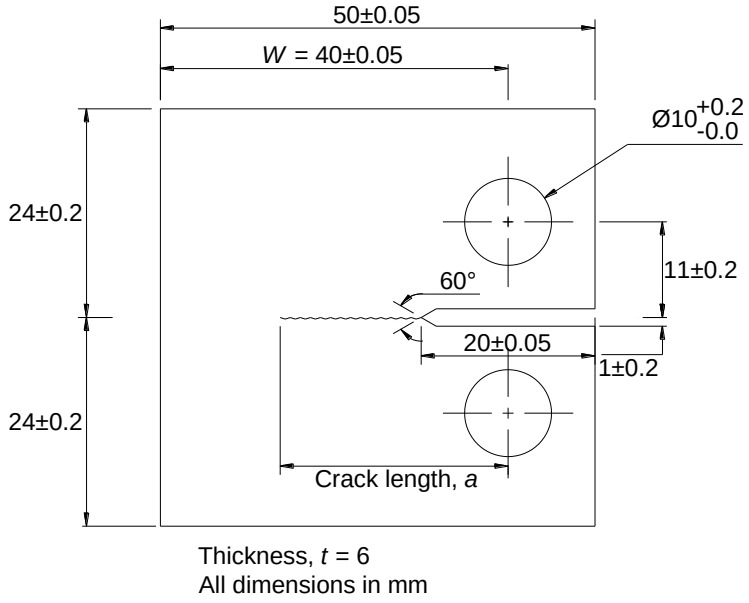

Figure 12. Engineering drawing of the used compact tension (CT) specimen in the current work. It should be noted that the crack length *a* and width of the specimen *W* are measured from the centerline of the loading holes.

The crack plane orientation for all specimen was longitudinal-transverse (L-T), namely the direction of the applied load was parallel to the rolling direction. Chevron

notch is usually used to cause fatigue crack to initiate at the middle thickness of the specimen, in order to achieve acceptable degree of straightness of fatigue crack front at the end of fatigue pre-cracking procedure. However, a straight through-crack starter notch is used for all specimens because it is simpler and can produce fatigue crack that conforms to the necessary requirement (May, 1970).

3.3. General experimental procedure

All tests were carried out at an ambient temperature of 22 ± 1 ºC, on a 100 kN capacity servo-hydraulic fatigue machine (MTS 810 Material Test System). The maximum capacity of the load cell was adjusted to 20 kN, in order to increase the accuracy of load application. The fatigue machine was controlled by the program TestStar^{TM} IIs (Model 793.00, Version 3.5c) developed by MTS Pty. Limited. Fatigue pre-cracking was carried out because most of the notch machining techniques (such as wire-cut, which was used in this work) would not be able to simulate the recommended sharpness of the root radius (0.08 mm) (ASTM E 651, 2009). Fatigue pre-cracking was done with a series of very low CA fatigue cycles (0.2 – 2.0 kN) up to a certain crack length a_i.

At the start of each test (after fatigue pre-cracking was done), the axial load was steadily increased at a rate of 0.05 kN per second, from zero to the minimum load in the fatigue loading cycle P_{min}. From thereon, a sinusoidal fatigue loading was applied which would oscillate between the P_{min} and the maximum load in the fatigue cycle P_{max}. The crack length was measured by surface observations (on one side of the specimen) using a travelling-stage microscope with a maximum magnifying power of 30 times. This crack measurement technique, however, has the drawback, of it being

difficult to measure the crack length at the very beginning of crack growth because the crack tip is often obscured by the plastic deformation at the free surface (ASTM E 647, 2009). This problem was reduced by polishing an appropriate area on the specimen surface, in which the crack was expected to grow and by using indirect lighting from a desk lamp.

3.3.1. CA fatigue test

Testing with CA loading was conducted to generate stable tearing under CA fatigue conditions in order to investigate its characteristics and determine the main parameters that control the onset and arrest of tearing. A total of six CT specimens (denoted as CA1 to CA6) were tested. Table 4 shows the applied cyclic loads. The CA fatigue cycle was defined as having constant P_{min} and P_{max}, constant ΔP and hence increasing ΔK, as shown in Figure 13a.

Table 4. Details of specimens loading for CA fatigue tests.

Specimen	CA1	CA2	CA3	CA4	CA5	CA6
P_{min} (kN)	0.2	0.3	0.4	0.5	1.2	0.4
P_{max} (kN)	2.0	3.0	4.0	5.0	4.0	4.0
Cycles/s	5	10	10	10	10	5

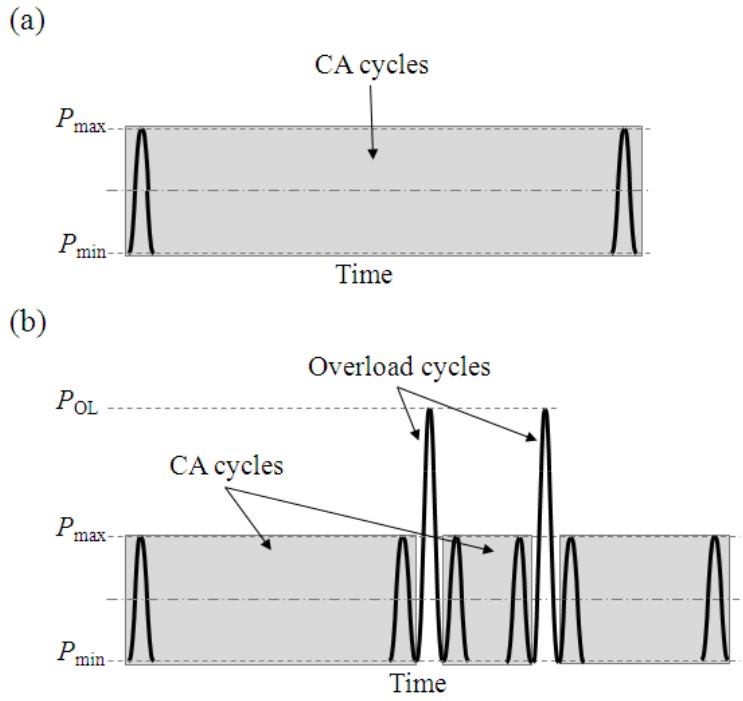

Figure 13. The sinusoidal fatigue cycles: (a) constant amplitude (CA) and (b) variable amplitude (VA). Shaded regions indicate constant amplitude.

3.3.2. VA fatigue test

Testing with VA loading was conducted to generate stable tearing under VA fatigue in order to investigate its characteristics and determine the main parameters that control the onset and arrest of tearing. A total of 32 CT specimens (designated as VA1 to VA32) were used for this test. The specimens were loaded with CA fatigue up to an initial crack length a_i as measured on the surface of the specimen. One or more high loads (overloads) P_{OL} of various levels were applied. The specimens were then subjected to CA fatigue to failure, using the same level of ΔP as was used prior to the application of overload. The VA fatigue condition is schematically illustrated in Figure 13b and details of specimen loading are listed in Table 5 to 7.

Table 5. Details of specimens loading for VA fatigue tests (background cycle of ΔP = 1.8 kN, R = 0.1, cycles/s = 5).

Specimen	a_i (mm)	P_{OL} (kN)	Specimen	a_i (mm)	P_{OL} (kN)
VA1	20.4	3.00	VA10	20.0	4.54
VA2	20.4	3.50	VA11	24.9	3.00
VA3	20.3	4.00	VA12	20.5	4.50
VA4	18.9	4.00	VA13	20.1	4.68
VA5	20.4	5.00	VA14	20.7	4.50
VA6	20.4	3.75	VA15	20.3	4.75
VA7	24.6	2.71	VA16	20.6	4.65
VA8	20.4	4.00	VA17	22.5	4.00
VA9	22.6	3.50	VA18	20.5	4.99

Table 6. Details of specimen loading for VA fatigue tests (background cycle of ΔP = 2.25 kN, R = 0.1, cycles/s = 5).

Specimen	a_i (mm)	P_{OL} (kN)	Specimen	a_i (mm)	P_{OL} (kN)
VA19	14.0	6.50	VA25	20.6	4.79
VA20	20.3	4.25	VA26	20.4	4.90
VA21	20.3	4.36	VA27	20.5	4.86
VA22	20.4	4.51	VA28	20.3	4.95

Specimen	a_i (mm)	P_{OL} (kN)	Specimen	a_i (mm)	P_{OL} (kN)
VA23	20.3	4.65	VA29	20.4	5.00
VA24	20.0	4.93			

Table 7. Details of specimen loading for VA fatigue tests (background cycle of increasing ΔP, R = 0.1, cycles/s = 5).

Specimen	VA30	VA31	VA32
P_{min} (kN)	0.3	0.35	0.4
P_{max} (kN)	3.0	3.5	4.0
P_{OL} (kN)	4.99	4.99	5.01

The application P_{OL} in some specimens was done at a random initial crack length a_i, in order to investigate the minimum K-value that was required to produce a substantial macroscopic tearing jump. This critical K-value was then compared to the results from the CA tests. Some specimens were specifically loaded with CA fatigue up to an a_i of about 20 mm, which was followed by an application of overloads of various levels. The load ratio R for all VA tests was set at 0.1. It should be noted that in the VA test, some specimens failed during an application of P_{OL}. For example, specimens VA3, VA7 and VA10 failed at overloads, while specimens VA4 and VA5 failed during the finishing phase of CA fatigue.

The sequence effect of prior fatigue loading in the formation of stable tearing was minimised by ensuring the CA background fatigue was sufficiently low. This was

achieved by maintaining the ΔK at the end of the first block of CA background fatigue within the range of 7 MPa√m to 10 MPa√m and the terminal value of K_{max} for all specimens in between 27% to 37% of the estimated K_{Ic}, in compliance with the requirements of ASTM E 399 (2009).

It should also be noted that Chanani and Mays (1977) found that the effect of crack closure for this particular aluminium alloy and thickness was very minimal and therefore could be assumed to be negligible, even after the application of an overload. An interesting experiment has been conducted by Nicoletto (1989) to study the plastic deformation at the crack tip in 5 mm thickness, 7075-T6 aluminium alloy using moire interferometry. This method captures the fringe patterns on the side of specimen, which deform during loading. He concluded that the plasticity-induced crack closure only had a minor effect on crack growth retardation. These results are not surprising because Suresh (1983) concluded that the plasticity-induced crack closure is not a primary mechanism for retardation in a single overload VA sequence, and supported this assertion with empirical evidence from various materials (Lindley and Richards, 1974; Mills and Hertzberg, 1975; Brown and Weertman, 1978).

3.3.3. K_R curve test

Testing was conducted to develop the stress intensity factor resistance curve or K_R curve. This test was carried out according to ASTM E 561 (2009), which stipulated procedures for determining the resistance to fracture for metallic materials that exhibit ductile crack extension. The main difference between this standard and that for determining fracture toughness (ASTM E 399, 2009) is that it does not provide a minimum limit to specimen thickness (rather the thickness of the specimen can be the

actual thickness used in service), although its application is still limited to cases where the plastic zone size is negligible in comparison to the in-plane dimensions of the specimen.

A total of four CT specimens were used to develop the K_R curve. These specimens were fatigue pre-cracked up to the initial crack length a_i of 11.6 mm, 14.7 mm, 15.8 mm and 20.1 mm, respectively. The static loading of the specimen was done in displacement control, which had the advantage of allowing the determination of the K_R curve entirely up to the K_{plat}. The crack size measurement was done by direct measurement of crack size and carried out using travelling binocular microscope. The practice of dripping a droplet of recorder ink to indicate the progression marking of the crack tip had been superseded since it was found that the aqueous stain could adversely affect the fracture response of some metals (Hertzberg, 1996). The crack length a_p was measured periodically (a change in crack length of about 1 to 2 mm) for evaluation of *K*-values. Each measurement of crack length a_p was carried out after the crack had stabilised.

3.4. Fracture surface examination and measurement

The literature review in Chapter 2 indicated that there are various macroscopic parameters that may affect the occurrence of stable tearing. In aluminium alloys, it was experimentally established that the main controlling parameters are the crack front line length l (Forsyth and Ryder, 1961; Forsyth, 1976, 1978, 1983; Bowen and Forsyth, 1977, 1978, 1981; Forsyth and Bowen, 1981) and the unfractured ligament (Vlasveld and Schijve, 1979, 1980). The theoretical analysis of stable tearing based on

the energy methods (Sih, 1981; Ivanova, 1982b) suggested that the area of tearing could also be a controlling parameter.

The macroscopic characteristics of the tearing were viewed and measured at high magnification using a digital microscope (Brand: CAM DIG Microscope USB) with a magnification between 20 to 400 times. Typical macrographs of fracture surfaces exhibiting multiple bands of CA and VA tearing are shown in Figure 14, which displays the fracture surfaces of one side of the specimen and the crack growth direction is from left to right. The stable tearing area was also analysed using a scanning electron microscope (SEM).

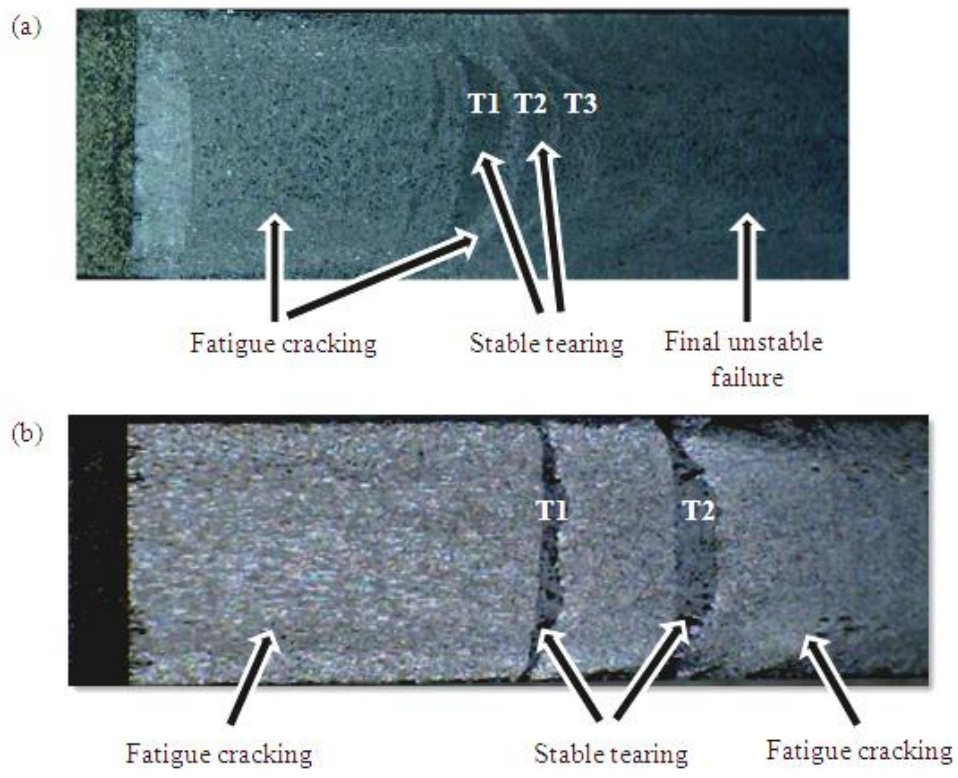

Figure 14. Examples of macrographs of fracture surfaces as captured by a digital microscope for: (a) CA tearing (specimen CA4), and (b) VA tearing (specimen VA20).

The analysis of the stable tearing shape was performed by importing key dimensions from macrographs of the fracture surfaces into AutoCAD, a computer-aided design program. The sequence of processes is shown in Figure 15. This was particularly useful because in some cases, especially under CA load cycles, there was little contrast between the macroscopic appearances of the tearing and fatigue areas. A similar technique was used to analyse the stable tearing area of various fractographs of various aluminium alloys from the literature.

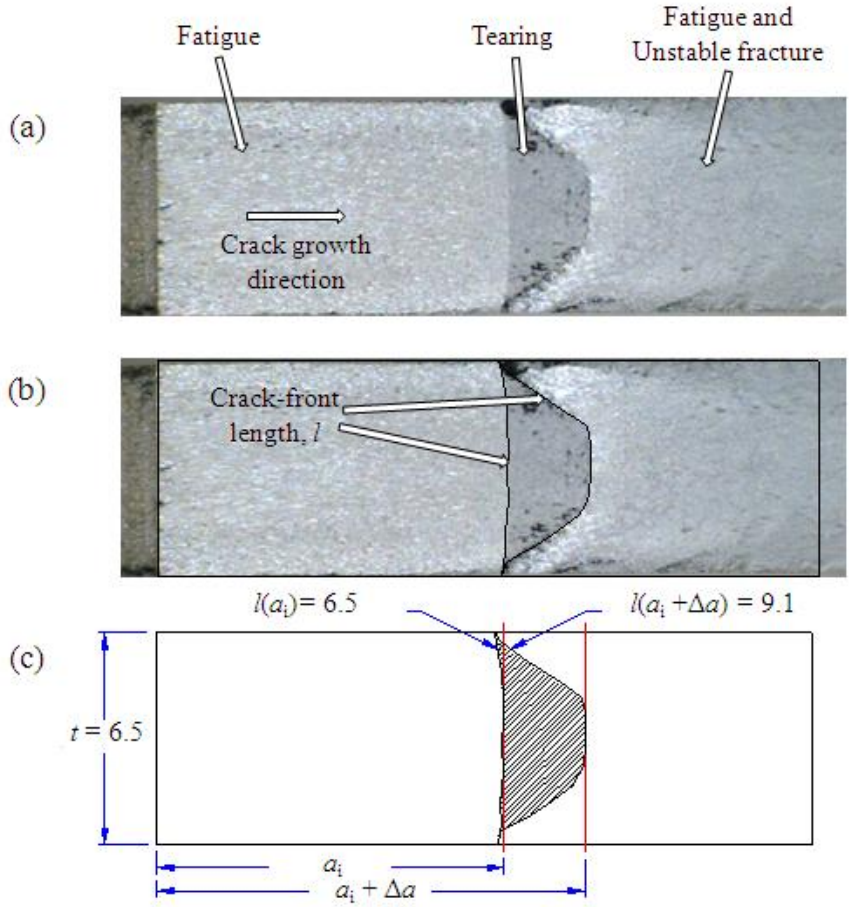

Figure 15. Examination and measurement of tearing parameters (specimen VA25). (a) Macrograph of fracture surface (one side only); (b) sketch of tearing surfaces; and (c) determination of crack length.

3.5. Determination of stress intensity factor *K*

The stress intensity factor at the initiation of stable tearing was determined by using the theoretical closed-form *K* solution for the CT specimen (Strawley, 1976) as given by Eq. (15):

$$K_{2D}(a) = \left(\frac{P}{t\sqrt{W}}\right) \times \frac{2+\frac{a}{W}}{\left(1-\frac{a}{W}\right)^{\frac{3}{2}}} \times f\left(\frac{a}{W}\right) \tag{15}$$

where P = applied load, t = specimen thickness, a = crack length, W = specimen width and $f\left(\frac{a}{W}\right)$ is the non-dimensional function defined in Eq. (16).

$$f\left(\frac{a}{W}\right) = 0.886 + 4.64\left(\frac{a}{W}\right) - 13.32\left(\frac{a}{W}\right)^2 + 14.72\left(\frac{a}{W}\right)^3 - 5.6\left(\frac{a}{W}\right)^4 \tag{16}$$

Eq. (15) was derived based on a one-dimensional analysis of the crack front, which implicitly assumes that the crack front is straight, and is valid for $\frac{a}{W} \geq 0.35$. It should also be noted that all data in this study satisfied this condition.

All of the crack fronts at the initiation of stable tearing, for example as shown in Figure 14, were in compliance with the requirements outlined by ASTM E 399 (2009), and the *K*-value at initiation of each stable tear was determined by substituting the initial crack length a_i and overload P_{OL} into Eq. (15). The construction of the K_R curve involved the determination of two stress intensity factors. The $K_{2D}(a_i)$ was determined

by substituting the crack length a_i into Eq. (15), and then using this to determine the plastic zone size $r_{y,R}$, given in Eq. (17).

$$r_{y,R} = \frac{1}{2\pi}\left(\frac{K_{2D}(a)}{\sigma_Y}\right)^2 \tag{17}$$

In effect, Eq. (17) is the plastic zone correction factor, proposed by Irwin (1960), to account the effect of plastic strains on the crack tip. The effective crack length a_e was determined by adding the individual a_p to its respective $r_{y,R}$, to account for the significance of plastic deformation under plane stress conditions. The K_R was then calculated by substituting a_e into Eq. (15), namely

$$K_R = K_{2D}(a_e) \tag{18}$$

The stress intensity factor K_R was then plotted against the crack length a_p and the change in effective crack length Δa_e, defined as a_e - a_o. a_o is the crack length at the end of fatigue pre-cracking procedure.

The thickness of the specimen was less than that required for a fully-developed plane strain condition, but it has been established that plane strain conditions can still exist at the mid-thickness region even in a very thin specimen (Janssen *et al*., 2006, Steigerwald and Hanna, 1962, Schwalbe, 1979, Banerjee, 1981, Schwalbe and Setz, 1981). Due to extensive curvature of the crack front at stable tearing arrest, the *K*-values were estimated using the finite element (FE) method.

3.6. Definition of areal and width ratios

Significant curvature of the crack fronts complicated the measurement of the tearing area. To simplify this task, the stable tearing crack jump length Δa was defined to represent the difference between the measured crack length (at the specimen centre) at stable tearing arrest and onset, as shown in Figure 16a. Macroscopic examination of the stable tearing which was produced in this study under VA fatigue revealed that the tearing often featured an apparently straight crack front at both the tearing onset and the central portion of tearing arrest. To simplify the analysis of stable tearing, a generalised model was proposed to represent the stable tearing crack front as a trapezoidal shape, as illustrated in Figure 16a.

The trapezoidal front at the tearing arrest was defined such that the area enclosed by the trapezoidal front and the straight line $x = a_i$ was equal to the area enclosed by the actual crack front and the straight line $x = a_i$, as indicated in Figure 16a. This equal area condition could be expressed mathematically as

$$A_c \equiv 2 \int_{a_i}^{a_i+\Delta a} Z(x)\,\mathrm{d}x = \frac{(b+t)}{2}\Delta a \qquad (19)$$

where $z = Z(x)$ denoted the actual stable tearing crack front and A_c was defined as in Figure 16b. The dotted straight line at the initiation of tearing connects the crack length at both surfaces of the specimen, while the dotted straight line at tearing arrest overlaps the most advanced tip of the crack front. The dotted straight line at tearing arrest is always perpendicular to the surface of the specimen, but this is not necessarily the case for the dotted straight line at tearing onset. The areal ratio was defined as

$$\text{Areal ratio} = \frac{A_c}{A_c + A_l} \tag{20}$$

A_l was defined as the ligament areas as shown in Figure 16b. Eq. (20) furnished the required relationship for determining the crack front width *b*, provided that the actual crack front was known. If the area of tearing can be represented as a trapezium (to be discussed later) as illustrated in Figure 16a, and the total area (A_c + A_l) in the denominator can be approximated as a rectangle of area $t \times \Delta a$,

$$\frac{A_c}{A_c + A_l} = \frac{\frac{b+t}{2}\Delta a}{t \times \Delta a} \tag{21}$$

$$\frac{b}{t} = \frac{2A_c}{A_c + A_l} - 1 \tag{22}$$

Eq. (22) defines the width ratio of stable tearing. The areal ratio was determined by measuring the tearing fracture surface, and then used to determine the width ratio.

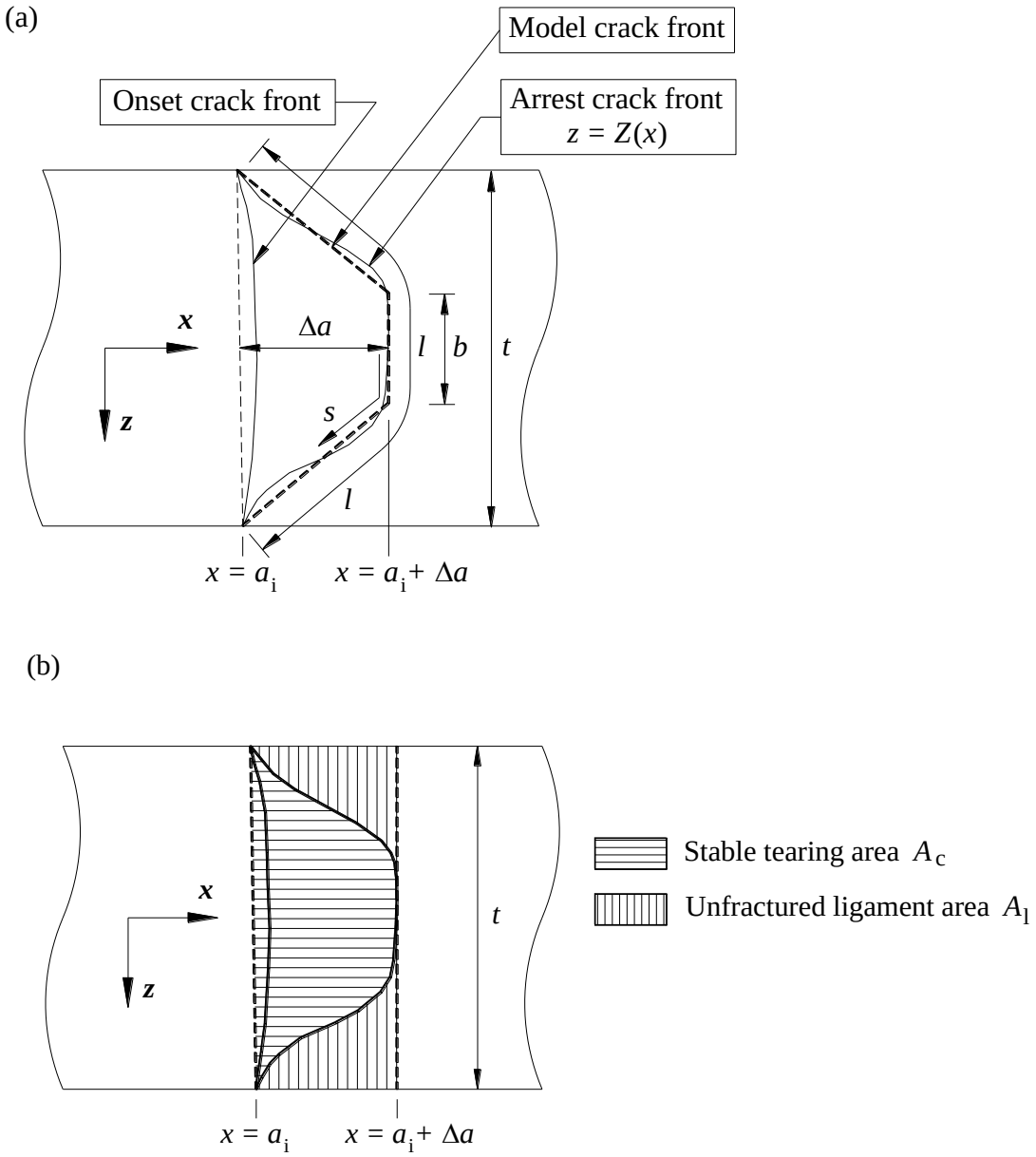

Figure 16. Simplification of stable tearing shape: (a) The definitions and geometric properties of stable tearing areas; and (b) definition of areas.

Chapter 4. Results of Experimental Testing

4.1. Various tearing parameters measured from this study

4.2. Resistance curve plot

4.3. Theoretical validation of the small-scale yielding conditions

The results of the experimental testing are presented in this chapter. A total of 56 tears are produced from this study and various parameters of these tears are quantified.

4.1. Various tearing parameters measured from this study

Tables 8 to 11 show the various measured parameters for each tearing produced under conditions specified in Tables 4 to 7, respectively. The tear bands on the fracture surface of each specimen were numbered according to the sequence of occurrence; thus an individual tear might be $CA1^1$, where CA1 was the specimen and superscript 1 was the first tear band on that specimen. The final tear, which continued to final unstable fracture, was marked as superscript F, for example $CA1^F$ for specimen CA1. Some of the specimens from VA tests failed at the application of P_{OL}, such as VA13 and VA16, and were also listed for reference purposes. It should be noted that the $K_{2D}(a_i)$ at the moment of failure ranged from 30 to 37 MPa$\sqrt{m}$, for VA7 and VA24, respectively. There were 14 CA tears and 42 VA tears generated in this study. Figure 17 shows examples of fatigue fracture surfaces of specimens which were loaded with single P_{OL} at a_i of about 20 mm. The significance of this observation is discussed in Chapter 5.

Table 8. Details of measured parameters for CA tests.

Tear no.	Δa (mm)	l (mm)		$K_{2D}(a_i)$	$\frac{A_c}{A_c + A_l}$	$\frac{b}{t}$
		$l(a_i)$	$l(a_i + \Delta a)$	(MPa√m)		
CA1[1]	0.6	7.3	7.8	35.4	0.66	0.32
CA1[2]	0.8	7.7	8.6	39.9	0.62	0.24
CA1[F]	-	8.6	-	51.5	-	-
CA2[1]	0.2	1.2	1.3	36.5	-	-
CA2[2]	0.3	6.8	7.1	38.1	-	-
CA2[3]	0.2	7.3	7.6	40.5	0.60	0.20
CA2[4]	0.7	7.5	8.4	43.1	0.63	0.26
CA2[5]	1.0	8.5	9.2	50.7	0.59	0.18
CA2[F]	-	9.2	-	60.6	-	-
CA3[1]	0.8	7.0	7.9	35.9	-	-
CA3[2]	0.7	8.3	9.2	40.6	0.64	0.28
CA3[F]	-	8.9	-	44.6	-	-
CA4[1]	0.6	6.9	7.5	36.4	-	-
CA4[2]	0.6	7.0	7.7	39.5	-	-
CA4[3]	0.9	8.7	9.6	43.3	0.64	0.28
CA4[F]	-	9.4	-	50.1	-	-
CA5[1]	0.8	7.5	8.2	34.7	0.61	0.22
CA5[2]	0.4	8.1	8.6	37.9	0.65	0.30
CA5[3]	2.0	8.1	9.8	41.9	0.61	0.22
CA5[F]	-	9.2	-	52.0	-	-
CA6[1]	0.3	7.6	8.1	35.9	0.68	0.36
CA6[2]	0.4	7.9	8.2	37.9	0.66	0.32
CA6[3]	0.6	8.2	9.0	40.6	0.64	0.28
CA6[4]	1.3	8.8	10.0	43.9	0.66	0.32
CA6[F]	-	10.0	-	53.3	-	-

Table 9. Details of measured parameters for VA tests (background cycle of ΔP = 1.8 kN, R = 0.1, cycles/s = 5).

Tear no.	Δa (mm)	l (mm)		$K_{2D}(a_i)$	$\frac{A_c}{A_c + A_l}$	$\frac{b}{t}$
		l (a_i)	l ($a_i + \Delta a$)	(MPa$\sqrt{m}$)		
VA1[1]	0	6.8	6.8	22.9	-	-
VA1[2]	0	6.8	6.8	24.4	-	-
VA1[3]	0	6.8	6.8	26.5	-	-
VA1[4]	0	6.7	6.7	27.0	-	-
VA1[5]	0.2	6.7	6.9	29.0	0.59	0.18
VA1[6]	1.3	6.8	8.0	33.9	0.65	0.30
VA1[7]	3.0	6.9	10.0	44.0	0.64	0.28
VA1[F]	-	9.1	-	68.0	-	-
VA2[1]	0	6.8	6.8	26.7	-	-
VA2[2]	0.1	7.0	7.0	29.1	0.62	0. 24
VA2[3]	0.3	7.0	7.3	31.8	0.62	0.24
VA2[4]	0.2	7.2	7.5	34.4	0.61	0.22
VA2[5]	0.9	7.5	8.5	38.2	0.65	0.30
VA2[6]	1.7	8.0	10.2	43.5	0.64	0.28
VA2[F]	-	9.0	-	53.8	-	-
VA3[1]	0.4	6.8	7.0	30.3	0.65	0.30
VA3[2]	1.8	6.6	8.4	33.1	0.70	0.40
VA3[3]	2.0	7.2	9.7	39.2	0.67	0.34
VA3[F]	-	9.6	-	50.8	-	-
VA4[1]	0.1	4.7	4.8	27.4	-	-
VA4[2]	0.2	6.6	6.7	29.7	-	-
VA4[3]	0.2	7.3	7.4	31.1	-	-
VA4[4]	1.3	6.8	8.0	33.8	0.63	0.26
VA4[5]	1.5	7.6	9.0	39.4	0.60	0.20
VA4[6]	0.6	7.7	8.3	37.6	0.64	0.28

Tear no.	Δa (mm)	l (mm)		$K_{2D}(a_i)$	$\frac{A_c}{A_c + A_l}$	$\frac{b}{t}$
		$l\,(a_i)$	$l\,(a_i + \Delta a)$	(MPa√m)		
VA4[7]	0.4	8.2	8.5	41.6		0.28
VA4[F]	-	8.4	-	46.1	-	-
VA5[1]	2.4	6.9	10.0	38.2	0.64	0.28
VA5[2]	0.7	7.1	7.8	35.5	0.68	0.36
VA5[3]	0.9	7.6	8.7	43.4	0.64	0.28
VA5[F]	-	8.7	-	54.7	-	-
VA6[1]	0.5	6.7	6.8	30.2	0.60	0.20
VA6[2]	1.1	6.7	7.7	33.6	0.66	0.32
VA7	-	6.6	-	30.2	-	-
VA8[1]	1.1	6.6	7.3	30.6	0.68	0.36
VA9[1]	1.2	6.7	7.0	32.3	0.66	0.32
VA10	-	6.6	-	33.8	-	-
VA11[1]	3.2	6.7	10.4	34.6	0.67	0.34
VA12[1]	1.9	6.7	7.9	34.7	0.67	0.34
VA13	-	6.6	-	35.0	-	-
VA14[1]	1.5	6.7	7.7	35.3	0.65	0.30
VA14[2]	1.5	7.0	7.7	37.1	0.59	0.18
VA15[1]	2.5	6.6	8.7	36.1	0.65	0.30
VA16	-	6.6	-	36.3	-	-
VA17[1]	2.9	6.6	9.4	36.6	0.67	0.34
VA18[1]	4.2	6.6	11.8	37.1	0.65	0.30

Table 10. Details of measured parameters for VA tests (background cycle of ΔP = 2.25 kN, R = 0.1, cycles/s = 5).

Tear no.	Δa (mm)	l (mm)		$K_{2D}(a_i)$	$\frac{A_c}{A_c + A_l}$	$\frac{b}{t}$
		l (a_i)	l ($a_i + \Delta a$)	(MPa√m)		
VA19[1]	2.0	6.6	8.7	32.0	-	-
VA20[1]	0.9	6.7	7.2	32.3	0.65	0.30
VA20[2]	1.7	6.7	7.5	35.2	0.67	0.34
VA21[1]	0.5	6.7	6.9	33.1	0.70	0.40
VA22[1]	2.0	6.7	8.2	34.7	0.70	0.40
VA23[1]	1.3	6.7	7.7	35.3	0.69	0.38
VA24	-	6.6	-	36.6	-	-
VA25[1]	3.0	6.5	9.1	37.3	0.64	0.28
VA26[1]	2.0	6.7	8.2	37.4	0.65	0.30
VA27[1]	3.5	6.6	11.5	37.6	0.65	0.30
VA28[1]	2.8	6.6	9.0	37.6	0.62	0.24
VA29[1]	3.3	6.6	9.6	38.2	0.63	0.26

Table 11. Details of measured parameters for VA fatigue tests (background cycle of increasing ΔP, R = 0.1, cycles/s = 5)

Tear no.	Δa (mm)	l (mm)		$K_{2D}(a_i)$	$\frac{A_c}{A_c + A_l}$	$\frac{b}{t}$
		l (a_i)	l ($a_i + \Delta a$)	(MPa√m)		
VA30[1]	2.7	6.6	9.1	38.3	0.68	0.36
VA31[1]	2.2	6.8	8.4	38.4	0.62	0.24
VA32[1]	3.5	6.8	10.2	39.5	0.65	0.30

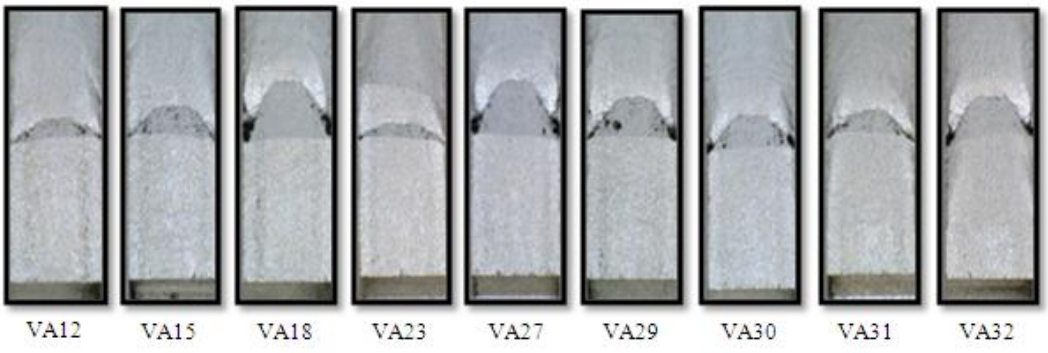

Figure 17. Some of the macrographs showing fracture surfaces of VA tearing with a P_{OL} applied at a_i = 20 mm.

4.2. Resistance curve

The typical plot of effective stress intensity factor K_R versus initial crack length a_p for four specimens is shown in Figure 18a, whilst the plot of K_R versus effective crack length Δa_e is shown in Figure 18b. The data points of K_R versus Δa_e can be represented by a power equation as follows

$$K_R = 42.89(\Delta a_e)^{0.514} \tag{23}$$

The empirical function has a very strong positive correlation with R^2 approximately equals to unity.

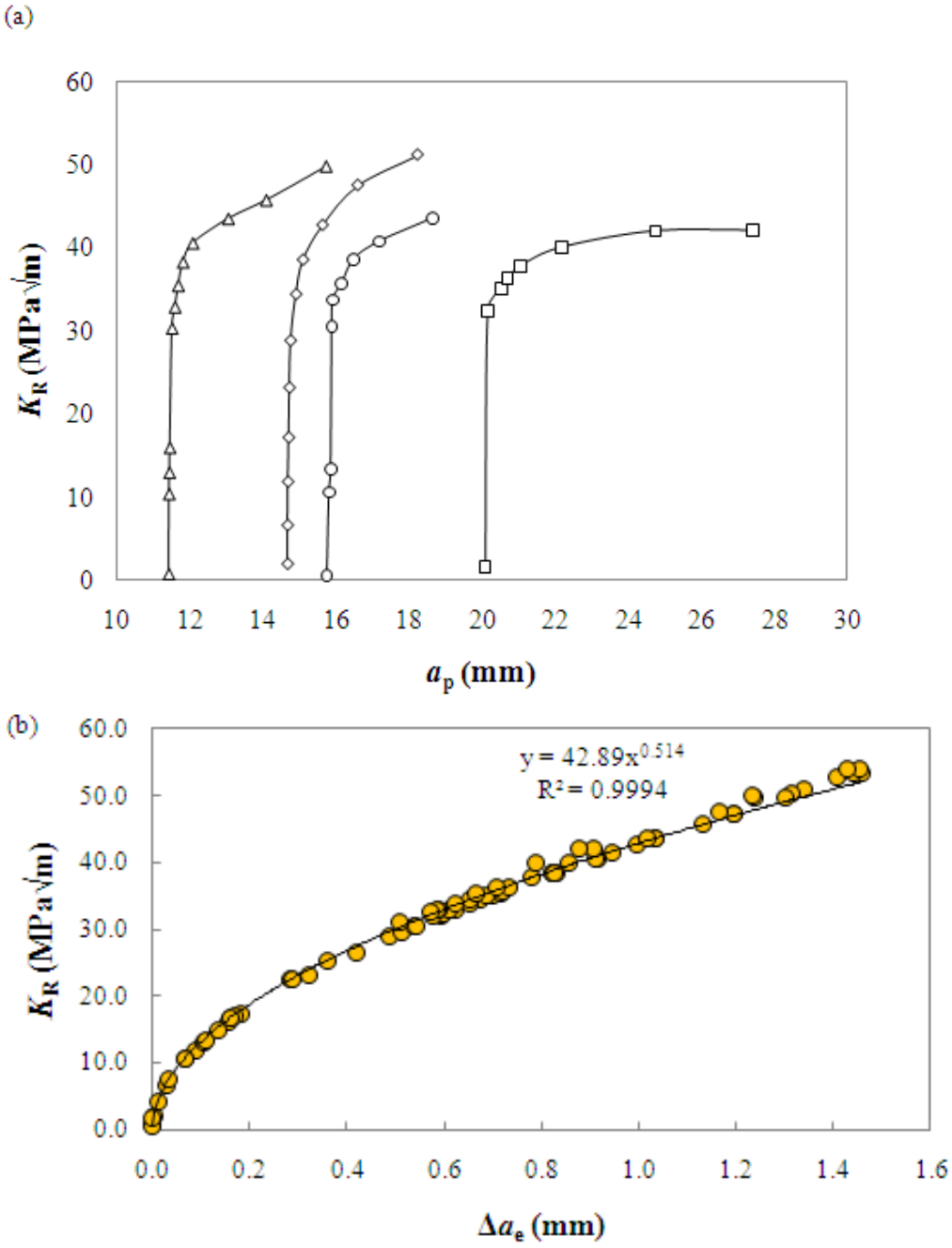

Figure 18. The resistance curve of 6.5 mm thick 7075 aluminium alloy CT specimens, (a) typical plot of K_R against initial a_p; and (b) plot of K_R against Δa_e.

4.3. Theoretical validation of small-scale yielding conditions

The theoretical plastic zone size due to each overload was small in comparison with the distance from the crack to any free surface edges of the specimen, to ensure that linear-elastic fracture mechanics (LEFM) were applicable in this study. The small-scale yielding conditions were checked according to several requirements. In particular, the remaining uncracked ligament ($W - a$) must be greater than $2.5\left(\frac{K_{Ic}}{\sigma_Y}\right)^2$ (ASTM E 399, 2009). Figure 19 shows that all of the tearing data comply with this requirement.

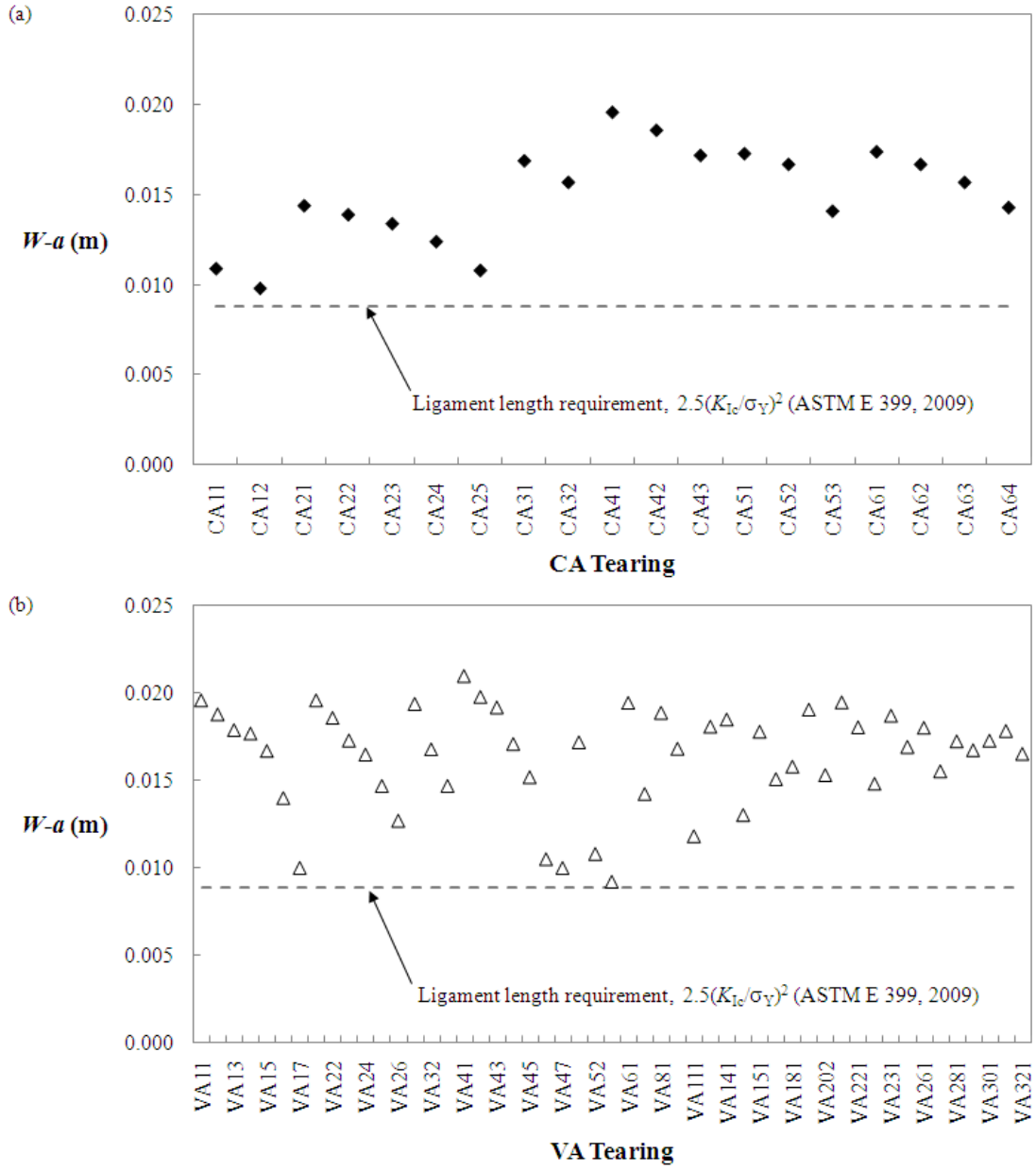

Figure 19. Validation of small-scale yielding for tearing data according to the ligament length requirement of ASTM E 399 (2009), (a) CA tearing and (b) VA tearing. The last number for each specimen is superscript as in Table 8 – 11.

The small-scale yielding condition has also been checked according to the requirement of ASTM E 561 (2009), which states that the size of the remaining uncracked ligament ($W - a$) must be greater or equal to eight plastic zone sizes. The

plastic zone size is calculated according to Eq. (17) by substituting $a = a_i + \Delta a$ for all tearing data and $K_{2D}(a)$ is determined by Eq. (15) with $P = P_{OL}$. Figure 20 shows that most of the CA and VA tearing data comply with the small-scale yielding conditions according to the ASTM E 561 (2009). There are five tearing data that do not comply with this requirement, and these tearing are the final tear in a given specimen that occurs prior to the final unstable separation.

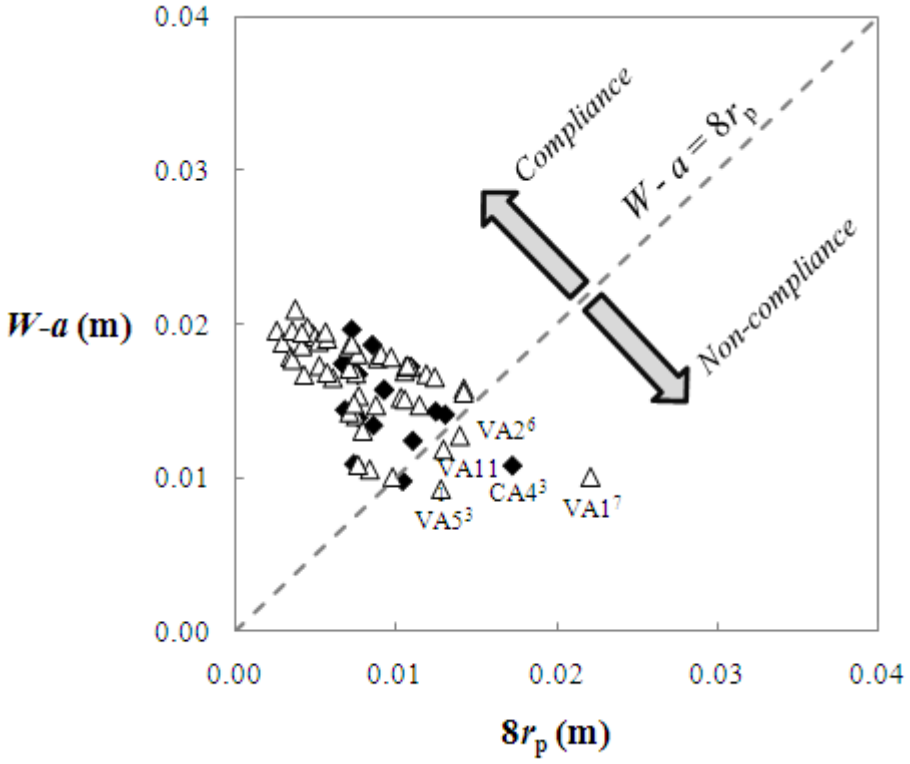

Figure 20. Validation of small-scale yielding for CA and VA tearing data according to the ligament length requirement of ASTM E 561 (2009).

Chapter 5. Critical Assessment of Existing Models

This chapter evaluates the significance of various measured tearing parameters, and assesses the effectiveness of the existing empirical models (Forsyth, Schijve and K_R curve models). These analyses provide some insight into the influence of the stress intensity factor K on CA and VA tearing crack jump length Δa. The CA and VA tearing crack jump length Δa are compared to the theoretical plastic zone size and the static resistance curve plot is compared with the stable tearing crack jump length Δa. Multiple stable tears generated in this study and experimental data from the literature are then used to develop a new predictive model, which idealises the shape of tearing and incorporates some of the key parameters of stable tearing. The new predictive model is supported by a combination of experimental testing and computational simulation. It relates the stress intensity factor parameters at the onset of stable tearing and arrest to the stable tearing crack jump length and the curved geometry of the crack front. This chapter ends with comparisons between the model's predictions and the experimental results, which show excellent agreement.

5.1. Some observations and measurements of stable tearing characteristics

5.1.1. Macroscopic ranges

The macroscopic examination and measurement of both CA and VA tears in this study show that the geometry of tearing varies significantly in a continuously-varying range, covering three broad geometrical types. Type I and Type II are usually observed under CA fatigue and VA fatigue, respectively, whilst Type III can be observed under both loading conditions.

Type I is tearing which has crack front line length l less than the thickness of the specimen t such as shown in Figure 14a (specimen CA4) and also has been observed on the fracture surface of specimen CA2. This tearing is usually fully contained in the central section of the specimen, and is typical of the pop-in crack growth, seen during fracture toughness tests, such as reported by Logsdon (1976). In certain steels, Pearson (1968) observed that these localised tears accumulated and merged together, first in the central region and finally appearing on the side of the specimen after nearly 100 CA fatigue cycles.

Troshchenko and Pokrovskii (1983b) suggest that the accuracy of their prediction model can be reduced by the presence of this type of tearing, while the Forsyth model, which is fundamentally based on the observation that $l \geq t$, is inapplicable. As noted by Vlasveld and Schijve (1980), Eq. (7) in particular is only applicable for $l \geq t$. This centrally localised tearing has been suggested to occur for reasons that include sporadic distribution of the main alloying elements (Vlasveld and Schijve, 1980), local inhomogeneity of the material and asymmetrical loading (Forsyth, 1978), the presence of micro-defects (Hertzberg, 1996) or the through-thickness constraint (Ab Rahman *et al*., 2010a).

Type II tearing stretches all through the thickness of the specimen, but has a slight crack jump length Δa and has been observed on the fracture surface of specimens VA1, VA2 and VA4. As a result, tearing of this type usually has l longer than the specimen thickness t, but can be observed as a single, relatively thin dark line on the fatigue fracture surface. This makes it difficult to differentiate this tearing from other progression marks on fatigue surfaces, and therefore inappropriate, if the two conditions are only differentiated by the degree of plastic deformation. This type of

tearing is usually observed under VA fatigue conditions, and hence is analogous to the macro-band observed by Hertzberg (1996), which resulted from variation in the applied stress intensity factor. The Forsyth model can be used to estimate the K, but the Schijve model is not meant for this type of tearing, as the model is only useful if Δa is significantly greater than zero.

Type III tearing features an l larger than t and has significant Δa. and has been observed on the fracture surface of all specimens. This tearing is readily noticeable and usually appears as crescent- or tongue-shaped bands (Forsyth and Ryder, 1961). Both Forsyth and Schijve models are developed based on this tearing type and therefore are applicable to this type of tearing. It should also be noted that the type I and II tears do not have significant effect on the overall fatigue crack growth life, and therefore the crack growth rate is still governed by the Paris relationship (Paris region in Figure 3). For this reason, the application of a stable tearing prediction model will become redundant.

5.1.2. Microscopic characteristics

It has been established in section 2.5 that the occurrence of stable tearing in material of intermediate thicknesses under CA conditions can be associated with the transition of a fatigue crack from a tensile mode (flat fracture surface) to the shear mode (slant fracture surface), in which the crack front becomes more curved during the process. Macroscopically, these fracture conditions means that tearing produced under CA fatigue involves formation of shear lips on the specimen CA1, as illustrated in Figure 21.

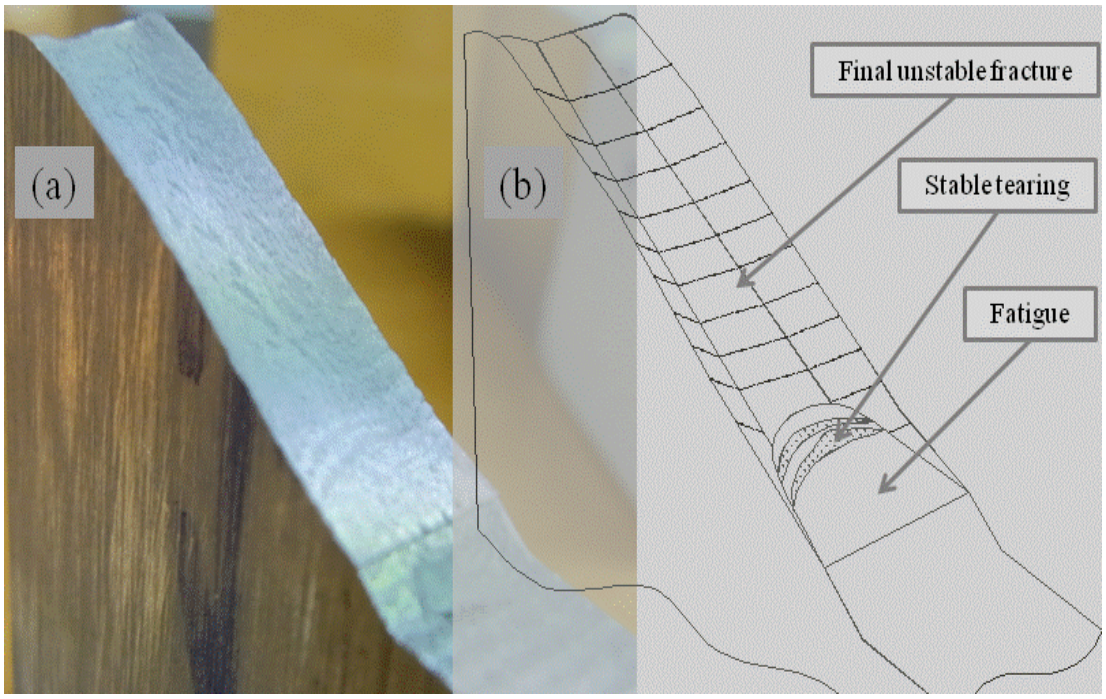

Figure 21. Transition of fatigue-tearing crack growth under CA fatigue appears to be associated with transformation from flat to slant fracture surface (specimen CA1).

Examination of the fracture surfaces of the specimens tested in this study showed that the occurrence of VA tearing does not involve a notable change in crack plane, however, detailed examination of the VA tearing surfaces revealed that each tear appears to form on different steps, as shown in Figure 22 of specimen VA3; the difference in height between plane T1 and T3 in Figure 22 is about 1.36 mm. A similar observation has been observed in some steels, such as by Rungta *et al*. (1985) (as shown in Figure 23) and Stepanenko *et al*. (1984).

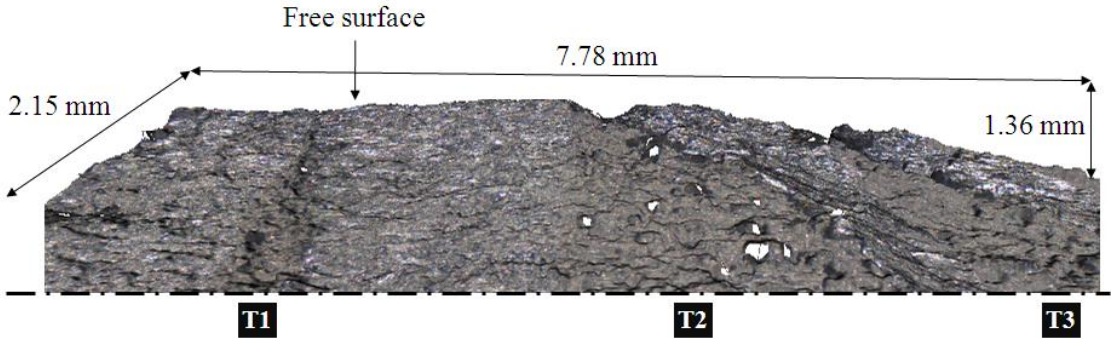

Figure 22. Surface analysis by three-dimensional microscope shows apparent steps in VA tearing (specimen VA3). The first tearing (marked as T1) is formed on a different plane than T2 and T3 (on one side of the specimen). The difference in height between the plane T1 and T3 is measured at 1.36 mm. The crack grows from left to right and the dashed line approximates the centreline.

The change in crack plane in VA tearing has been associated with crack branching, which usually occurs during an overload (Suresh, 1983). The crack appears at an angle on the free surface, which indicates that the cracking mechanism of stable tearing in VA conditions is similar to the CA conditions. This implies that the crack jumps at the mid-thickness region (in plane strain), while in the regions close to the free surface, cracking occurs on a slanted plane (in plane stress). In CA conditions, the crack continues to grow on the slanted plane because the subsequent fatigue cycles have relatively high ΔK, but in VA sequences, the crack on the surface has to realign and grow on the flat plane because of the lower subsequent ΔK. This latter cracking mechanism contributes to the retardation of fatigue crack growth following an overload (Fleck, 1985). It should be noted that crack branching is one of the mechanisms that causes crack growth retardation. It was pointed out in section 2.4 that

other retardation mechanisms are also possible such as crack tip blunting and an increase in crack front line length, though none of these mechanisms can be regarded as a primary contributor to crack retardations.

It should also be noted that the fatigue crack growth period, after the first occurrence of stable tearing in CA conditions, is not considerable in comparison to the overall fatigue crack growth life, as shown in Figure 21. As discussed in 2.7.4 of this thesis, it can be expected that the subsequent tearing and fatigue crack growth will also occur in quick succession, which then leads to the final separation of the specimen.

The absence of shear lips in VA tearing may also contribute to the lower first onset stress intensity factor $K_{2D}(a_i)$ compared to CA tearing. This will be discussed in section 5.1.5. According to Krafft *et al*. (1961), a larger plastic zone (or deformation) by virtue of shear deformation at the edge of the specimen increases the resistance of material to fracture, potentially explaining the higher $K_{2D}(a_i)$ value which is observed for CA tearing compared to that for the tearing produced under VA conditions.

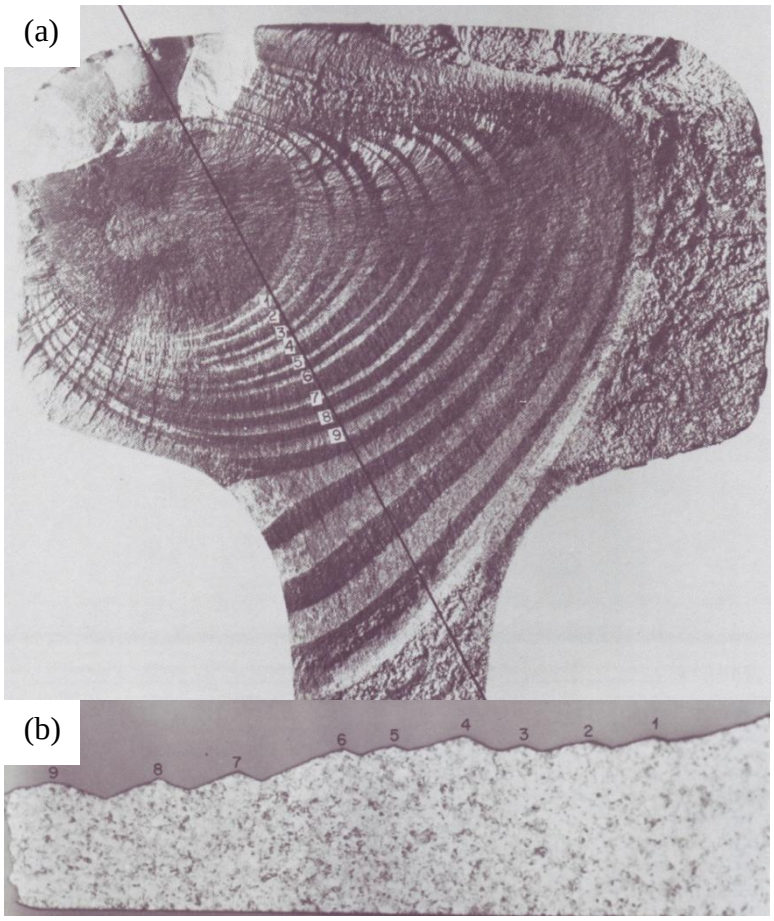

Figure 23. The cross section of a steel railroad head in (b), along a diagonal line in (a) shows each tear was produced on different planes (Vander Voort, 1992).

SEM images of the fracture surfaces of fatigue and stable tearing crack growths on specimen VA30 are shown in Figure 24 to Figure 27. These images are taken from the central region of fracture surfaces. Figure 24 shows the boundary between the fatigue and tearing. It reveals that at microscopic level, the actual crack front is tortuous, as reported in the literature (Forsyth, 1978). Fatigue striations can be observed at high magnification (Figure 24b) on the fatigue crack growth area, but at higher magnification it can be shown that the striation spacing is not always perpendicular to the direction of crack growth, but its direction is mainly influenced by

the secondary inter-metallic particles, as shown in Figure 25. This observation is supported by Xue *et al*. (2007), who suggested that the initiation of fatigue damage in this alloy occurs at the inclusion made of iron-rich inter-metallic particles.

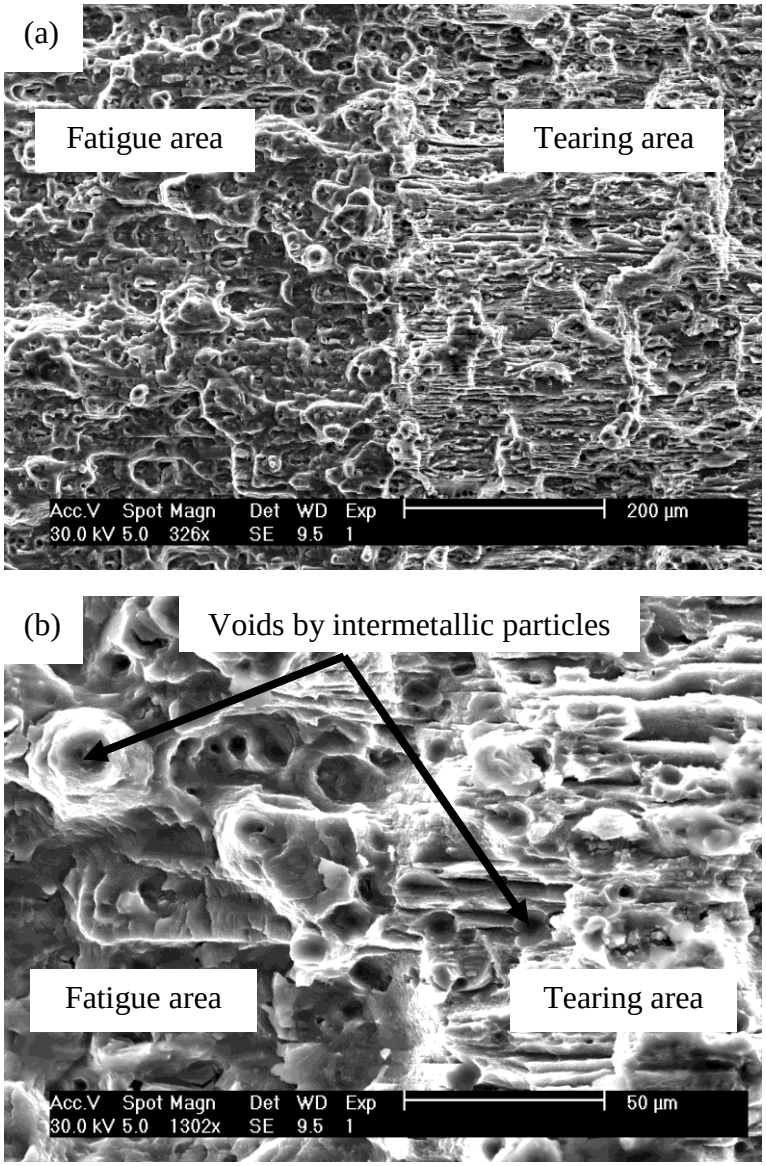

Figure 24. SEM images of fatigue to tearing crack growth transition (specimen VA15) at different levels of magnification, (a) 326 x and (b) 1302 x. The crack growth direction is from left to right.

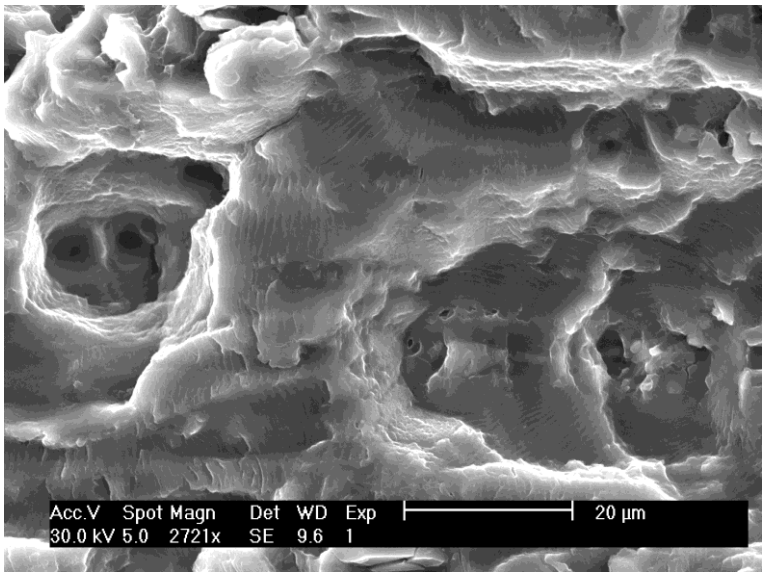

Figure 25. Striation features as observed in fatigue crack growth area (specimen VA15). The crack growth direction is from left to right.

There are three types of second-phase particles that are present in this type of aluminium alloy; the largest of these particles are the secondary inter-metallic phases of iron (Fe) and silicon (Si) (Bucci *et al*., 1980). Achon *et al*. (1996) observed that these coarse particles are randomly distributed and resulted in higher strength of 7075 aluminium alloy in comparison to 7475 alloy. Their presence is readily seen on a fracture surface and appeared as craters or holes, as shown in Figure 24 and Figure 26.

In addition to these secondary phase particles, the tearing surface is dominated by river patterns running parallel to the crack growth direction, which are typical of cleavage fracture (Anderson, 2005). The initiation of cleavage is caused by a sharp microcrack provided by the secondary phase particles (Cottrell, 1958; Anderson, 2005). This result is not surprising as it has been discussed in section 2.1, that stable tearing fracture surface can be predominated either by cleavage- or ductile-like

fracture. Drar (1995) has shown that it is possible for metals to have mixed fracture mechanisms, whereby interparticle void coalescence (ductile fracture) and transgranular cleavage occur on the same fracture surface. It has been indicated in section 3.1, that the 7075 alloys are the lack in terms of ductility, and therefore the cleavage fracture can be expected to predominate the tearing surface.

Figure 26 shows that the fatigue crack growth area subsequent to tearing appears to be smooth. This striationless feature has been associated with the roughness-induced crack closure that contributes to the retardation of crack growth (Suresh, 1983). This view is rather controversial, as other researchers such as Shih and Wei (1974) have suggested this feature is evidence of plasticity-induced crack closure. The present author believes that both of these explanations are practically sensible, but depending on property of materials, one mechanism may be more pronounced in some alloys, but may not be in others.

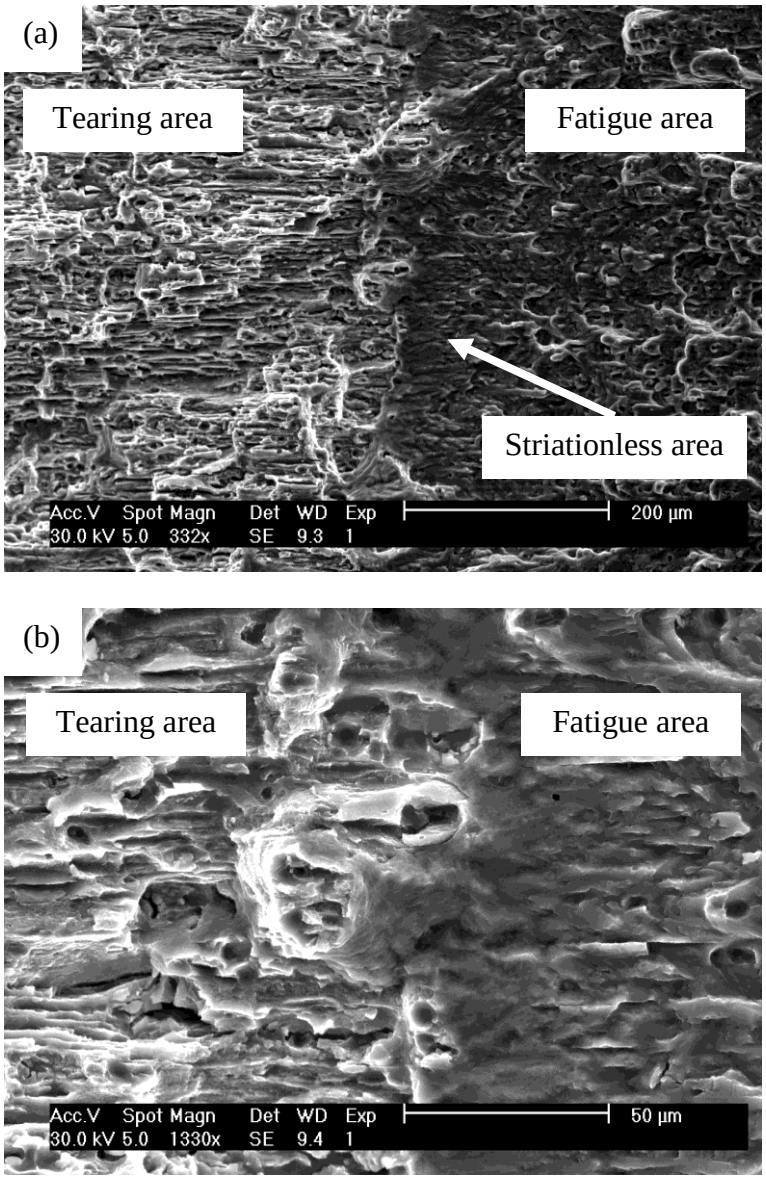

Figure 26. SEM images of tearing to fatigue crack growth transition (specimen VA15) at different levels of magnification, (a) 332 x and (b) 1330 x. The crack growth direction is from left to right.

Another notable feature of stable tearing surface, as observed in this study, is the presence of multiple secondary cracks, which are parallel to the crack growth direction. These cracks can also be observed on the CA tearing surface near the final

unstable fracture. Vlasveld and Schijve (1979) suggested that these cracks are resulted from plastic deformation, and the crack can be seen even after the specimen fails. It is noted in Figure 27b that these cracks appear at both side of tearing area, and therefore can be associated with the crack branching, which is created during the application of an overload. It has been established in section 5.1.2 that an application of overload causes the crack near the surface to deviate from the crack plane, and this crack occurs on the slanted plane. This crack should join the stable tearing crack jump, which occurs on the flat plane at the mid-thickness region, as schematically shown in Figure 28b. However, as the fatigue crack growth during the subsequent fatigue cycles tries to revert back to the flat crack plane by growing on the unfractured ligaments (Figure 28c), no further crack can occur on the slanted plane. Therefore, this dormant crack should appear as multiple discontinuous cracks on the stable tearing surface.

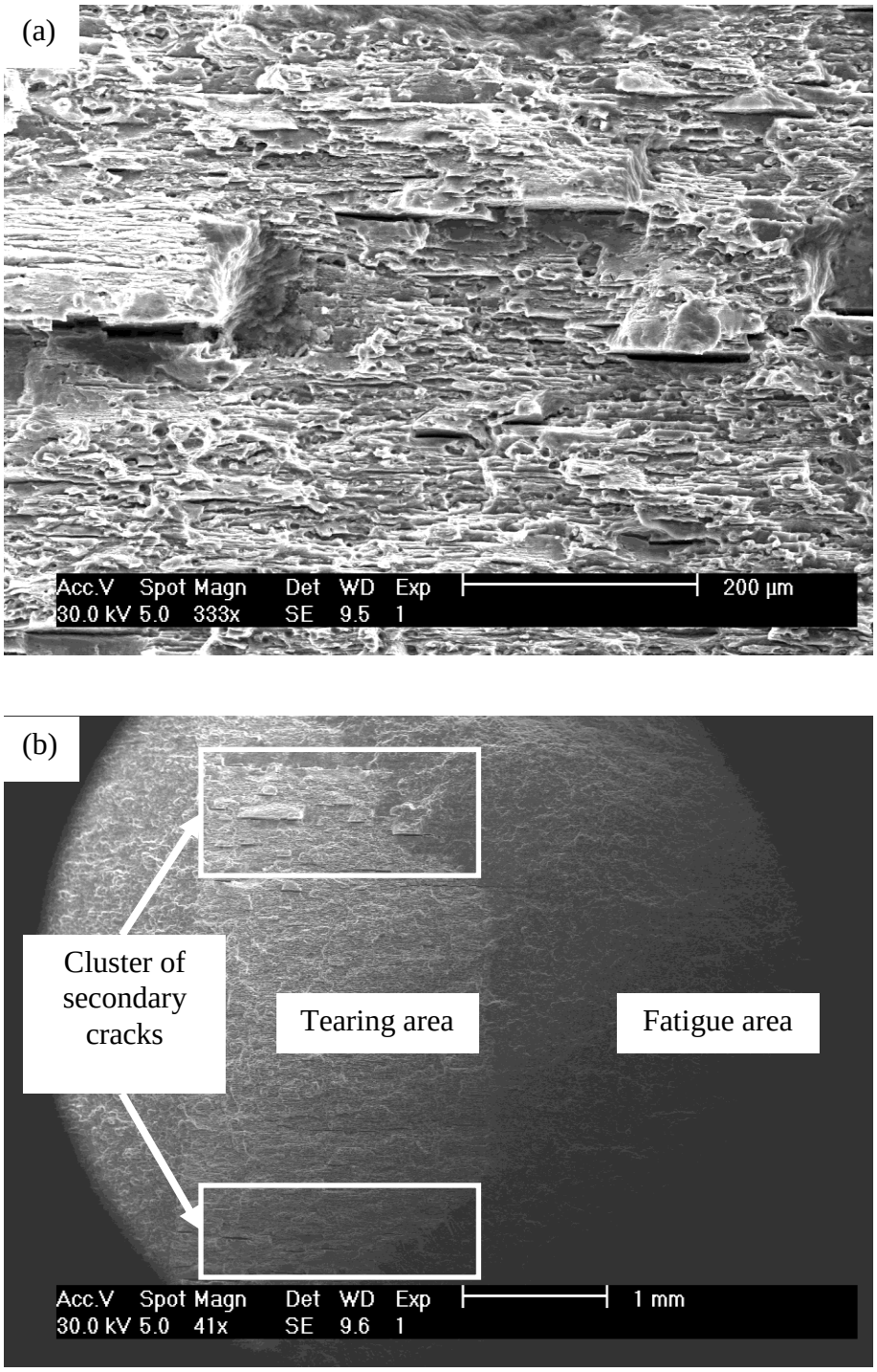

Figure 27. Secondary cracks, parallel to the crack growth direction on both sides of the tearing surface (specimen VA15) (a) 333 x and (b) 41 x. The crack growth direction is from left to right.

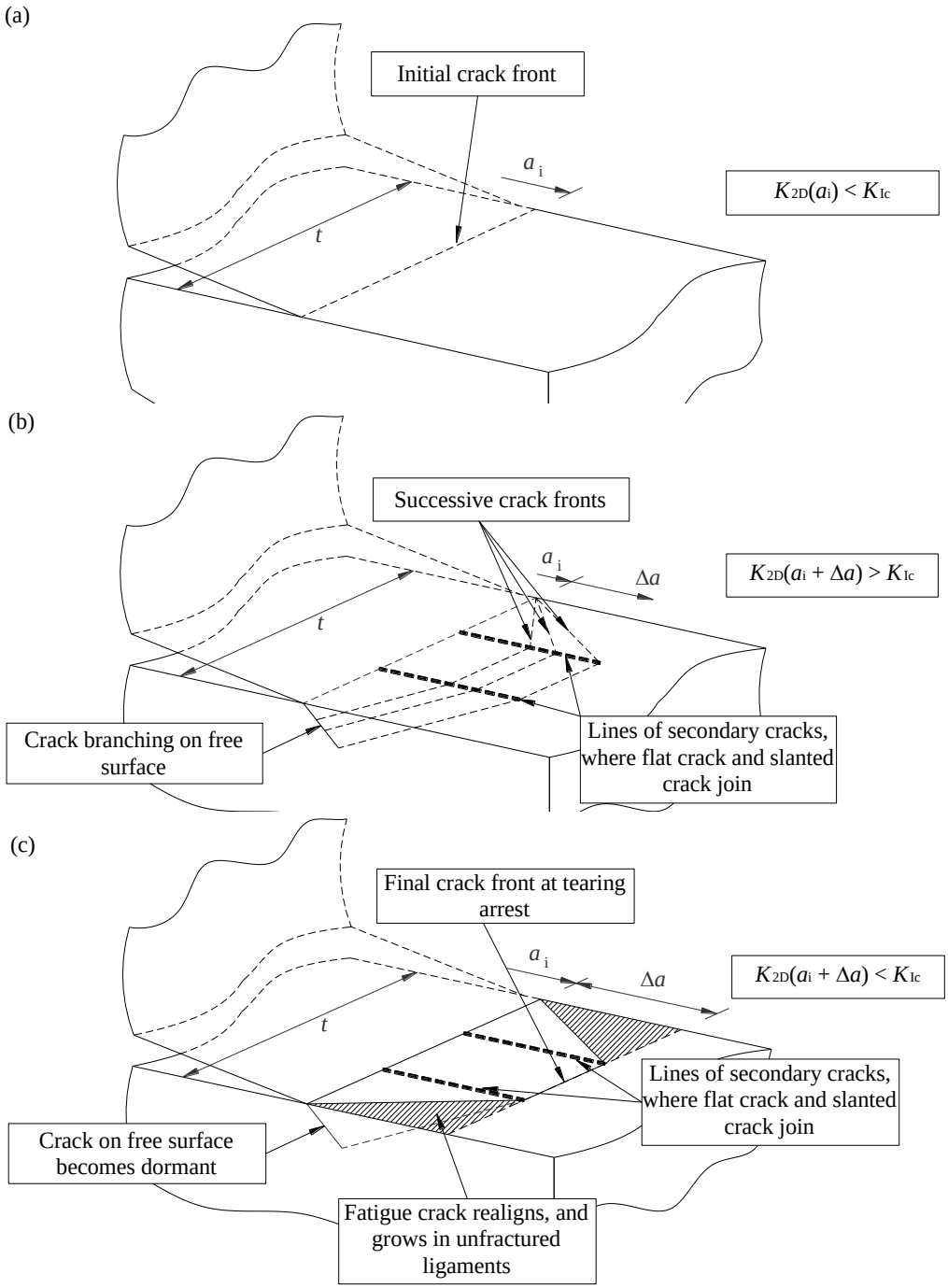

Figure 28. The formation of secondary cracks on a stable tearing area. (a) at initial stage of the overload; (b) the overload reaches the critical condition, and tearing starts to extend at the mid-thickness region, while the crack deflects at an angle at the free surface; and (c) the overload is removed and fatigue crack growth ensues on the unfractured ligaments, and the crack on the slanted plane becomes dormant.

5.1.3. Crack front line length

The Forsyth model depends on the $\frac{\sqrt{a}}{l}$ ratio, which suggests that this ratio is approximately constant (as in Eq. (4)) at both onset and arrest of tearing, while the ratio at tearing onset is slightly higher than at tearing arrest. An empirical result also suggests that the value of $\frac{\sqrt{a}}{l}$ at onset can be associated with K_{Ic} (Forsyth, 1976). Figure 29 shows the relationship between the $\frac{\sqrt{a}}{l}$ ratios at onset and arrest for tears produced under CA and VA fatigue conditions in this study. The plot indicates that the $\frac{\sqrt{a}}{l}$ ratios are not strictly constant for either onset or arrest of tearing, and that this is valid for both CA and VA fatigue conditions. It should be noted that the Forsyth model has been derived based on the measurement of multiple stable tearing crack growth on a single specimen. Therefore, the $\frac{\sqrt{a}}{l}$ ratio of a tear is directly influenced by the previous tear, and therefore it can be concluded that the constant $\frac{\sqrt{a}}{l}$ ratio can only be achieved for tears from the same specimen, as shown by Bowen and Forsyth (1981).

In addition, Figure 29 shows that the ratio of $\frac{\sqrt{a}}{l}$ at onset is higher than that at arrest in most of the tearing, especially the CA tearing, and therefore agrees with the results of Forsyth (1978). In contrast, some of the VA tearing produces equivalent $\frac{\sqrt{a}}{l}$

ratio at onset and arrest. The equality of onset and arrest $\frac{\sqrt{a}}{l}$ ratios is, as might be expected, usually occurred during the early phase of tearing formation on each specimen, where the extend of tear appears as insignificant and visually appears as an extended form of the localised deformation at the crack tip associated with overload.

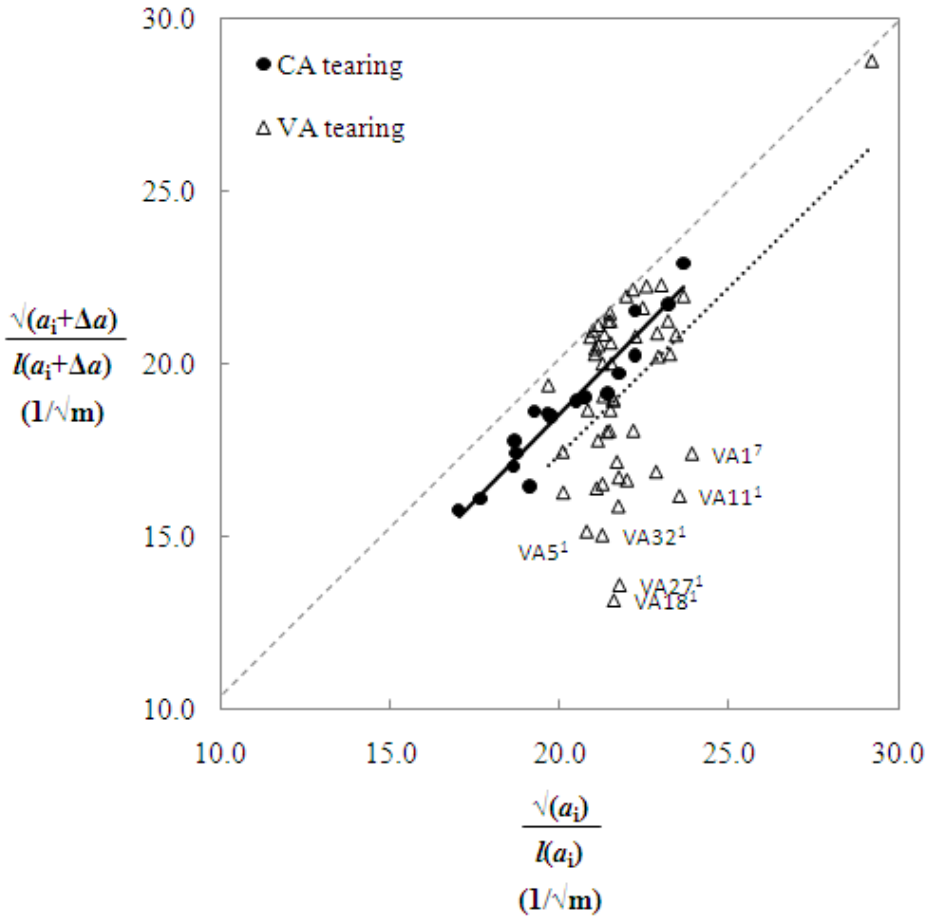

Figure 29. Plot of $\frac{\sqrt{a}}{l}$ at arrest against $\frac{\sqrt{a}}{l}$ at onset. The solid and dotted lines are the line of best fit for CA and VA tears, respectively, and the dashed line is the line of equal relation (Y = X).

Figure 29 also shows that all points lay on, or to one side of equal $\frac{\sqrt{a}}{l}$, and the onset of tearing displays a slightly higher $\frac{\sqrt{a}}{l}$ ratio. Figure 29 substantiates the general linearity of $\frac{\sqrt{a}}{l}$, suggested in the Forsyth model for CA tearing as shown by the solid line, but not for the VA tearing data. Table 12 shows that the standard deviation for VA tearing is higher in comparison to the CA tearing. The farthermost outliers are all associated with tearing under VA conditions, and these outliers are also associated with a large value of Δa. The complexity of these large tears (under VA tearing) causes difficulty in applying the Forsyth model for prediction of stable tearing jump length, which will be discussed in section 6.1.

Table 12. Average relative error and standard deviation of CA and VA tearing data.

	$\frac{\sqrt{a}}{l}$ ratio $\left(\frac{1}{\sqrt{\text{m}}}\right)$		$\frac{K}{l}$ ratio $\left(\frac{\text{MPa}\sqrt{\text{m}}}{\text{m}}\right)$	
	Average relative error	Standard deviation	Average relative error	Standard deviation
CA	7.2	2.7	1.1	3.2
VA	13.5	10.5	4.9	5.8

The results of this study suggest that the constancy of $\frac{\sqrt{a}}{l}$ as proposed by Forsyth in Eq. (4) cannot be considered as strictly correct, at least not for VA tearing in 7075 aluminium alloy. In CA conditions, however, while the ratio of $\frac{\sqrt{a}}{l}$ at onset of tearing has a tendency to be higher than at tearing arrest, as proposed by Forsyth in Eq. (5), the differences are relatively small, with most $\frac{\sqrt{a_\mathrm{i}+\Delta a}}{l(a_\mathrm{i}+\Delta a)}$ data lying apparently between 85% and 100% of $\frac{\sqrt{a_\mathrm{i}}}{l(a_\mathrm{i})}$ confirming the potential effectiveness of the Forsyth model as a useful engineering tool in representing fracture surface tearing.

Figure 30 shows the results in term of $\frac{K}{l}$ ratios. The plot of $\frac{K_{2\mathrm{D}}(a_\mathrm{i}+\Delta a)}{l(a_\mathrm{i}+\Delta a)}$ versus $\frac{K_{2\mathrm{D}}(a_\mathrm{i})}{l(a_\mathrm{i})}$, suggests that $\frac{K_{2\mathrm{D}}(a_\mathrm{i})}{l(a_\mathrm{i})}$ is up to 10% higher than $\frac{K_{2\mathrm{D}}(a_\mathrm{i}+\Delta a)}{l(a_\mathrm{i}+\Delta a)}$. The scatter of data points again imply that the linear relationship of the onset and arrest $\frac{K}{l}$ ratios can be assumed for the purposes of engineering representation of stable tearing behaviour on fracture surfaces:

$$\frac{K_{2\mathrm{D}}(a_\mathrm{i}+\Delta a)}{l(a_\mathrm{i}+\Delta a)} = \frac{K_{2\mathrm{D}}(a_\mathrm{i})}{l(a_\mathrm{i})} \qquad (24)$$

This result also implies that $K_{2\mathrm{D}}(a_\mathrm{i})$ is not always equal to K_{Ic}, as macroscopic examination of the fracture surface often suggests that $l(a_\mathrm{i})$ is slightly curved, which infers that $l(a_\mathrm{i}) > t$.

In summary, the results further substantiate Forsyth's proposition that crack front line length l can effectively be used to correction to the stress intensity factor, calculated based on the maximum crack length. The stronger correlation can be observed for CA data points rather than the VA data points. These results also emphasise a couple of difficulties with this empirical model. Firstly, the use of a maximum crack length in K calculation is clearly invalid, since it represents a notional stress intensity factor value while the real value should be affected by the crack front curvature. Secondly, the models revolve around visual measurements from fracture surfaces, which the information available from that inspection could be used more effectively in an alternative and more detailed analysis. The assumption made by Forsyth (Forsyth, 1976, 1978; Bowen and Forsyth, 1981) and Schijve (Vlasveld and Schijve, 1979, 1980) that $K_{2D}(a_i) = K_{Ic}$ at initiation of tearing will be discussed further in section 5.1.5.

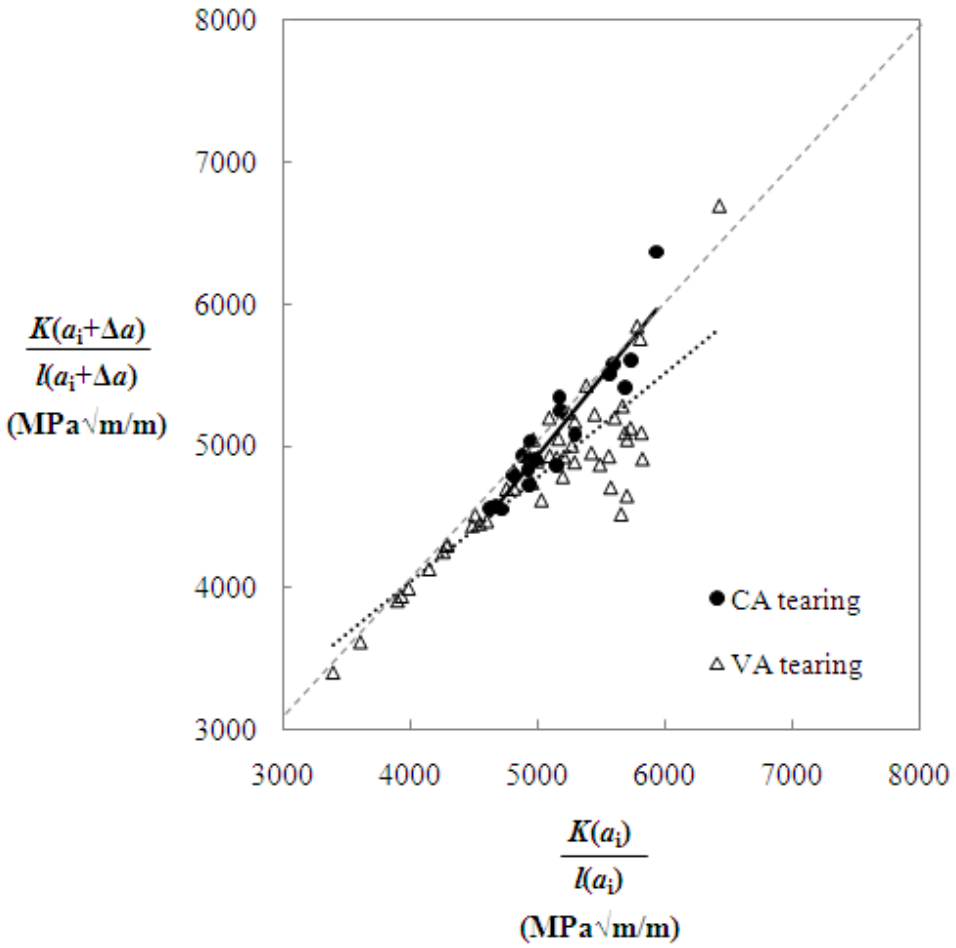

Figure 30. Plot of $\frac{K_{2D}}{l}$ at arrest versus $\frac{K_{2D}}{l}$ at onset. The solid and dotted lines are the line of best fit for CA and VA tears, respectively, and the dashed line is the line of equal relation (Y = X).

5.1.4. Crack front curvature

It has been established in section 2.5 that the crack front curvature results from the interaction effect between the plane strain and plane stress regions, are more pronounced in materials of intermediate thickness. The tearing can lead to a substantially curved crack front, which also means an increase in the crack front length, namely $l(a_i + \Delta a) > t$. Forsyth (1976, 1978) associated this change with a

return to “normal” fatigue crack growth, while Vlasveld and Schijve (1979, 1980) proposed a corrected *K*-value, based on fracture mechanics principles, to account for the effect of the trailing ligaments of the uncracked material. These ligaments, at both sides of a tear, hinder further crack advance, progressively, as the front tunnels ahead, until the increased resistance to advance prevents further tearing and causes the return to fatigue crack growth. Therefore, it can be concluded that both models are proposed based on similar foundation, namely the effect of crack front curvature on the stable tearing phenomenon.

It is also important to note that all of the stress intensity factors used in section 5.1.3 relate to the maximum crack length, which often occurs in the middle thickness of the specimen. In fact, both models for tearing (Forsyth and Schijve) have been developed based on the maximum crack length. At its simplest, and as acknowledged by the Schijve model, large tears (extensive crack jump length Δa) possess more acute crack front curvatures, which result in considerable portions of the crack front lagging behind – effectively providing the ligaments central to the Schijve model. On the other hand, Forsyth (1976, 1978) employed a relatively simpler approximation, proposing that the additional crack front line length could be linked to the *K*, as indicated by Eq. (7) and in Figure 7. This means that the stress intensity factor values used in the previous section (and by Forsyth), based on an assumption of no curvature, are only “notional” and a more detailed analysis of the true stress intensity factor at the mid-thickness point would lead to lower values of stress intensity factor, as will be discussed in section 5.4.2.2. The Schijve model acknowledges this, and attempts the correction using ligaments, while Forsyth uses crack line length as an empirical correction.

Therefore, while in early tearing, with relatively straight crack fronts, the "notional" maximum stress intensity factor can be assumed to represent the true stress intensity factor, this parameter may grossly overestimate the true stress intensity factor when significant crack front curvature is present. The determination of the actual *K*-value for a curved crack front is still not well established. Several attempts have been reported in the literature, but are limited to either a slightly curved crack front (Kuna, 1982; Burton *et al*., 1984; Yamamoto *et al*., 1987; Wu, 2006), usually resulted from fatigue pre-cracking procedure or an elliptical crack front (Shen and Guo, 2005; Zhang and Guo, 2007; Yu *et al*., 2008). Liu *et al*. (2005) proposed a more detailed analysis for the true stress intensity factor at various points along the curved crack front at tearing arrest using finite element analysis, and it seems clear that appropriate adjustments to the value of *K* may remove some of the anomalous behaviour observed in the results in the $\frac{\sqrt{a}}{l}$ and $\frac{K}{l}$ plots, namely Figure 30 and Figure 31, respectively. An alternative approach is to use a resistance curve (*R*-curve) analysis, establishing a crack growth resistance curve for the specimens used in this study, and details of this are presented in section 5.1.7.

5.1.5. Stress intensity factor

The experimental results in this work establish that stable tearing can be produced under CA and VA fatigue, and allow a comparison of tearing onset under the two fatigue load regimes. Figure 31a and b shows the values of stress intensity factor at the onset of tearing $K_{2D}(a_i)$ for the first significant tear in each specimen. Specimens

VA4 and VA5, which are being tested under VA loading but actually failed during the CA background loading part of the load history, are included and denoted as VA4[6] and VA5[2] respectively. The results show that the $K_{2D}(a_i)$ is not affected by the variation in P_{max} and P_{min} of the load cycles. Higher P_{min} in specimen CA5 and a lower cyclic frequency in CA6, as compared to specimen CA3 do not significantly affect the $K_{2D}(a_i)$ values. This implies that the occurrence of tearing is influenced by $K_{2D}(a_i)$, the magnitude of the stress intensity factor.

The $K_{2D}(a_i)$ is affected by the type of loading. The magnitude of $K_{2D}(a_i)$ ranges from 35 to 38 MPa√m (average 36 ± 2 MPa√m) under CA, while the VA values vary from 29 to 32 MPa√m (average 30 ± 1 MPa√m excluding specimen VA5 – see later). So both load types, CA and VA, exhibit constant but different level of $K_{2D}(a_i)$, indicating that these values represent some type of threshold K for tearing to occur under respective load cycle types.

Figure 31b and c shows the relationship between $K_{2D}(a_i)$ and Δa in the first significant tear occurrence in each specimen. It shows that the size of Δa follows the same trend as the $K_{2D}(a_i)$, namely a higher $K_{2D}(a_i)$ will result in higher Δa; this is discussed in more detail below. This result also supports the use of the stress intensity factor (in practice K_{max}) to represent the tear-controlling stressing condition along the crack front in the early tearing. However, as the tearing progresses and there is significant change in crack front shape, the amount of Δa starts to be sensitive to the type of load cycling.

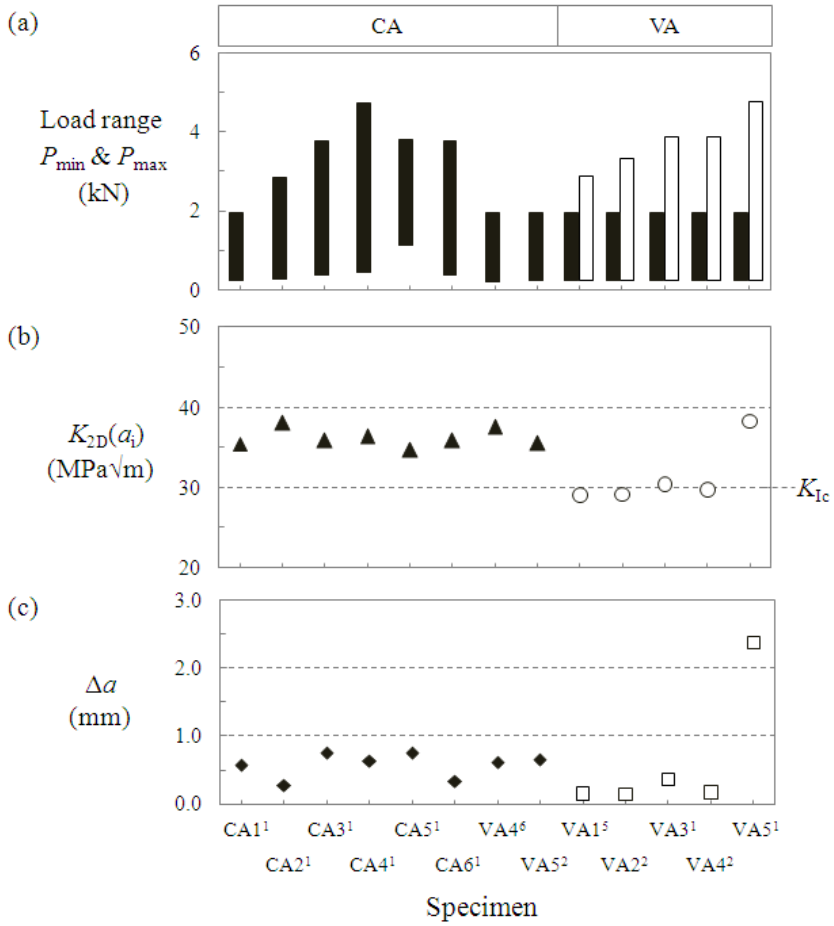

Figure 31. Effect of $K_{2D}(a_i)$ and load cycle on Δa; (a) load range subjected to specimen; (b) the values of stress intensity factor at the onset of tearing; and (c) tearing size.

The difference between CA and VA tearing can also be observed on the resultant Δa from the equivalent applied $K_{2D}(a_i)$. Figure 32 shows the effect of $K_{2D}(a_i)$ on the size of Δa. This shows that generally, and for similar $K_{2D}(a_i)$ conditions, the VA provides larger values of Δa than the CA loading, the $K_{2D}(a_i)$ at onset of VA tearing is lower than that required under CA condition and the size of Δa under VA sequences is markedly larger than that sustainable under CA. This implies that the CA loading is

conferring some level of resistance to tearing. An obvious question then, is how two loading arrangements, CA and VA, both of which reach the same peak load, can produce different crack advance? It seems reasonable to conclude that either (a) tearing starts at the same peak load, but is then retarded by some effect related to the large ΔK cycles in the CA history, or (b) the tearing onset occurs before peak load in VA case, allowing the tearing crack jump length Δa to progress further as the load rises to its peak (Figure 33).

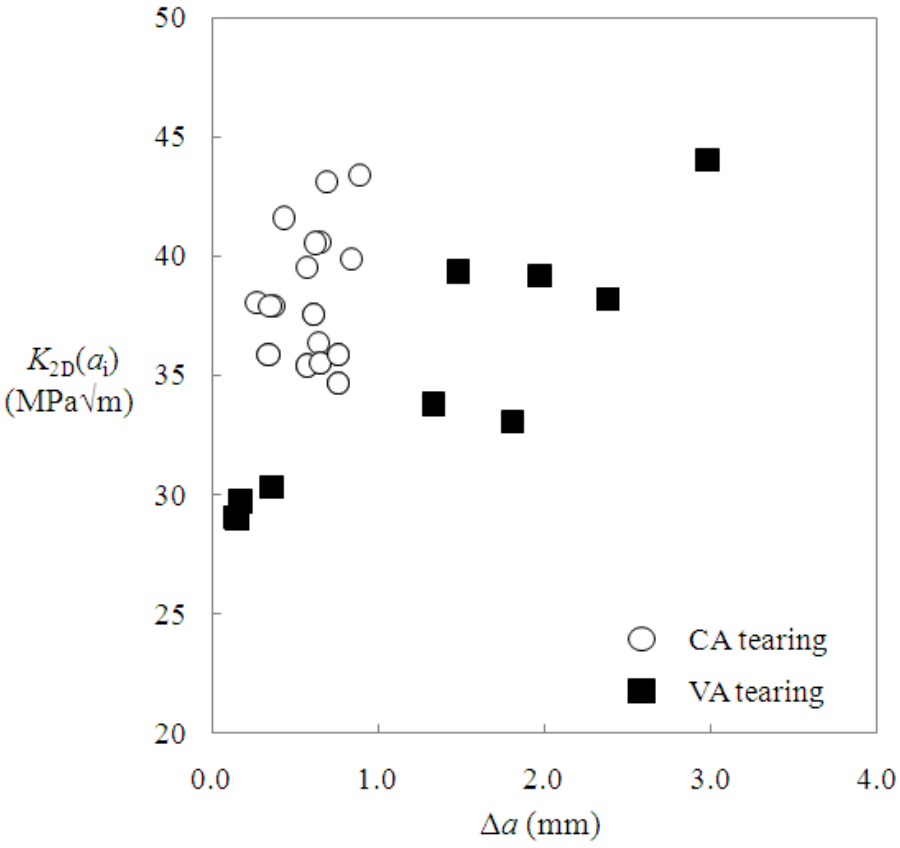

Figure 32. Effect of $K_{2D}(a_i)$ on Δa.

Both representations amount to the same thing – the CA loading cycles immediately before tearing provide some resistance to tearing, relative to the "sudden overload" case of the VA test. An example is specimen VA5 in Figure 31, where the first overload in VA happened to be at a high K and produced a large crack advance Δa. This is thought to be a prime example of the situation described in Figure 33, where the tearing may have started well before peak load. The effect appears similar to the effect observed by Clark (1979) and Jones and Brown Jr. (1970). For example, Clark (1979) noted that CA cycling effectively elevated K_q values for steels in fracture toughness testing. Indeed, this is why plane strain fracture toughness testing prohibits the use of high levels of prior fatigue loading (Brown and Srawley, 1966). Possible explanations include cyclic hardening or softening of the material near the crack tip after the high levels of cyclic strain associated with the constant amplitude loading, crack tip blunting, or residual stress effects.

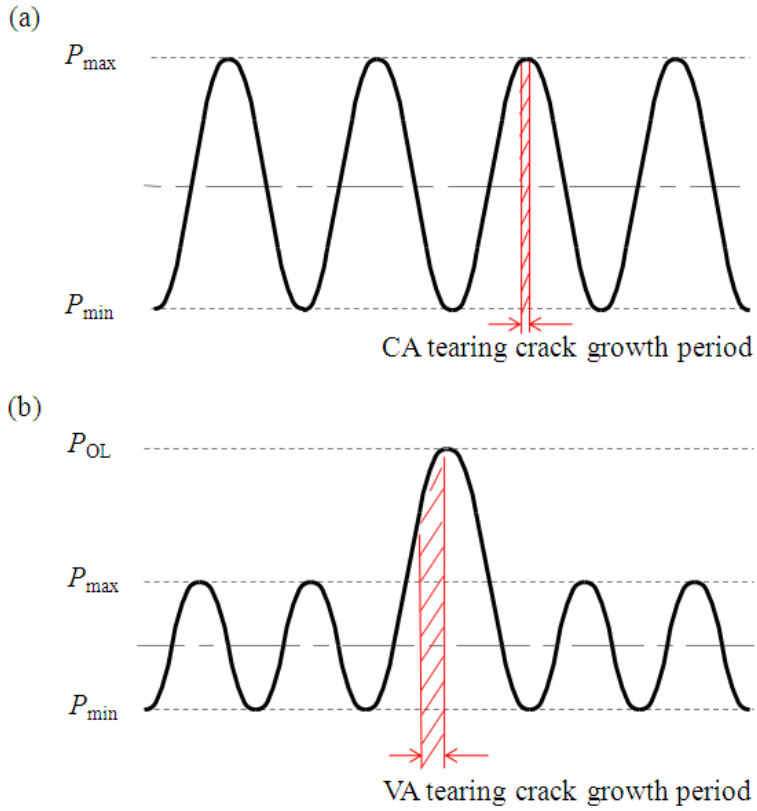

Figure 33. A possible effect of types of load cycle on the start of tearing jump length Δa: (a) CA tearing, and (b) VA tearing.

5.1.6. Plastic zone size

The importance of plastic zone size in tearing formation has been emphasised by empirical evidences in several studies (Troshchenko and Pokrovskii, 1983a, 1983b; Troshchenko *et al*., 1978; Kitsunai, 1985, 1986). The crack tip plastic zone is an enclosed volume around the crack tip, which prevents the stress singularity condition of linear elastic fracture mechanics. Fracture modelling to accommodate the existence of this zone of plasticity leads to a crack appearing to be longer than its physical size would suggest (Broek, 1986), and for practical applications, the theoretical size of the

plastic zone is usually added to the measured crack length from the surface, as will be discussed in section 5.1.7.

The two important aspects of the plastic zone are its size and shape. The shape of the monotonic plastic zone (Mode I) at the tip of a through crack is shown in Figure 34a. The shape of the cyclic plastic zone has been proposed to be the same as the shape of the plane stress plastic zone; however, its size is smaller due to reversed plasticity (Schijve, 2009). Schijve (2009) stated that the size of the plastic zone for plane stress and plane strain, as depicted in Figure 34b, can be estimated by Eq. (25) and Eq. (26) respectively.

For plane stress,

$$r_{y,\sigma} = \frac{1}{\pi}\left(\frac{K}{\sigma_Y}\right)^2 \tag{25}$$

For plane strain,

$$r_{y,\varepsilon} = \frac{1}{3\pi}\left(\frac{K}{\sigma_Y}\right)^2 \tag{26}$$

It should be noted that Ivanova (1982b) and Troshchenko (2009) modified Eq. (25) and Eq. (26), respectively, for estimating the stable tearing jump length Δa in their models.

The depth of the shear lip D from the side of the component (indicated in Figure 6), which deformed under plane stress, can also be estimated by Eq. (25) (Hertzberg,

1996). Vlasveld and Schijve (1979, 1980) used this equation to estimate the size of the plastically-deformed ligament (in the thickness direction) on both sides of tearing. Although their works were on VA tearing, where the shear lip was absent, they showed that this ligament was crucial in lowering the effective stress intensity factor (namely the stress intensity factor that drives the mid-thickness and deepest part of the tear), and thus resisting the occurrence of unstable fracture. The additional resistance to tearing in the plane stress region (after Krafft *et al*. (1961)) means that the tear does not advance easily near the surface, leaving a near-surface ligament, which retards that advance, despite tearing advancement in the central part.

Figure 34b shows the plastic zone shape based on the von Mises yield criterion. Another method of estimating the shape of plastic zone is to use the Tresca yield criterion, which would result in a slightly larger size and different shape (Broek, 1986). Whilst Hertzberg (1996) used the shape of the crack tip plastic zone shown in Figure 34b, other shapes have been proposed in the literature as discussed by Broek (1986). Notably, both Broek (1986) and Schijve (2009) agreed that the shape of the plastic zone as proposed by Tuba (1966), which fans away from the crack tip (in the direction of crack growth), gives the best estimate. It should also be noted that Bathias and Vancon (1978) concluded VA tearing can be associated with the later plastic zone shape.

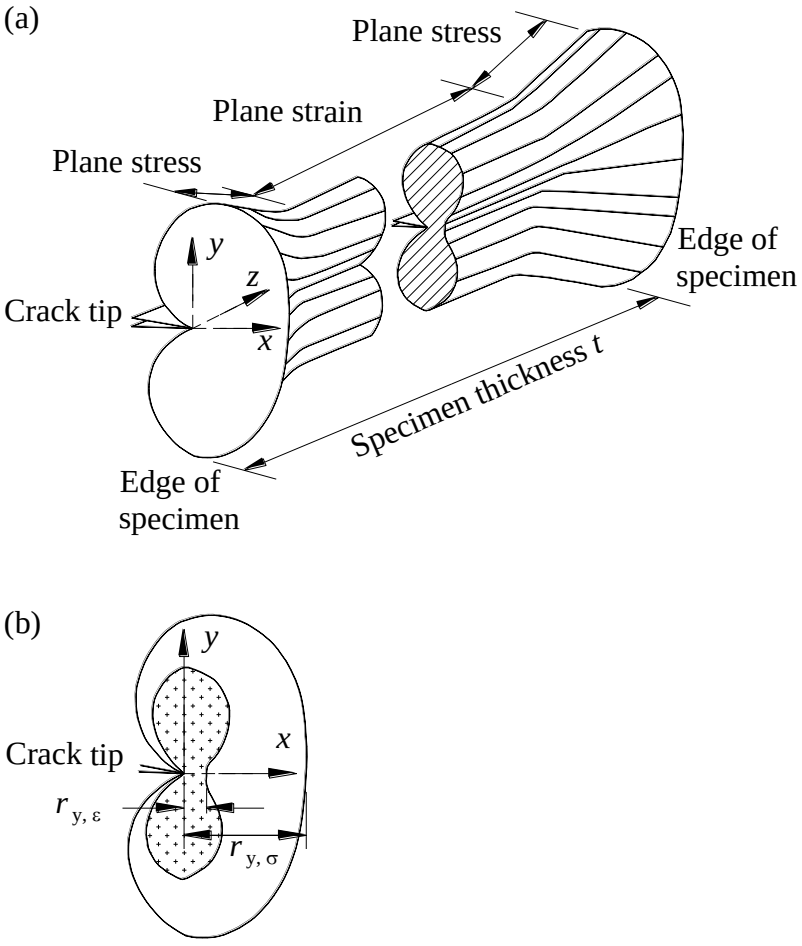

Figure 34. The two main characteristics of the crack tip plastic zone: (a) the shape of the monotonic plastic zone for Mode I (tensile) crack growth at the tip of a through crack, based on von Mises yield criterion; and (b) the theoretical size of plane stress and plane strain plastic zones (adapted from Stephens *et al*. (2001)).

Several plastic zone size equations have been proposed in the literature that relate to the extent of tearing jump in various metals. These formulas were modified to arrive at satisfactory correlation with the trends observed in test results. For instance, Ivanova (1982b) introduced a factor (denoted as ζ in Eq. (2)) that accounted for the

effect of ductility. Troshchenko and Pokrovskii (2003b) used the cyclic proportionality limit (denoted as σ_p^c in Eq. (14)) and suggested that there was a systematic relationship between the CA tearing crack jump length and the size of plastic zone in steels, and according to them, the crack jump length Δa can be estimated by Eq. (14). Other empirical evidence (Troshchenko and Pokrovskii, 1983a, 1983b; Troshchenko *et al*., 1978; Kitsunai, 1985, 1986; Bolotin, 1999a) has also emphasised the apparent relationship between the plastic zone size and the tearing crack jump length Δa.

The experimental results presented in section 4.1 are used to examine the relationship between the theoretical size of the plastic zone and the Δa for this particular alloy. It should be noted that previous empirical correlations between the Δa and the plastic zone size have been observed for CA tearing only. This study enables comparison to be made between the CA and VA tears. This analysis will also show whether the cessation of tearing occurs within the enclosed plastic zone that exists at the beginning of the tear or extends outside its theoretical size. In effect – does the crack resisting plane-stress zone provide some limit on the extent to which the central part of tear will advance?

The theoretical plastic zone size (at the initiation of tearing) is determined by Eqs. (2), (12), (14), (25) and (26), and the Δa data points are plotted as a function of r_y in order to evaluate any equation that can best describe the tearing data for this particular material. It is found that modification of Eq. (2) gives the best correlation with Δa, as illustrated in Figure 35. The modified plastic zone size formula is obtained as

$$\Delta a = \frac{1}{\pi}\left[\frac{K_{2D}(a_i + \Delta a)}{\frac{\sigma_Y + \sigma_U}{2}}\right]^2 \qquad (27)$$

In Eq. (27), the terms $K^R{}_{max}$ in the numerator and ($\zeta \times \sigma_Y$) in the denominator of Eq. (2) are replaced by $K_{2D}(a_i + \Delta a)$ and $\frac{\sigma_Y + \sigma_U}{2}$, respectively. It should be noted that the correction factor ζ in Eq. (2) can be assumed to be equal to 1 since the 7075 aluminium alloy is known for its low toughness (lack of ductility).

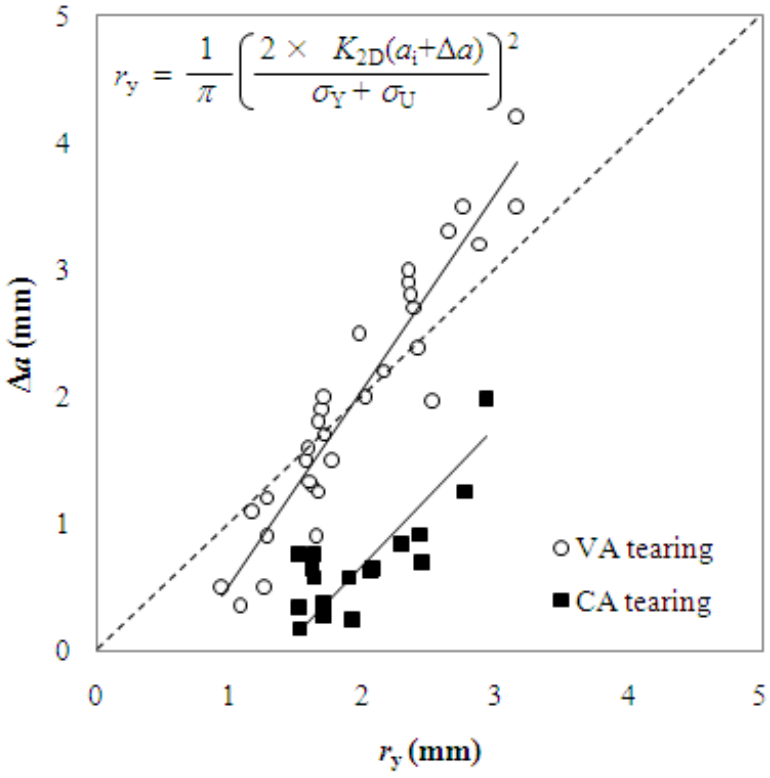

Figure 35. The relationship between the plane stress plastic zone size at the onset of tearing and the tearing jump length.

Figure 35 suggests that relationship between the plastic zone size and the CA tearing length is more complex than the tearing length under VA conditions. The non-unique relationship between the plastic zone size and the Δa under CA condition does not support the results of Troshchenko and Pokrovskii (2003b). On the other hand, the plot shows that in 7075 aluminium alloy, such a relationship *may* exist for VA tearing. It implies that the plastic zone size cannot be used directly to estimate Δa in 7075 aluminium alloy. Figure 35 suggests that the CA and VA tearing lengths increase as the size of the plastic zone increases. In addition to that, the plot also implies that as the crack progresses, the VA tearing jump length will extend beyond the theoretical plastic zone size ($r_y \geq 2$ mm), namely the cessation of tearing occurs outside the original plastic zone enclaves. This result is consistent with the observation that larger tearing is produced in VA rather than CA fatigue loading conditions, as reported in section 5.1.5. On the other hand, the CA tearing arrest in these tests always occurs within the initial plane stress plastic zone region. The reason for this smaller Δa *may* be associated with more opportunity in the CA case for developing a fracture-resistance or tearing-resistant plastic zone during the prior fatigue loading cycles, which also supports the trend observed in section 5.1.5. These conclusions, however, may only apply to the aluminium alloy 7075, as Hudson and Hardrath (1963) have shown that prior loading history could affect the size of subsequent tearing in aluminium alloy 2024-T4. In addition to that, the cessation of tearing could also be related to the crack front line length, as Bowen and Forsyth (1977, 1978) found that (in 7178-T6 aluminium alloy) an increase in 20% of crack front line length could cause a 30% reduction in ΔK. It seems likely, however, that crack front line length is more likely to be a consequence of the stress/strain and fracture conditions driving tearing.

5.1.7. Resistance curve

Slight variation in the shape of the *R*-curve (as shown in Figure 18a), as the crack progresses can be due to the difference in the initial crack front shape (Petrak, 1972) and the amount of crack deviation from the mid-plane (Cotterell, 1970). ASTM E 561 (2009) recommends that that crack deviation is limited ± 10º from the machined notch. A similar observation was reported by Schwalbe and Setz (1981), and they added that this characteristic was not observed in 2024-T3 or 7475-T761 aluminium alloys, which implied that this scatter could be due to the material property. This is supported by the SEM images in Figure 24 and Figure 26, which show that the distributions of intermetallic particles are uneven. Anderson (2005) stated that the K_R versus a_p plot for this particular thickness specifies the *K*-value at which ductile tearing commences. The results of this study show that the *K*-value at which ductile tearing starts is approximately equivalent to the first onset stress intensity factor for VA tearing. The tearing data from section 4.1 can be plotted onto the K_R versus Δa_e plot by using a technique proposed by Liu *et al*. (2005). The r_y is determined by substituting $K_{2D}(a_i)$ into Eq. (12) and a correction is used in this analysis to account the effect of crack front curvature (Liu *et al*., 2005).

In this analysis, a simpler approach is used by multiplying the Δa of stable tearing with the relative difference between the crack front line lengths at onset and arrest of each tear, namely

$$C = \frac{l(a_i + \Delta a) - l(a_i)}{l(a_i + \Delta a)} \tag{28}$$

Similar to Liu *et al*. (2005), the change in effective crack length Δa_e of static tearing can be defined as

$$\Delta a_e = \Delta a \times C + r_y \tag{29}$$

The $K_{2D}(a_i + \Delta a)$ versus $(\Delta a \times C + r_y)$ for CA and VA tears are plotted onto the K_R versus Δa_e plot (*R*-curve for static case), as depicted in Figure 36. It should be noted that this plot is obtained by multiplying each Δa with its corresponding *C*. The result shows satisfactory agreement with the *R*-curve, except for VA tearing with large Δa, which deviates from the trend of *R*-curve as the crack progresses. The small scatter is due to large differences between the crack front line length at arrest and onset. There are also five data points ($\Delta a \times C + r_y > 1.5$ mm) that fall beyond the range of the *R*-curve. In fact, the static *R*-curve for the high range of Δa is unavailable because the data points violate the crack deviation requirement.

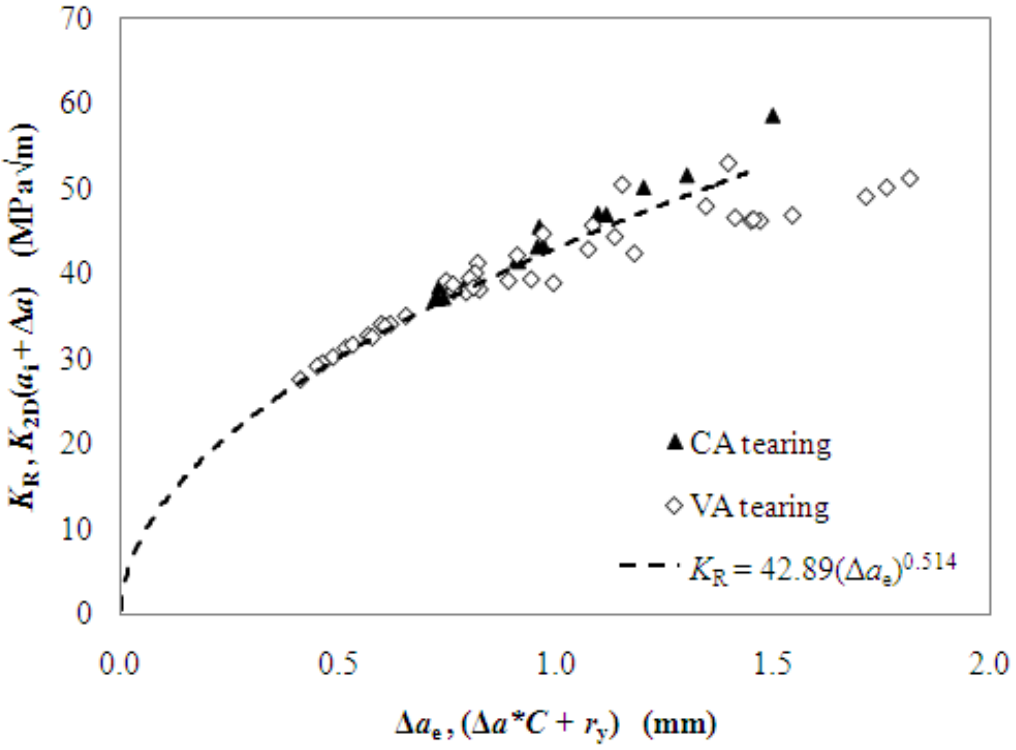

Figure 36. The combined *R*-curve and scatter of tearing jump length. The Δa values are corrected by individual *C*.

An alternative approach is to use an average *C*, as proposed by Liu *et al*. (2005) to represent a generic correction factor for stable tearing occurrence in specific thickness. With an average of about 0.13, a closer agreement can be achieved as illustrated in Figure 37. Therefore, by utilising Eq. (23) and for C = 0.13, the tearing data can be approximated by the following relationship

$$K_{2D}(a_i + \Delta a) = 42.89(\Delta a \times C + r_y)^{0.514} \qquad (30)$$

Eq. (30) suggests that given both $K_{2D}(a_i)$ and C, Δa can be estimated through some regression analysis. It implies that the *R*-curve approach can be used to estimate the

Δa of both CA and VA tearing, as opposed to the results of Liu *et al*. (2005). This approach, however, may have two limiting factors, namely the determination of the *R*-curve and the use of correction factor *C* that can represent a range of thickness of a material. It has been established that the *R*-curve is very dependent on the thickness of the material (Heyer and McCabe, 1972), and therefore estimation of Δa is only possible on an *R*-curve of equivalent thickness.

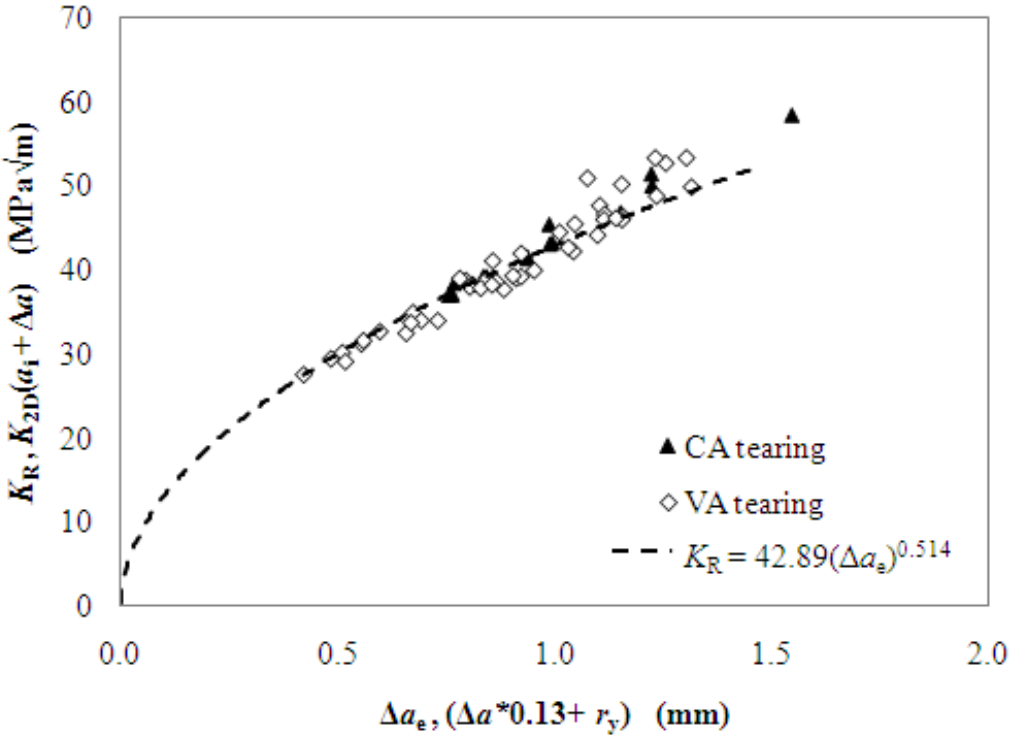

Figure 37. The combined *R*-curve and scatter of tearing jump length. The Δa values are corrected by an average *C* of 0.13.

The *C*-value can only be determined from fracture surface measurement, but for engineering simplicity, it can be assumed to be constant, as proposed by Liu *et al*.

(2005) and further substantiated by this study (as shown in Figure 38). Both of these limitations are further analysed by using empirical results of Vlasveld and Schijve (1979, 1980) for 6.35 mm and 12.7 mm thick aluminium alloy 7075 aluminium alloy. Eq. (30) has been rearranged to estimate the predicted Δa, and the results are plotted in Figure 38, where $C = 0.13$ has been used for all thicknesses. For the present results, the predicted Δa and measured Δa are in good agreement for small tears, and the predicted Δa overestimates the measured Δa as the tear size increases. This deviation can be due to the limitation of *R*-curve, which has been developed according to LEFM conditions.

Figure 38 also shows that the prediction Δa is in good agreement with the measured Δa for 6.35 mm thick specimen, but relatively poor correlation for thickness 12.7 mm. Besides the effect of thickness and the *C*, the scatters in these results can also be due to the fact that all of the data used in this comparative analysis have substantially large Δa, whilst the *R*-curve developed in this study does not include these high ranges of Δa as the static data already violates the LEFM conditions.

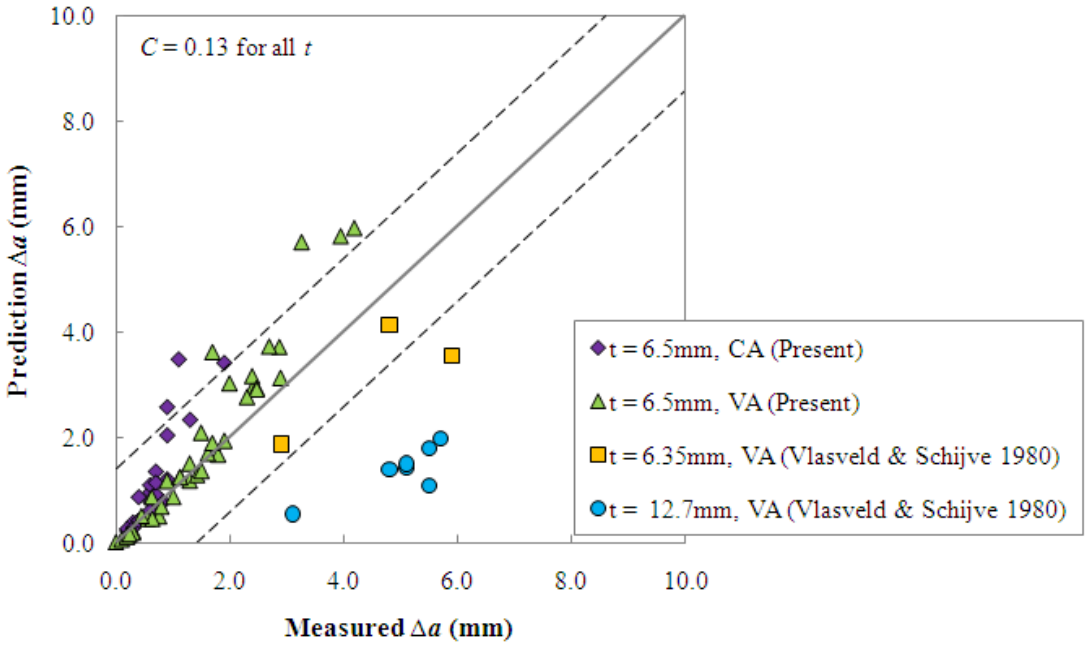

Figure 38. Comparison between the model prediction by *R*-curve method and the measured Δ*a*, for similar type of aluminium alloy but with different thicknesses, with *C* = 0.13. The solid line is the line of equal relation and dashed lines indicate ± 1.0 mm error.

The overall results also show that both data points are distributed in such a way that their clusters are approximately parallel to the line of equal relation. It implies that appropriate adjustments to the value of *C* for specific thickness may result in better correlation, as suggested by Liu *et al*. (2005). In this particular case, an improved correlation can be observed if *C* = 0.10 and 0.05 are used for 6.35 mm and 12.7 mm thick data points, respectively, and the results are shown in Figure 39. The observed discrepancy between the measurements and model predictions may also be due to neglecting the thickness effect on the shape of the *R*-curve, but this effect can be compensated by proper adjustments of the *C*-value.

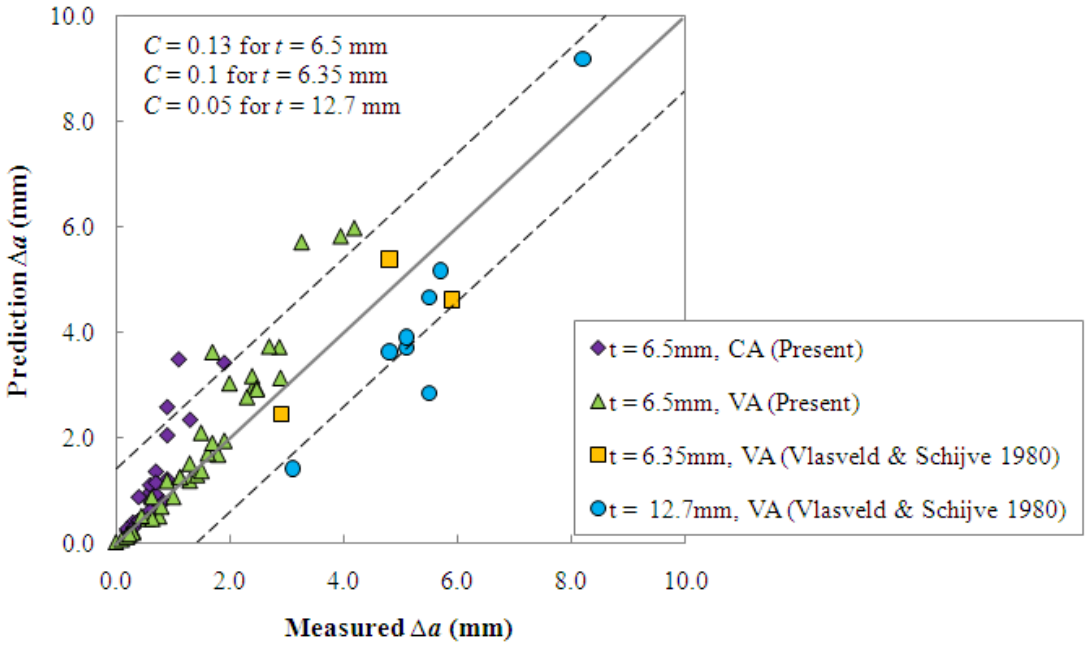

Figure 39. Comparison between the model prediction by *R*-curve method and the measured Δa, for similar type of aluminium alloy but with different thicknesses, with specific *C*-value for each thickness. The solid line is the line of equal relation and dashed lines indicate ± 1.0 mm error.

Therefore, it can be concluded that the *R*-curve method is viable to predict the stable tearing jump length Δa, especially for relatively small Δa. However, this technique is very dependent on the type of material, thickness of the specimen and to some extent the correction factor to account for the effect of crack front curvature *C*. Another noteworthy conclusion is that this result further substantiates the notion that there are some similarities of crack growth behaviour between the static and fatigue conditions, as reported in the literature (Schwalbe, 1979).

5.1.8. Evaluation of the existing predictive models

In Chapter 2, it has been established that stable tearing is a very significant technical issue during the fatigue crack growth assessment of the post-failure analysis of fracture surfaces or quantitative fractography. The ability to predict the tear behaviour in various aluminium alloys is presently limited to estimating the conditions for the first onset of stable tearing (Molent, 2010) and, more importantly, does not enable prediction of the jump in crack length. Stable tearing is also not included in fatigue predictive models, and so the presence of significant tearing can greatly complicate the derivation of a crack growth history which can be matched to a crack growth model. An ability to integrate the stable tearing model into overall fatigue life prediction models would therefore be a major advance in fatigue crack growth prediction capability and accuracy.

Several theoretical models have been proposed for analysing stable tearing, but an important aspect to be recognised is that these theoretical formulations have not yet been developed to the point of being useful candidates for engineering analysis of fracture surfaces. Another complication is that constants in these theoretical formulations depend on the type of material, and there is no standardised experimental method to determine these constants. In addition to that, experimental techniques used by researchers have been rather complicated and time-consuming.

For aluminium alloys, two notable empirical models have been proposed. Byrnes *et al*. (2000) examined the models of Forsyth and Schijve, using specimens with various thicknesses, and concluded that the model of Forsyth, which utilised the change in crack front length as the main controlling parameter at onset and arrest of

CA tearing, appeared to give reasonably good agreement with the experimental observations. In relation to the Schijve model, they noted that it gave poorer agreement than the Forsyth model, and also highlighted the relative complexity of the Schijve approach, in which one particular issue was that the determination of variable α, namely the angle of the restraining ligament made to the specimen's side, in Eq. (10), is not a straight-forward procedure. For simplification and greater accuracy, Vlasveld and Schijve (1979, 1980) had determined α based on the measurement of tearing on 12.7 mm thick specimens, and assumed this parameter to be a constant. Ab Rahman *et al*. (2010b) reported that the α is not a constant and varies significantly for different tearing cases, which may explain the poorer correlation between the Schijve model prediction and the results of Byrnes *et al*. (2000).

Although extensive research has been carried out on stable tearing, no single study exists which adequately covers the prediction of stable tearing jump length. Besides an attempt made by Liu *et al*. (2005), previous studies have not dealt with the simulation aspect of stable tearing. However, much of the research up to now has been descriptive in nature, and qualitatively, it can be established that stable tearing has mainly occurred in material of intermediate thickness and therefore is more important in engineering practice. This also implies that stable tearing in very thick or thin specimen lacks practical interest because they are either very unstable or involve plasticity, respectively.

Extensive analyses have been conducted to understand stable tearing characteristics in steels. The Troshchenko model, in particular, is shown to provide a good prediction of fatigue crack growth and stable tearing growth up to the final unstable failure. The application of this model, however, is limited to thick steel being

tested at very low operating temperatures. In this case, the similarity principle and the physical meaning of K can still be justified. The application of the Troshchenko model in aluminium alloy is rather limited due to two main reasons: (i) the occurrence of stable tearing in aluminium alloys is often observed in intermediate thickness materials, and hence the application of the K criterion must be checked against the small-scale yielding conditions, as shown in section 4.3; and (ii) the critical K at the first onset of tearing in aluminium alloys is equivalent to the K_{Ic}, and although this condition is retained by the crack front in the mid-thickness region, the final unstable failure is prevented by material at near surface (in plane stress). Several functions have been proposed to estimate Δa in steels, but these empirical equations are calibrated with experimental results, and hence their applications are rather limited.

5.2. New concept and parameters of stable tearing

In development of this new model, the term stable tearing crack jump length Δa has been defined as the difference between the measured crack length (at the specimen centre) at stable tearing arrest and onset. The stable tearing structural model (in Figure 40) idealises the crack front at the arrest of stable tearing as two straight sections; (1) the central portion of the crack front that is perpendicular to the specimen surfaces, and (2) the inclined segments that separate the tearing area from the unbroken ligaments.

With this model, the tearing arrest is assumed to occur when the stress intensity factor K at the central straight portion of the crack front is equal to the plane-strain fracture toughness K_{Ic}. Arrest is associated with a condition where any further increase in jump length is resisted by the remaining ligaments near the specimen surface, and would result in a reduced K. The trapezoidal shape of the tearing arrest front is characterised by two parameters, the crack jump length Δa and the frontal width b.

Determination of these two variables requires a unified fracture criterion that can account for the transition from plane stress to plane strain and the complex elastic-plastic deformation of the unbroken ligaments. Due to the lack of a validated, unified fracture criterion (to be discussed in section 6.3), here a semi-analytical model is proposed, consistent with a key observation, described below, concerning the tearing arrest crack front.

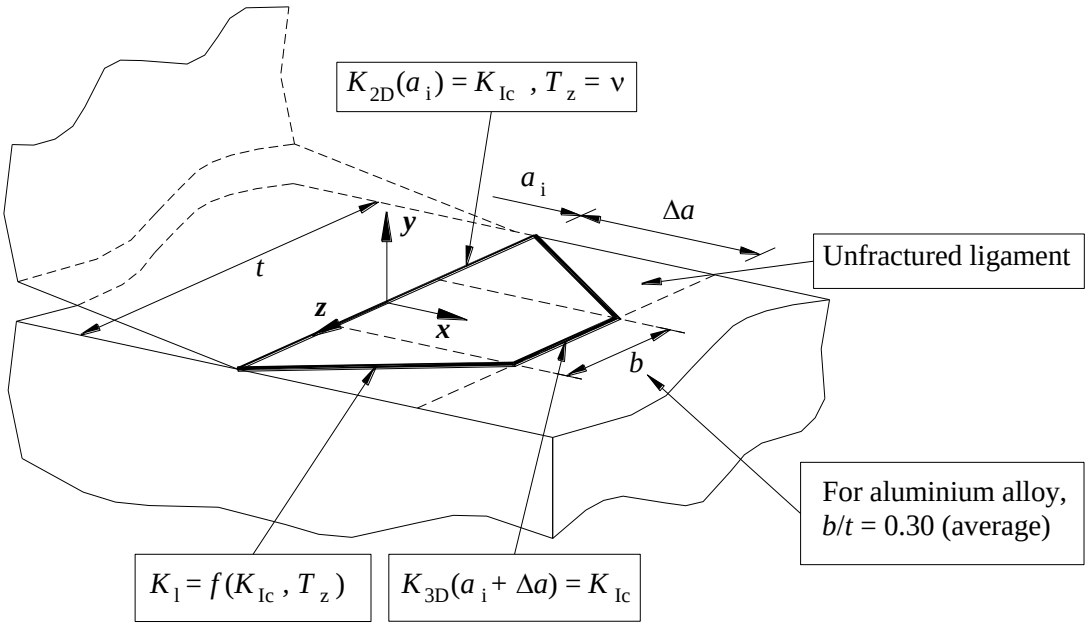

Figure 40. A structural model for stable tearing in aluminium alloy indicating the fracture conditions of stable tearing onset and arrest.

A detailed examination of the large number of experimental results obtained by various authors seems to indicate that the ratio between the area of stable tearing band A_c and the area of the unbroken ligament (indicated as A_l in Figure 16b) is approximately constant. Alternatively, the ratio of the stable tearing band A_c and the area A_l bounded by $x = a_i$ and $x = a_i + \Delta a$, referring to Figure 16b, is close to constant. A summary of the areal ratio $\frac{A_c}{A_c + A_l}$ calculated from the present investigation and a large number of experimental data reported in the literature is given in Table 13.

Table 13. Detailed examination of stable tearing on various aluminium alloys.

Material	t (mm)	No. of tears	$\frac{A_c}{A_c + A_l}$ (average)	$\frac{b}{t}$ (average)	Source
7075-T651	6.5	71	0.65	0.30	Present results
7075-T6	10	4	0.68	0.36	Vlasveld and Schijve (1980)
7075-T651	12.7	3	0.62	0.24	
7075-T7	12.7	2	0.61	0.22	
2024-T3	10	3	0.62	0.24	
7050-T7451	3	7	0.62	0.24	Liu *et al*. (2005)
	6	4	0.63	0.26	
	9	3	0.66	0.32	
7178-T6	4.5	10	0.64	0.28	Forsyth (1976)
2618	10	3	0.65	0.30	Bathias and Vancon (1978)
2024	10	2	0.67	0.34	
7075-T6	5	4	0.65	0.30	Vardar and Yildirim (1990)
7050-T7451	6	6	0.65	0.30	Byrnes *et al*. (2000)
	12	4	0.65	0.30	
	12.5	4	0.68	0.36	
	25	3	0.70	0.40	
Average			0.65	0.30	

Table 13 lists the areal and width ratios for a large number of stable tearing reported in the literature, for a range of thicknesses and aluminium alloys. It also lists the average of these parameters from the present study. The tears from the literature were produced under either CA or VA conditions. As highlighted in the literature

review, most of the specimens' thickness can be categorised as intermediate, whereby substantial interactions between the plane strain and plane stress conditions can therefore be expected to occur during the formation of each tearing. A very thin (3 mm) and thick (25 mm) specimen was included for comparison purposes. The tears in the thick material were produced on a single CT specimen, exposed to a constant-ΔK loading conditions (through load shedding) and each tear was produced at $K_{2D}(a_i)$ of slightly less than the K_{Ic}. It implies that tearing in thick specimens is less stable and does not conform to the critical conditions of $K_{2D}(a_i) = K_{Ic}$.

It can be seen from the data presented in Table 13 that the areal ratio is approximately constant, namely,

$$\frac{A_c}{A_c + A_l} = \frac{b+t}{2t} \approx 0.65 \text{ (average)} \tag{31}$$

According to Eq. (31), this constant areal ratio is equivalent to a constant frontal width ratio $\frac{b}{t}$, which has an overall average approximately equal to 0.30; individual values for $\frac{b}{t}$ are also listed in Table 13. The constancy of width ratio $\frac{b}{t}$ indicates that the depth of plane stress penetration from the free surface is approximately constant, similar to the assumption used in the Schijve model (Vlasveld and Schijve, 1979, 1980) to derive the slope factor associated with the plastically deformed ligament. It is also important to note that the constant $\frac{b}{t}$ ratio is mostly observed in aluminium alloys, which can be categorised as having intermediate thickness as listed in Table 13.

A comparison between the actual shapes of stable tearing and the proposed model is shown in Figure 41. The three stable tears were produced under similar background fatigue loading of ΔP = 1.8 kN, but at increasing overloads P_{OL}, which are 4.50 kN, 4.75 kN and 4.99 kN respectively. The $\frac{\Delta a}{t}$ ratios for these three stable tears are determined from the fracture surface to be equal to 0.23, 0.32 and 0.64 respectively. The shape of the proposed stable tearing model resembles very closely the actual geometry of the stable tearing crack front. For these three stable tearing jump lengths, the frontal width ratio $\frac{b}{t}$ is approximately the same and equal to 0.30.

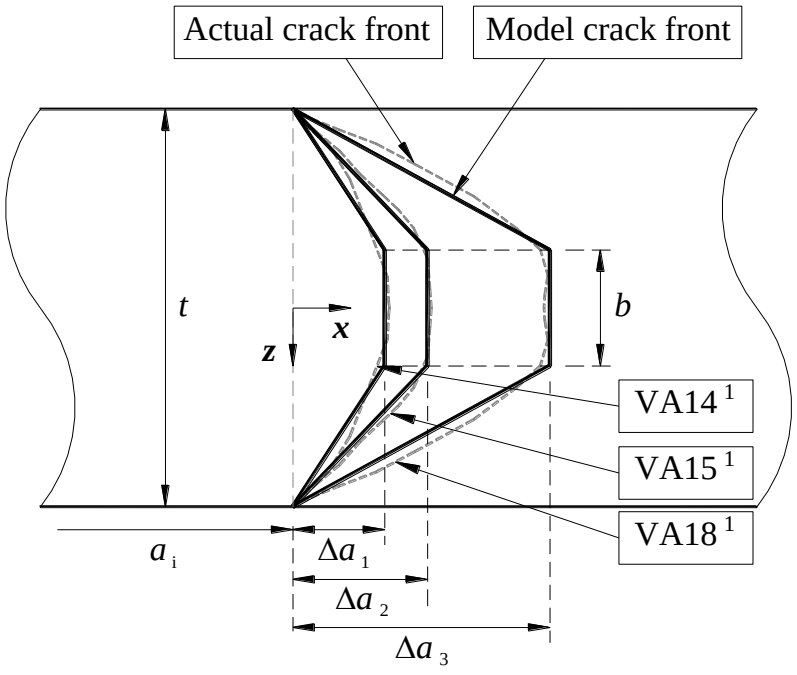

Figure 41. Comparison between actual shapes of stable tearing and the model in FE analysis. The crack grows from left to right.

5.3. Fracture conditions for the new model

The fracture condition at onset of tearing has been discussed in section 5.2. The onset of tearing is assumed to occur at the stress intensity factor value that is equivalent to fracture toughness of the material. The fracture condition at the arrest of stable tearing can be expressed as:

$$K_{3D}(a_i + \Delta a) = K_{Ic}, \quad \text{for } |z| \le \frac{b}{t} \tag{32}$$

For the stable tearing crack model shown in Figure 40, the stress intensity factor at the straight portion of the crack front $K_{3D}(a_i + \Delta a)$ depends on two non-dimensional parameters: $\frac{\Delta a}{t}$ and $\frac{b}{t}$,

$$\frac{K_{3D}(a_i + \Delta a)}{K_{2D}(a_i)} = H\left(\frac{\Delta a}{t}, \frac{b}{t}\right) \tag{33}$$

where the functional relationship H can be determined using the finite element method. Details are presented in the next section.

Along the inclined portion of the crack front, the stress intensity factor depends on the level of triaxial stress constraint parameter T_z, which is defined by (Guo, 1993),

$$T_z = \frac{\sigma_{zz}}{\sigma_{yy} + \sigma_{xx}} \tag{34}$$

where σ_{zz}, σ_{yy} and σ_{xx} are the stress components in the coordinate system shown in Figure 42a and b. Theoretically, the T_z is a function of specimen thickness, namely $T_z = f(t)$, and is equivalent to the Poisson's ratio v under plane strain conditions and equal to zero under plane stress conditions (Guo, 1993). The T_z has been used extensively to describe the stress state for elliptical cracks (Shen and Guo, 2005; Zhang and Guo, 2007; Yu *et al*., 2008), and is further employed by this study to characterise the stress state in stable tearing crack front curvature. Due to the loss of the through-thickness constraint along the inclined segments, the T_z-value drops below the plane strain value. Hence the plane strain condition exists predominantly at the flat crack front of the stable tearing arrest.

At the inclined section of the crack front at stable tearing arrest, the T_z should increase from zero at the free surface to Poisson's ratio v at the centre of the specimen. Along the inclined segments, the critical stress intensity factor is dependent on the constraint, but a unified criterion is not available. This new finding that the width ratio $\frac{b}{t}$ is approximately constant for a range of component thickness, between 4 mm to 24 mm, as presented in Table 13, forms the basis of a new semi-analytical predictive model for stable-tearing. The functional relationship H in Eq. (33) can be determined, once for all conditions, using the FE method by varying the ratio of $\frac{\Delta a}{t}$ while the width ratio $\frac{b}{t}$ is kept constant. It should also be noted that the idealisation of stable tearing shape into a trapezoid-like geometry also makes it easier to determine the K-value at tearing arrest from the FE analysis. As discussed in section 5.1.4, significant crack front curvature can be observed in large Δa. Details of this investigation will be

described in section 5.4. Alternatively, the proposed stable tearing model can be combined with the Forsyth and Schijve models to yield improved predictive algorithms, and this will be discussed in Chapter 6.

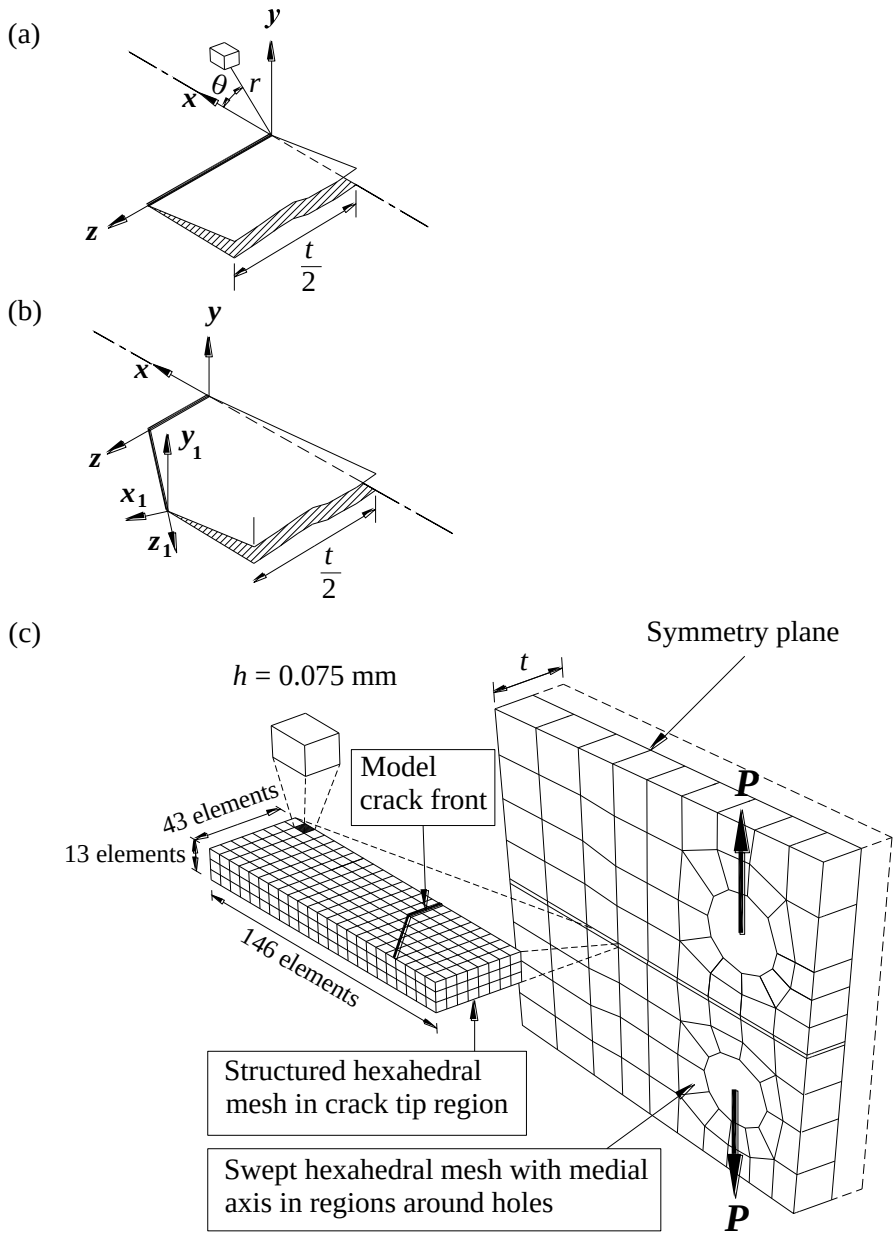

Figure 42. Definition of coordinates for (a) straight crack front and (b) model crack front; and (c) details of FE model and its mesh configuration.

5.4. Computational method for determining parametric relationship

5.4.1. Finite element model

To determine the functional relationship H in Eq. (33), a finite element model was created using Abaqus version 6.9 (2009). In order to effectively model the effect of crack front curvature to the through thickness stress intensity factor, a three-dimensional (3D) model was required. The FE model was a CT specimen with thickness equal to the half-thickness of the actual specimen (t = 6.5 mm) and the initial-crack-length-to-specimen-width ratio $\frac{a_i}{W}$ of 0.5 (W = 40 mm).

The solid model had a 3D modelling space, the type was deformable and its base feature was solid and extruded. The rectangle drawing tool was used to draw a rough approximation of area of the CT model, while constraints and dimensions were used to refine the CT model according to the required size. Two circles were drawn on the sketch of the CT model to represent the loading holes. The vertical distance between the centre of the circle and the perimeter point was set to zero in order to achieve high-quality mesh (Abaqus, 2009). The sketch of CT model was then extruded to the depth of 3.25 mm (half-thickness).

The material was assumed to be a homogeneous solid section with properties typical of a 7075 aluminium alloy, as shown in Table 3. The FE model was subjected to monotonic loading, while the crack front was held stationary. Loading was simulated by applying pressure on the upper and lower surfaces of the top and bottom of the loading holes, as shown in Figure 43. The pressure was determined based of a uniform distribution of stress acting on the top and bottom areas of the loading holes (Flabel, 2005), given by the following,

$$\text{Pressure at loading holes} = \frac{P_{OL}}{D \times t} \tag{35}$$

where P_{OL} is the applied overload, D is the diameter of the loading holes and t is the thickness. Flabel (2005) noted that the actual stress function is more complex and indicated that the Eq. (35) is sufficient to represent the loading condition.

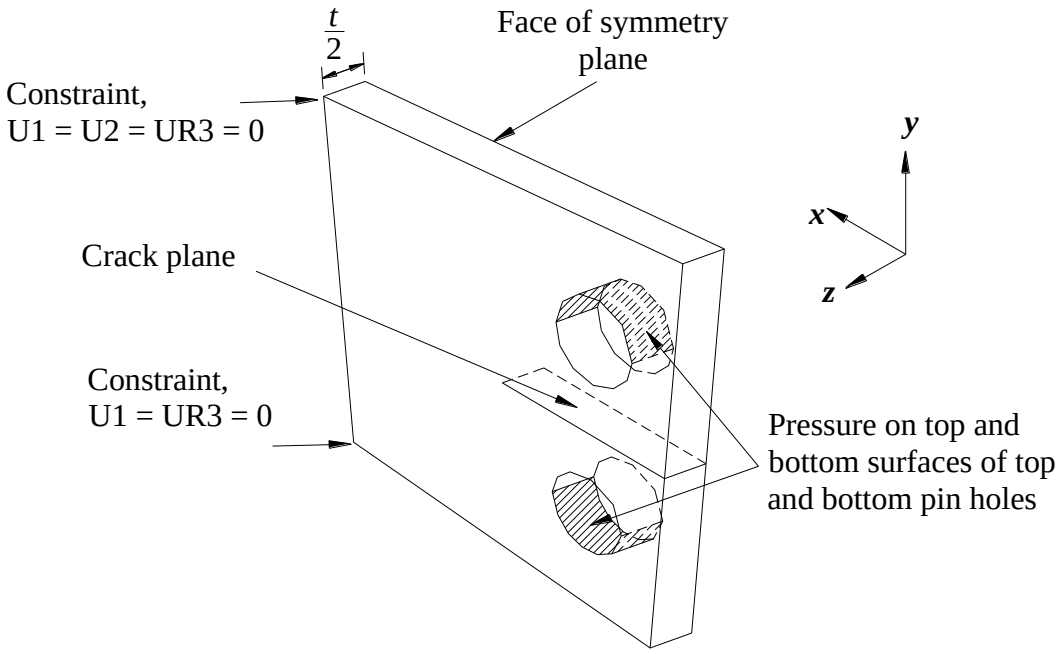

Figure 43. Loading and constraints of the solid model.

Figure 43 also shows the constraints applied to the FE model. Appropriate boundary condition was imposed to the plane of symmetry. The bottom edge at the free end of the model was fixed from moving in the *x*- (U1 = 0) and *y*- (U2 = 0) directions, and rotating in the *z*-axis (UR3 = 0), where *U* is the displacement. The top

edge at the free end of the model was constraint from moving in the *x*-direction (U1 = 0) and rotating in the *z*-axis (UR3 = 0). The local coordinates for straight and stable tearing crack fronts are shown in Figure 42a and b, whilst some details of the FE model are shown in Figure 42c.

The solid model was partitioned into 11 sections. The edge of each partition was seeded, and the number of seeds was based on either, the desired element size in the partition that contained the crack tip, or on the minimum required number of elements, so as to control the total number of mesh elements in order to minimise the time needed for simulating the model. The crack tip was enclosed within a small volume of high density mesh elements. The size of the smallest cubic element *h* in the crack front volume for fully elastic condition was 0.075 mm, which was adequate to comply with the mesh requirement condition indicated by Lei (2008). The mesh elements were represented by an 8-node linear brick (type C3D8R) with reduced integration and hourglass control.

The ratio of the smallest element size to crack length $\frac{h}{a}$ was $\frac{3}{800}$, which is significantly finer than the ratio used by Liu *et al.* (2005) and Shi *et al*., (2010). For example, Liu *et al*. (2005) used $\frac{h}{a} = \frac{2}{105}$ for similar analyses. There were 139,750 elements for the mesh configuration used, as shown in Figure 42c. The crack tip stress field was calculated using the extended finite element method (XFEM). The crack was modelled as a shell element and then assembled together with the solid model. The crack was assigned as an edge crack, and the XFEM Crack Growth was selected as an analysis procedure.

The main advantage of XFEM is that it allows alteration of the crack front profile without the need to change the mesh of the FE model (Abaqus, 2009), namely the mesh configuration is independent of the crack. This method was established by Belytschko and Black (1999), who introduced enrichment functions to represent displacement jump across crack face and singularity. The introduction of this computational technique is considered to be an important achievement in computational fracture mechanics (Abdelaziz and Hamouine, 2008) and is being applied in various engineering problems (Abdelaziz and Hamouine, 2008; Fries and Belytschko, 2010).

The through-thickness three dimensional stress intensity factor K_{3D} was determined by using the stress method, as described by Anderson (2005). Paths were created from the coordinates along the crack front to the end of high density mesh volumes. The stress component in the *y*-direction (S11) was used to determine the K_{3D}, while the stress components in the *x*-, *y*-, and *z*-directions (denoted as S22, S11 and S33 in Abaqus, respectively) were used to determine the T_z. A similar method has also been used by Kwon and Sun (2000), who further noted that the advantage of this technique is that it is independent of through-thickness constraint conditions. The K_{3D} on the crack plane at every point along the crack tip is given the following expression,

$$K_{3D} = \lim_{r \to 0} \left[\sigma_{yy} \sqrt{2 \pi r} \right] \text{ at } \theta = 0 \qquad (36)$$

The σ_{yy} is the stress component normal to the crack plane; r is the distance from the crack tip in the x-direction; and θ is defined as in Figure 42a. The K_{3D} was estimated by plotting $\sigma_{yy}\sqrt{2\pi r}$ against r and extrapolating the curve to $r = 0$. The small-scale yielding conditions are studied by using a similar model under elastic-plastic condition, and the numerical result for $\frac{\Delta a}{t} = 0.64$ is shown in Figure 44.

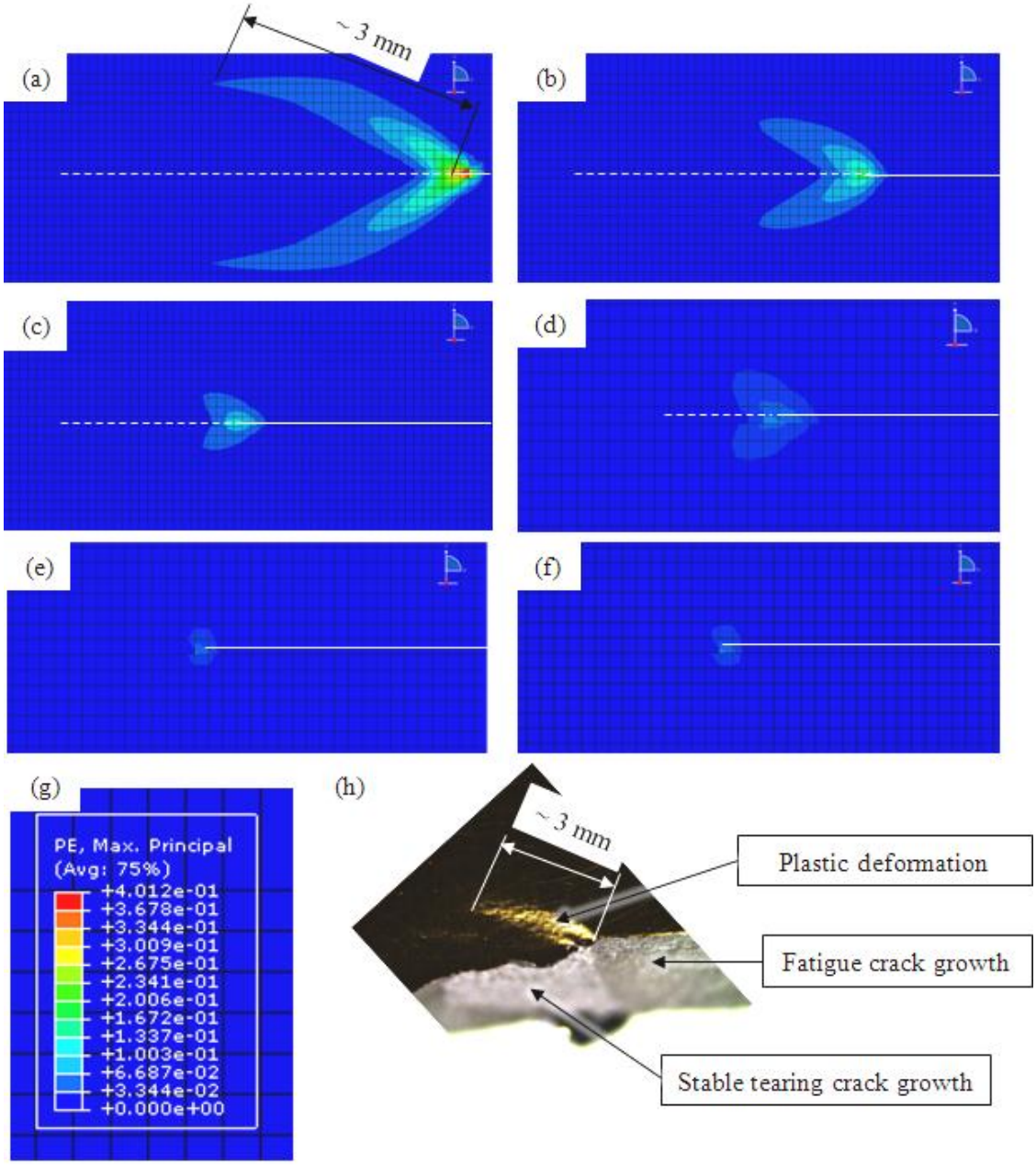

Figure 44. The through-thickness maximum principal strain along the inclined crack front ((a) to (d)) and flat crack front ((e) and ((f)): (a) z = 3.25 mm, at free surface, (b) z = 2.60 mm, (c) z = 1.95 mm, (d) z = 1.30 mm, (e) z = 0.65 mm, (f) z = 0 mm, mid-thickness, (g) legend, (h) physical observation of plastic deformation. Size of element is 0.09 mm. The crack grows from right to left.

Figure 44 shows that:

(i) The computed shape of plastic strain (Figure 45a) is generally comparable to the shape of plastic zone as proposed by Tuba (1966) and also similar to the shape of plastic deformation on the side of specimen during overload (Figure 45h). It can also be shown that the size of this deformation and the angle it made to the crack line (shown in Figure 45 as a horizontal line) are approximately equivalent.

(ii) Figure 45a to d show the plastic strain along the inclined crack front. The maximum distance of plastic strain in front of the crack tip (in the forward direction) is 3.0 mm and is less than Δa (= 4.2 mm). This implies that the plastic strain is contained within the ligament area (or volume).

(iii) Figure 45e and f show the plastic strain along the flat crack front. The size of plastic strain is about 0.20 mm, which is slightly less than the plastic zone size determined based on the fully-elastic analysis, estimated at 0.28 mm.

In actual, high plastic strain at the free surface causes the crack to deviate. The current application of XFEM is not yet able to simulate this condition (crack deflection/branching), while it is a formidable task to use contour integrals to model this condition in FE. Another notable conclusion is that this result supports the use of K in stable tearing analyses (Vlasveld and Schijve, 1980; Bowen and Forsyth, 1981; Glinka *et al*., 1984) and in various fatigue crack growth retardation models following overloads, such as proposed by Wheeler, Willenborg and Elber (Schijve, 2009b).

5.4.2. Verification of finite element model

5.4.2.1. Straight crack front

To validate the FE model, computational analysis was carried out for the special case of a straight-front crack, with the results being compared against available solutions. In this case, it is known that, due to the plane strain condition prevailing near the centre of the specimen, the stress intensity factor, denoted here by a subscript 3D, is greater than the plane stress solution from two-dimensional analysis. The ratio can be expressed in terms of the Poisson's ratio of the material (Kwon and Sun, 2000),

$$\frac{K_{3D}}{K_{2D}} = \sqrt{\frac{1}{1-\nu^2}} \quad \text{for } \Delta a = 0 \tag{37}$$

Two different meshes were employed in the present study, comprising 10 and 43 slices of through-thickness elements, as shown in Figure 45. In general, the results of the present study show that the K_{3D} is approximately constant all through the thickness except at the free surface. The ratio $\frac{K_{3D}}{K_{2D}}$ is in good agreement with Eq. (37). These results demonstrate that the current method can produce satisfactory estimation of K_{3D} at the mid-thickness region, namely $\frac{z}{t} \leq |0.4|$.

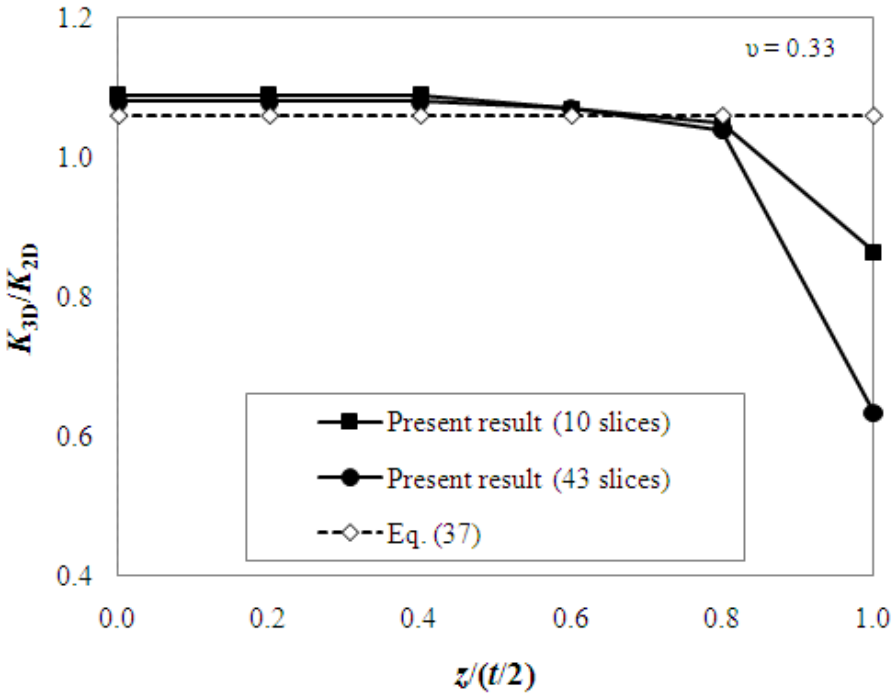

Figure 45. FE analysis of straight crack front (fully elastic condition) shows the dimensionless stress intensity factor inferred from the stress method.

The constant K_{3D} indicates that the plane strain condition dominates the $\frac{z}{t} \leq |0.4|$ range. This is supported by the normalised plot of the triaxial stress constraint parameter T_z as shown in Figure 46. It should be noted that all stress components were extracted along the path that was perpendicular to the crack front, in the coordinate system as defined in Figure 42a. Figure 46 also shows that the results of the present study support the notion that the $\frac{z}{t} \leq |0.4|$ range is indeed under plane strain condition and are in good agreement with the result of Guo (1995).

It is also important to note that at the free surface, the K_{3D} should decrease to zero, but it has been recognised by Kwon and Sun (2000) and Ortiz *et al*. (2006) that this condition is very hard to achieve even using very fine meshes. The sensitivity of

the K_{3D} at the free surface to the mesh refinement is consistent with the results of this study, which show that the K_{3D} at free surface is significantly reduced when the number of through thickness elements are increased from 10 to 43 slices.

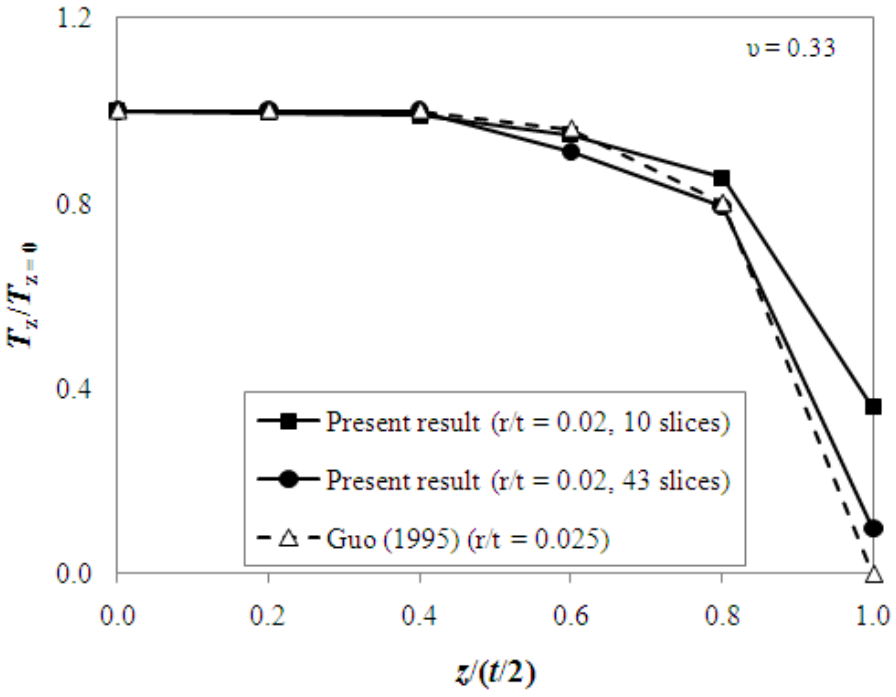

Figure 46. FE analysis of straight crack front analysis shows the normalised out-of-plane constraint for straight crack front at distance $r \approx \frac{t}{50}$ from the crack tip.

5.4.2.2. Curved crack front

The K_{3D} for three tearing shape factors as depicted in Figure 41 was estimated and compared to the results of Liu *et al*. (2005), who studied the K_{3D} distribution of the curved crack front in 6 mm and 12 mm 7050-T7451 aluminium alloy coupons. Figure 47a shows that the result of the present study at $\frac{\Delta a}{t}$ = 0.23 is in good agreement with that of Liu *et al*. (2005) at $\frac{\Delta a}{t}$ = 0.24. Figure 47b compares the K_{3D} at $\frac{\Delta a}{t}$ = 0.32 and $\frac{\Delta a}{t}$ = 0.64 from the present study and at $\frac{\Delta a}{t}$ = 0.44 from Liu *et al*. (2005), which further verifies the current FE model. It should be noted that the determination of K_{3D} close to the free surface is not possible due to lack of mesh element. Inspections of the computational results confirm the following observations:

(a) The mid-thickness region has constant K_{3D} values, which indicate that this region is under plane strain;

(b) Increasing $\frac{\Delta a}{t}$ will result in an increase of K_{3D} near the specimen surface to exceed the K_{3D} at mid-thickness. This result supports the physical observation of fatigue crack growth, whereby faster fatigue crack growth occurs at the free surface after each stable tearing jump; and

(c) Simplification of the stable tearing shape into a trapezoidal shape does not have a strong effect on the K_{3D} distribution.

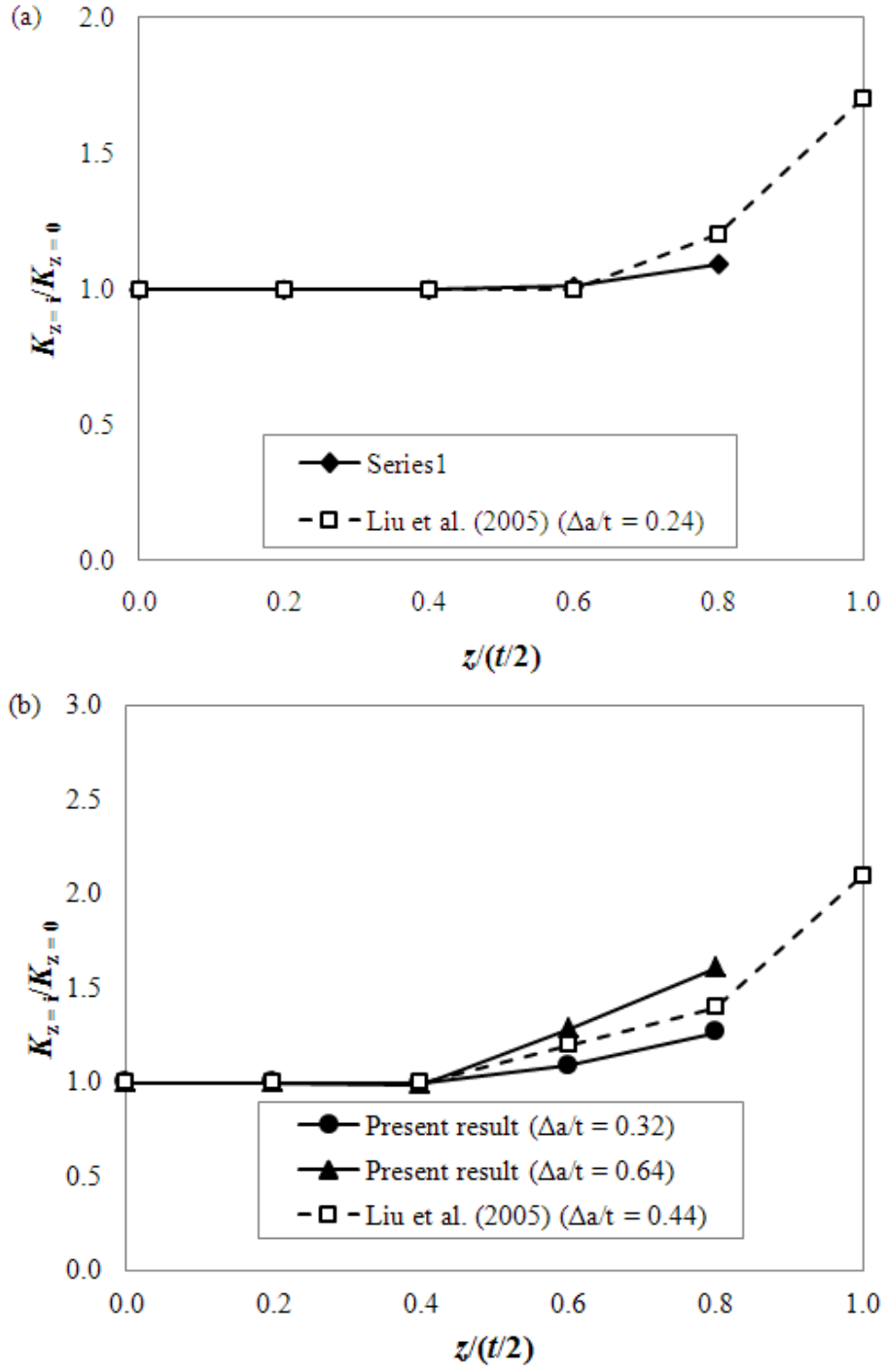

Figure 47. FE analysis (fully elastic) of various curved crack fronts at stable tearing arrest. Dimensionless through-thickness stress intensity factor of the present results and Liu *et al*. (2005) for, (a) $\frac{\Delta a}{t}$ = 0.23 and 0.24; and (b) $\frac{\Delta a}{t}$ = 0.32, 0.44 and 0.64.

Another important point to note is that the higher K_{3D} near the specimen surface is accompanied by lower through-thickness constraint factor T_z. The T_z value along the inclined segment of the crack front is shown in Figure 48. The parameter s is measured along the crack front from the centre line and l is the crack front line length, as illustrated in Figure 16a. It can be concluded that the T_z distribution for several curved-front profiles is quite similar to that for the straight front. In the following, the focus will be on the K-values at the mid-thickness region, where the plane strain region prevails and the K is shown to have a constant value. It should be noted that the value of T_z at the free surface is not included due to the problem associated with corner singularity (Zhao *et al*., 2007). It should also be noted that the plot of normalised K + T_z for three crack front profiles shows that these values are constant along the central portion of the crack front and varied along the inclined crack front, as shown in Figure 49.

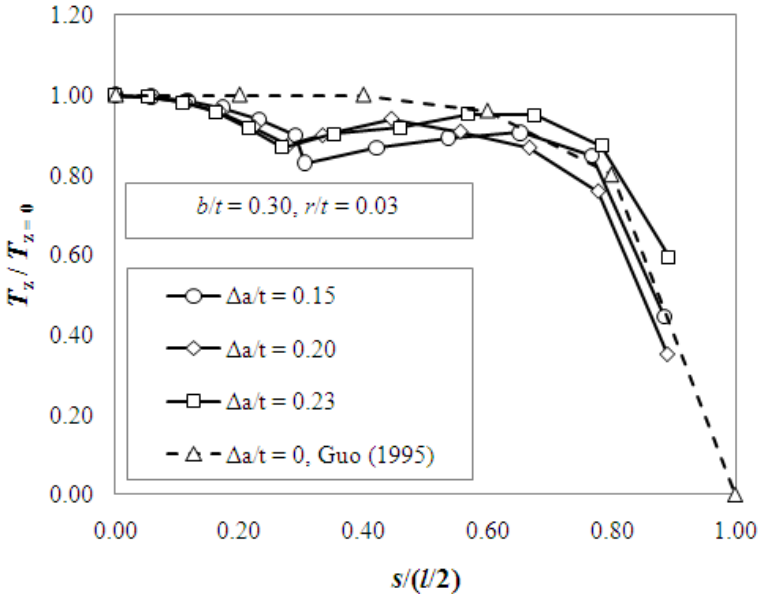

Figure 48. Numerical results of fully elastic condition comparing the T_z of straight- and the curved-fronts.

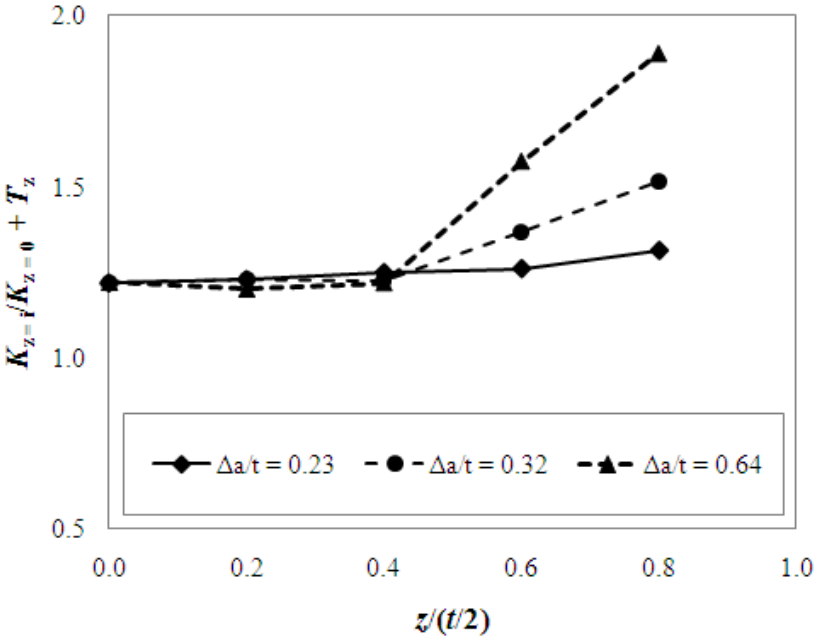

Figure 49. The plot of normalised $K + T_z$ for three crack front profiles.

5.4.3. Numerical solution

The computed K-values or K_{3D} at the mid-thickness ($\frac{z}{t} = 0$) for each stable tearing arrest in Figure 41 were normalised by the K-values at initiation. The K-values at initiation or K_{2D} are determined by using Eq. (15). The K_{2D} and K_{3D} basically represent the cracking conditions at the onset and arrest of stable tearing respectively. Figure 50 shows the plot of $\frac{K_{3D}}{K_{2D}}$ against the tearing shape factor $\frac{\Delta a}{t}$, at a $\frac{b}{t}$ ratio of 0.30. The data points at each $\frac{b}{t}$ ratio can be represented by linear relationship.

$$\frac{K_{3D}(a_i + \Delta a)}{K_{2D}(a_i)} = \sqrt{\frac{1}{1-\nu^2}} + \phi\left(\frac{\Delta a}{t}\right) \qquad (38)$$

where ϕ is a function of $\frac{b}{t}$ as depicted in Figure 50 and at $\frac{b}{t}$ = 0.30, ϕ = – 0.645. Eq. (38) also incorporates the relationship proposed by Kwon and Sun (2000) for the $\frac{K_{3D}}{K_{2D}}$ ratio of a straight-front crack, as indicated in Eq. (37) and implies that the K_{3D} decreases as the Δa increases, for a given load especially for $\frac{b}{t}$ < 0.9. It is hypothesised that this decrease leads to the tendency of the crack to arrest. In contrast, the K_{3D} increases as the Δa increases at $0.9 < b/t < 1.0$, which indicates that the tearing is *less* stable and that unstable failure is imminent.

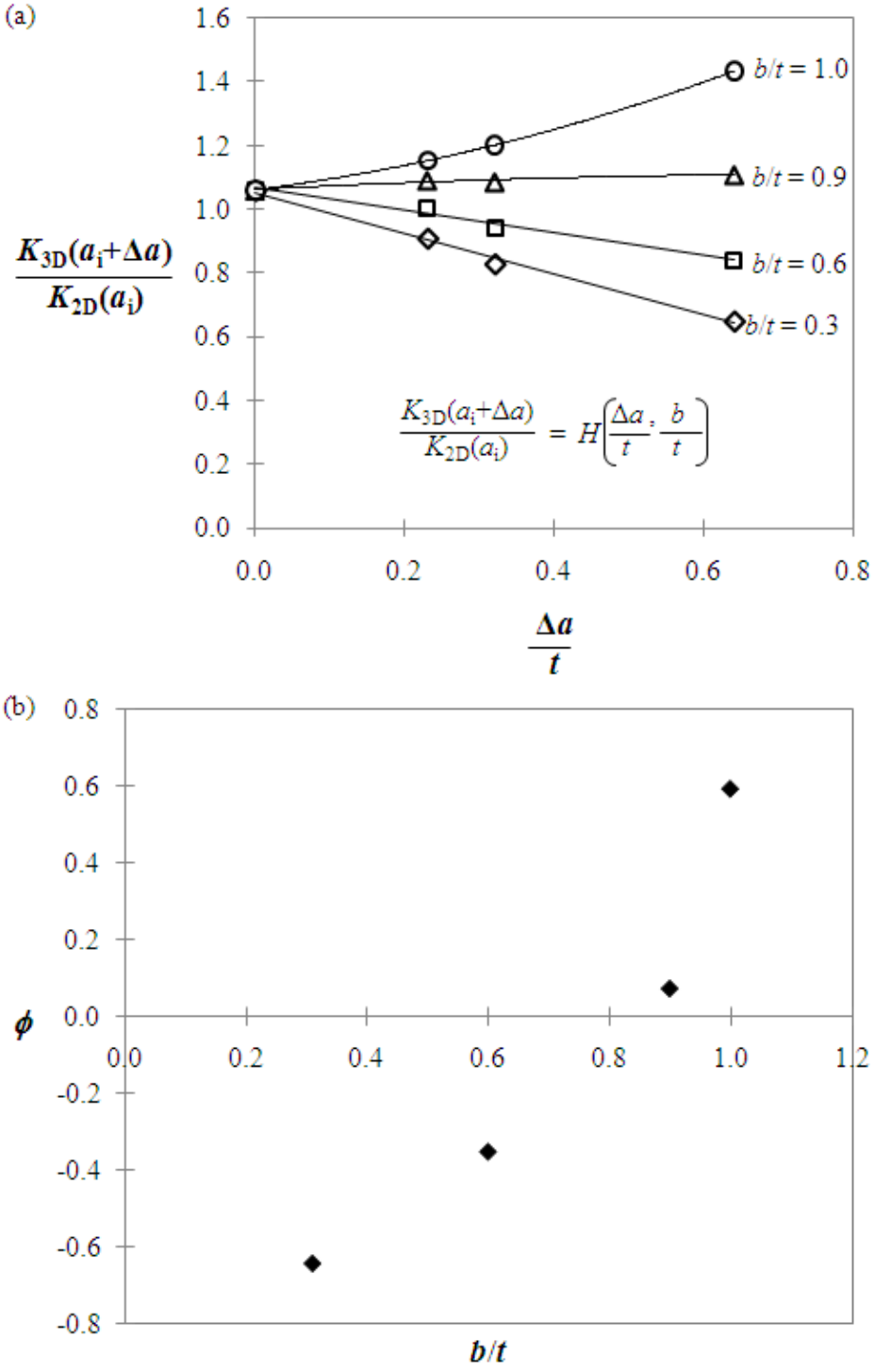

Figure 50. Parametric solutions for model crack front: (a) Relationship between the K at mid-thickness and stable tearing jump length Δa at various $\frac{b}{t}$ ratios; and (b) relationship between ϕ and the $\frac{b}{t}$ ratio.

Combining Eqs. (38) with Eq. (32), the tearing arrest condition can be expressed as

$$\frac{K_{\mathrm{Ic}}}{K_{\mathrm{2D}}(a_{\mathrm{i}})} = \sqrt{\frac{1}{1-\nu^2}} + \phi\left(\frac{\Delta a}{t}\right), \tag{39}$$

Eq. (39) can be rearranged to yield the following explicit expression for the crack jump length Δa

$$\Delta a = \frac{t}{\phi}\left(\frac{K_{\mathrm{Ic}}}{K_{\mathrm{2D}}(a_{\mathrm{i}})} - \sqrt{\frac{1}{1-\nu^2}}\right) \tag{40}$$

where ϕ = – 0.645, which provides a convenient closed-form solutions for the stable tearing crack jump length, for a given applied overload, where $K_{2D}(a_i)$ is determined by substituting P of Eq. (15) by the applied overload.

5.5. Comparison between model prediction and experimental data

The solution in Eq. (40) has been used to estimate the stable tearing crack jump length Δa for various aluminium alloys of different thickness investigated in this study and the literature. A total of 134 stable tears have been analysed, these having been produced under either CA or VA fatigue. It should be noted that the thickness ranged between 2.76 mm to 25 mm, and most of the aluminium alloys are from the 7XXX series, in addition to two types of aluminium alloys from the 2XXX series. The predicted Δa values are compared with the actual Δa in Figure 51. The overall results

show that the FE solution produces good prediction of the stable tearing crack jump length in various aluminium alloys and thicknesses. Table 14 shows the average relative errors for each material. The positive and negative values indicate underestimation and overestimation, respectively. The average relative errors suggest that the new model overestimates and underestimates Δa in seven classes (alloy, thickness, load condition) of materials.

Table 14. Average relative errors of the new stable tearing prediction model.

Class of material (alloy, thickness, load condition)	Average relative error
2024, 10 mm, VA	+ 0.189
2618, 10 mm, VA	– 0.073
7050, 3 mm, VA	– 0.961
7050, 6 mm, VA	+ 0.101
7050, 12 mm, VA	+ 0.295
7050, 12.5 mm, VA	+ 0.166
7050, 25 mm, VA	+ 0.768
7075, 5 mm, VA	– 0.102
7075, 6.35 mm, VA	+ 0.002
7075, 6.5 mm, CA	– 1.373
7075, 6.5 mm, VA	– 0.474
7075, 12.7 mm, VA	0.142
7178, 2.76 mm CA	– 0.631
7178, 4.5 mm CA	– 0.537

The observed discrepancy between the measurements and model predictions may be due to the variation of the stable tearing shape, which is not always symmetrical about the mid-plane. The tearing shape can cause error in determining the areal and width ratios, as suggested in Figure 52, which shows that the width ratios $\frac{b}{t}$ of CA and VA tearing in the present study are slightly varied. This is not surprising as it has been established in section 5.1.1 that the VA tearing in the early stage has relatively small Δa. The small Δa, as shown by T1 in Figure 14b, can be associated with asymmetrical tearing arrest and also result in difficulties of measuring the tearing parameters. This issue complicates the determination of the K at the initiation of stable tearing and hence affects the accuracy of the prediction. Another issue related with asymmetrical tearing shape is illustrated in Figure 53. For this particular tear, the width ratio $\frac{b}{t}$, determined by the areal ratio in Eq. (22) is equivalent to 0.33. However, macroscopic measurement suggests that the $\frac{b}{t}$ can be as high as 0.43.

Forsyth (1978) proposed that the crack length should be taken as the maximum crack length $a_{\max}$ at the tip of the crack front usually at the mid-thickness region. However, for in-service predictability of stable tearing, it is recommended that the crack length should be measureable from the free surface, as is the case in this study. The asymmetrical tearing shape can also cause error in measuring Δa, as also depicted in Figure 53.

The new model suggests that the FE formulation provides predictions of satisfactory accuracy and hence can be used as an effective engineering tool in relating the crack jump length with the applied loads. It should be noted that in this study, the crack growth at surface is assumed to not occur. This assumption is correct for a small

overload, as discussed in section 5.1.2. Numerical results shows that the variation of crack front geometries near the free surface has negligible effect on the plasticity-induced crack closure (Alizadeh *et al*., 2007; Matos and Nowell, 2008), and hence it can be deduced that the plasticity effect by unfractured ligaments in stable tearing formation is not significant. It should also be noted that the present application of XFEM does not enable crack branching.

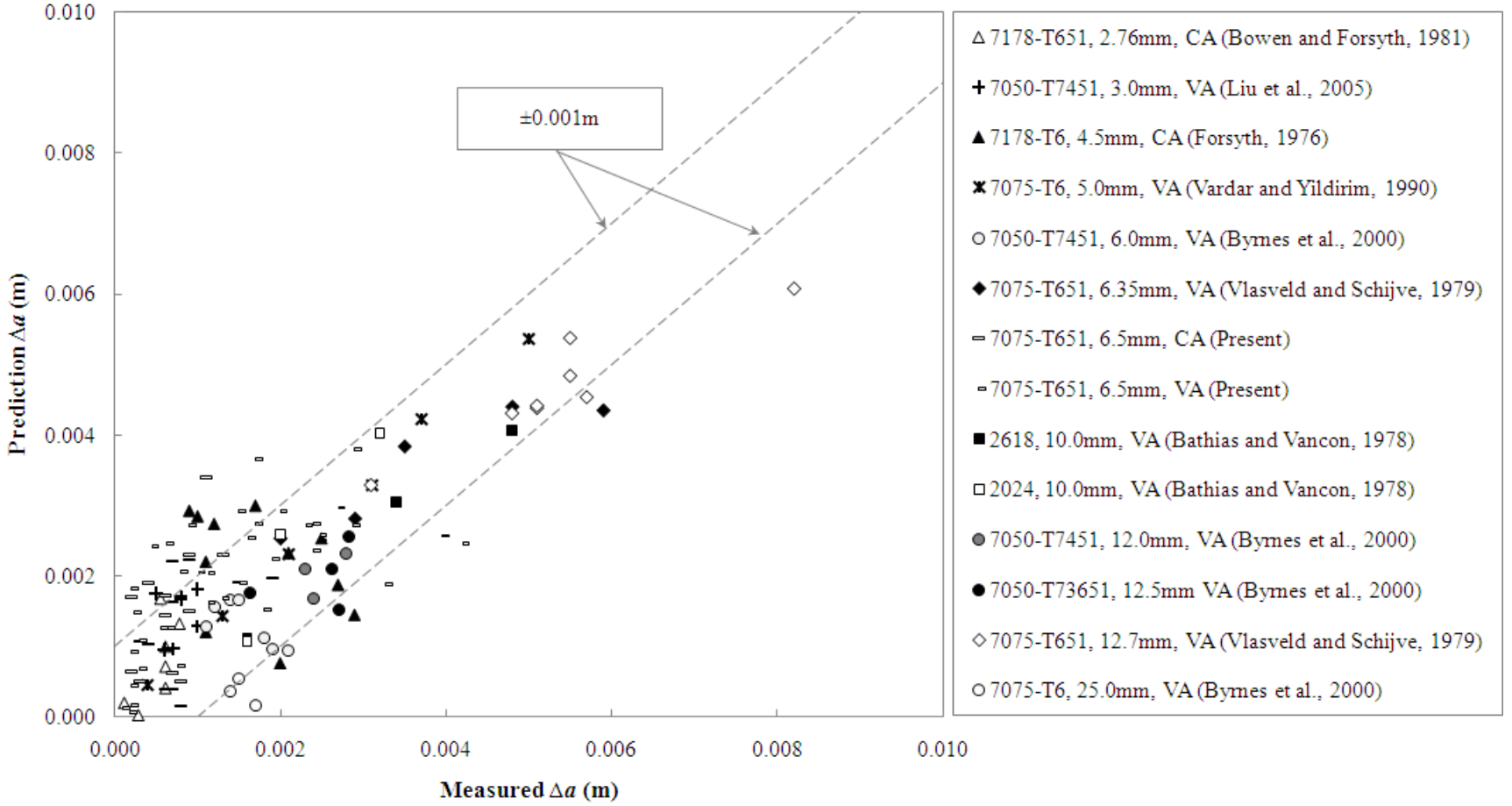

Figure 51. Comparison between the semi-analytical model prediction based on finite element method model (fully elastic condition) and actual measurement from present research and the literature. The dashed lines indicate ± 0.001 m error.

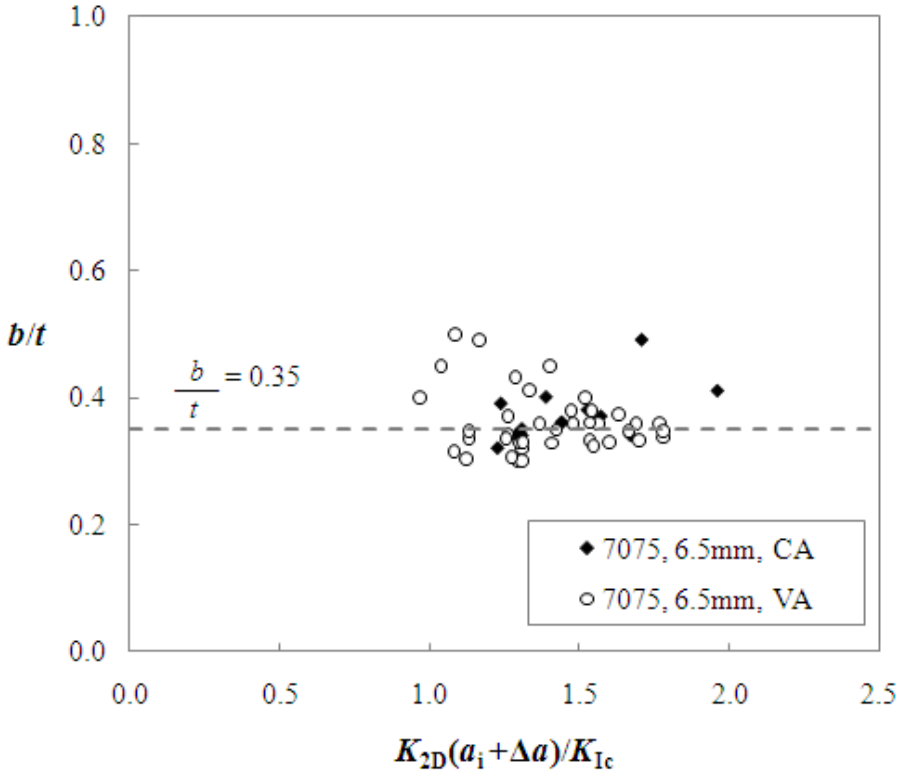

Figure 52. The plot of width ratio $\frac{b}{t}$ versus the stress intensity factor ratio.

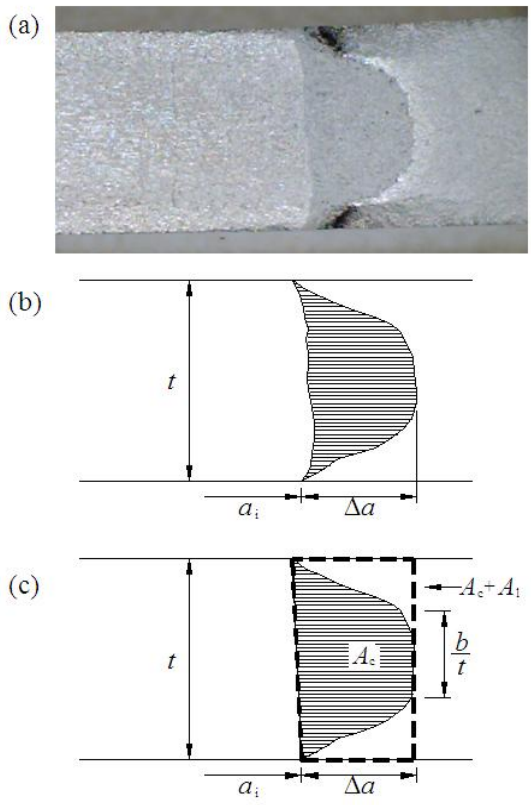

Figure 53. Error due to asymmetrical tearing shape on specimen VA11 (t = 6.5 mm).

Chapter 6. Empirical Analysis

6.1. Extended Forsyth model

6.2. Extended Schijve model

6.3. Analysis of empirical failure criteria

This chapter presents the extended Forsyth and Schijve models, which use the idealised shape of tearing in the new model to provide alternative methods for predicting stable tearing jump length. Each of these extended models is validated by using various empirical results from the literature, and shows fairly good agreement between the prediction and measured stable tearing crack jump length. The advantages and disadvantages of each model are presented and discussed. Due to the lack of a validated, unified fracture criterion, the numerical results of elastic-plastic conditions are used to investigate the use of continuum model for void nucleation.

6.1. Extended Forsyth model

An alternative predictive tool can be formulated by extending the Forsyth concept (Bowen and Forsyth, 1981) of stress intensity factor being proportional to crack front line length l, as stated in Eq. (7). Basically, the $K_{2D}(a_i + \Delta a)$ is the notional K based on the maximum crack length at stable tearing arrest. According to the present stable tearing model presented in Figure 40a, the total length of the trapezoidal crack front can be written as

$$l(a_i + \Delta a) = b + \sqrt{(t-b)^2 + 4\Delta a^2} \tag{41}$$

Substituting Eq. (41) into Eq. (7) and combining with the fracture criterion given by Eq. (32) yields the following relationship,

$$K_{2D}(a_i + \Delta a) = \frac{K_{Ic}}{t}\left(b + \sqrt{(t-b)^2 + 4\Delta a^2}\right) \qquad (42)$$

The crack jump length Δa can be readily solved iteratively. By setting $\frac{b}{t} \approx 0.30$, the solution results of Eq. (42), with K_{2D} being given by Eq. (15), are presented in Figure 54.

In the case of long cracks, *i.e.* $\Delta a << a_i$, the above relationship can be simplified to give the following explicit expression,

$$\Delta a = \frac{t}{2}\sqrt{\left(\frac{K_{2D}(a_i)}{K_{Ic}}\right)^2 - \frac{b}{t}\left(2\frac{K_{2D}(a_i)}{K_{Ic}} - 2\right) - 1} \qquad (43)$$

Eq. (43) provides another closed-form solution for the crack jump length. The results are plotted in Figure 55, where the crack front width ratio $\frac{b}{t} \approx 0.30$.

The solutions in Eq. (42) and Eq. (43) have been used to estimate the stable tearing crack jump length Δa for various aluminium alloys of different thickness investigated in this study and the literature, by using the similar tearing data in section 5.5. The predicted Δa values are compared with the actual Δa in Figure 54 and Figure 55. The overall results show that the two methods produce satisfactory prediction of the stable tearing crack jump length in various aluminium alloys and thicknesses. The prediction by the extended Forsyth model of Eq. (42) shows few overestimations (by iteration method), whilst the prediction underestimates when the $K_{2D}(a_i + \Delta a) \approx K_{2D}(a_i)$ assumption is used. It should also be noted that the Eq. (42) cannot be used to predict the Δa in 25.0 mm because the applied $K_{2D}(a_i)$ is marginally less than K_{Ic}.

Therefore, within the limitation of the proposed models, it can be concluded that both models give similar predictive performance and can be used as alternative approaches to Eq. (40) in providing estimation to Δa. In section 5.1.3, it has been established that application of Forsyth model is often limited to the marginally small tear, whereby its $\frac{\sqrt{a}}{l}$ ratio at onset and arrest is almost equivalent. Since the large VA tearing usually has relatively longer crack front length than at its onset, the accuracy of the Forsyth model is therefore reduced, as depicted in Figure 54 and Figure 55.

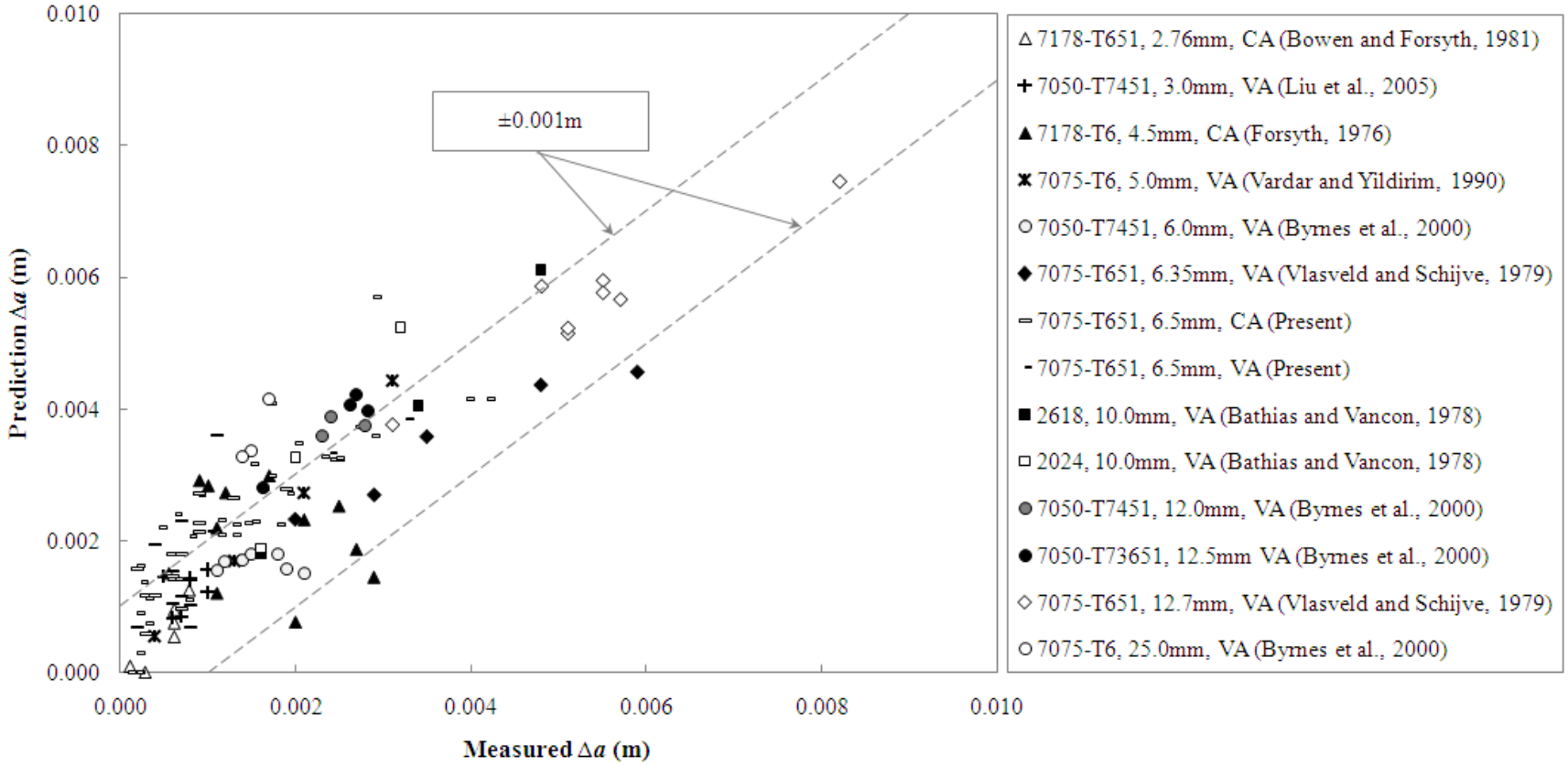

Figure 54. Comparison between the extended Forsyth model prediction (by iteration method) and the actual measurement from present research and the literature. The dashed lines indicate ± 0.001 m error.

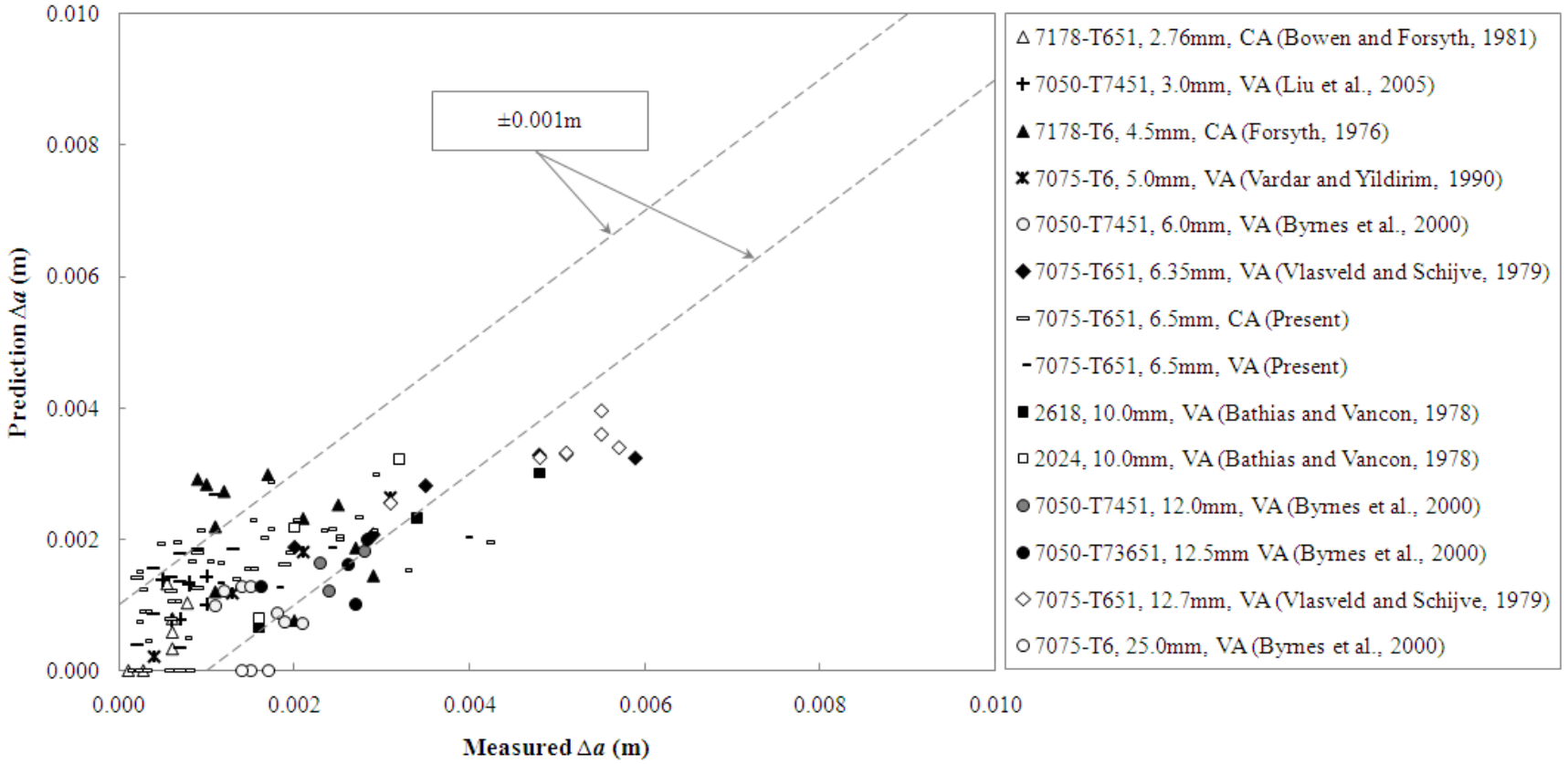

Figure 55. Comparison between the extended Forsyth model prediction (by assuming $K_{2D}(a_i + \Delta a) \approx K_{2D}(a_i)$) and the actual measurement from present research and the literature. The dashed lines indicate ± 0.001 m error.

6.2. Extended Schijve model

It has been highlighted that the application of the Schijve model is complicated by the need to determine α, which is a function of the angle of the restraining ligament made to the specimen's side, and the adoption of this model as a prognostic tool necessitates a capability to estimate this angle. According to the present stable tearing model presented in Figure 40a, for $\frac{b}{t}$ = 0.30, the angle between the inclined crack front and the side of the specimen is given by

$$\beta = \arctan\left(\frac{0.7t}{2\Delta a}\right). \tag{44}$$

Substituting Eq. (44) into (10) gives

$$\alpha = \arctan\left(\frac{0.7t}{2\Delta a}\right) - \frac{1}{\pi\Delta a}\left(\frac{K_{\mathrm{Ic}}}{\sigma_{\mathrm{Y}}}\right)^2, \tag{45}$$

from which the new expression for K_{I} can be derived, as given in Eq. (45).

$$K_{\mathrm{I}} = \frac{4\sigma_{\mathrm{Y}}}{t}\sqrt{\frac{a_{\mathrm{i}}+\Delta a}{\pi}}\left[\Delta a \times \arctan\left(\frac{0.7t}{2\Delta a}\right)\right]\left[\sqrt{1+\frac{2a_{\mathrm{i}}}{\Delta a}} - \frac{a_{\mathrm{i}}}{\Delta a}\arccos\left(\frac{a_{\mathrm{i}}}{a_{\mathrm{i}}+\Delta a}\right)\right] \tag{46}$$

,

Eq. (46) can be substituted to Eq. (8), which makes it possible to solve the relationship for Δa by regression analysis. Vlasveld and Schijve (1979, 1980) proposed the $K_{2\mathrm{D}}(a_{\mathrm{i}}) = K_{\mathrm{Ic}}$, and this is only applicable for the first onset of tearing. In reality, multiple

stable tearing bands may ensue, and therefore it is more appropriate to generalise Eq. (8) into the following,

$$K_{2D}(a_i + \Delta a) = K_{2D}(a_i) + K_l \qquad (47)$$

where $K_{2D}(a_i)$ = K_{Ic} for the first onset of tearing. It should also be noted that the iteration method is complicated by the complexity of Eq. (46), and for simple validation purposes, Figure 56 shows the plot of the $K_{2D}(a_i + \Delta a)$ against $K_{2D}(a_i)$ + K_l.

Figure 56 shows that the extended Schijve method can produce satisfactory prediction of Δa. The main limitation of this method is that the expression for K_l is complicated and careful analysis is required to arrive at the final estimation of Δa. However, it should be noted that the difficulty in determining the β parameter, as discussed in section 5.1.8, has been eliminated by adopting Eq. (44). Eq. (44) further implies that α is not a constant for a specific thickness, but depends on the Δa. However, it should be noted that the effect of β and α to the accuracy of the prediction capability of Schijve formulation may not be very significant, as suggested in Figure 57. In Figure 57, the predicted β is calculated according to Eq. (43), while the measured β is determined from the macroscopic examination of tearing. This result implies that there is notable discrepancy between the prediction and measured values of β, but this inconsistency has minimum effect on the accuracy of the extended Schijve model. In fact, as noted by Vlasveld and Schijve (1979, 1980), Eq. (9) is very sensitive to Δa. This implies that a relatively accurate measuring technique must be employed in order to achieve excellent prediction.

This analysis also shows that although the Schijve model was derived from the VA tearing, the new extended model can also be used for CA tearing. It should be noted, however, that notable scatters can be observed in tearing data for 7178-T6, thickness t = 4.5 mm, which can be due to the fact that these tears are produced in a single specimen, while the Schijve formulation is developed based on a single tear in a specimen. It has been emphasised in sections 5.5 that these discrepancies can be associated with excessive influence of excessive crack front curvature and plane stress conditions as fatigue crack grows. The comparison between the Δa and plastic zone size in section 5.1.6 0has shown that this effect is more pronounced in large Δa.

Another notable improvement of the new extended Schijve model is that its application is not limited to materials of intermediate thickness, but now can be used for either thin or thick material materials as well. Vlasveld and Schijve (1980) suggested that tearing in a very thick specimen should have small ligaments because a large fraction of the crack front will be under plane strain, while in a very thin specimen, plane stress will be dominant. The idealisation of the stable tearing shape into a trapezoidal shape however enable tears in a very thick or thin specimens to be predicted, and therefore further verified the usefulness of the new model proposed in section 5.2.

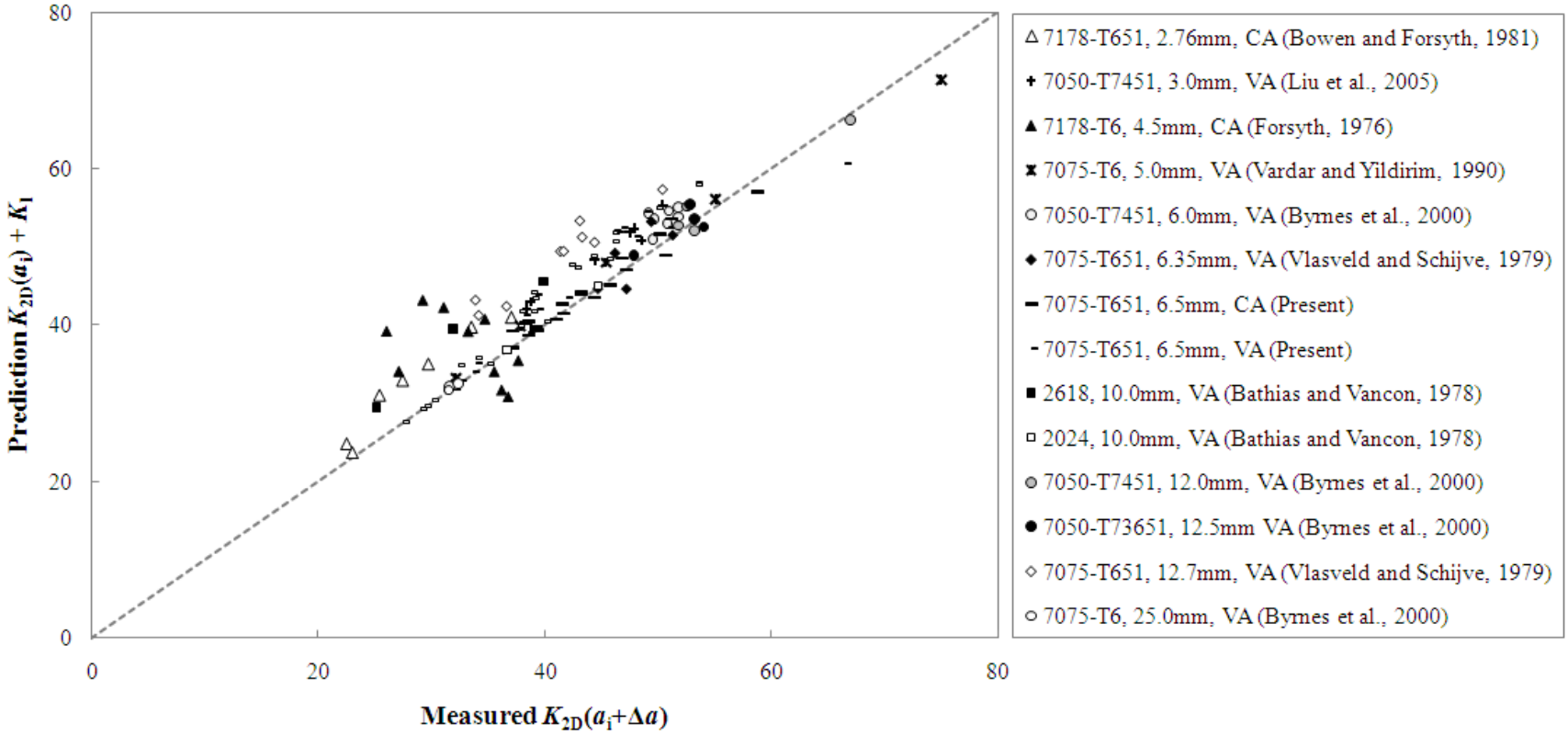

Figure 56. Comparison between the model prediction and actual measurement from present research and the literature by using the extended Schijve model. The dashed diagonal line represents a line of equal relationship.

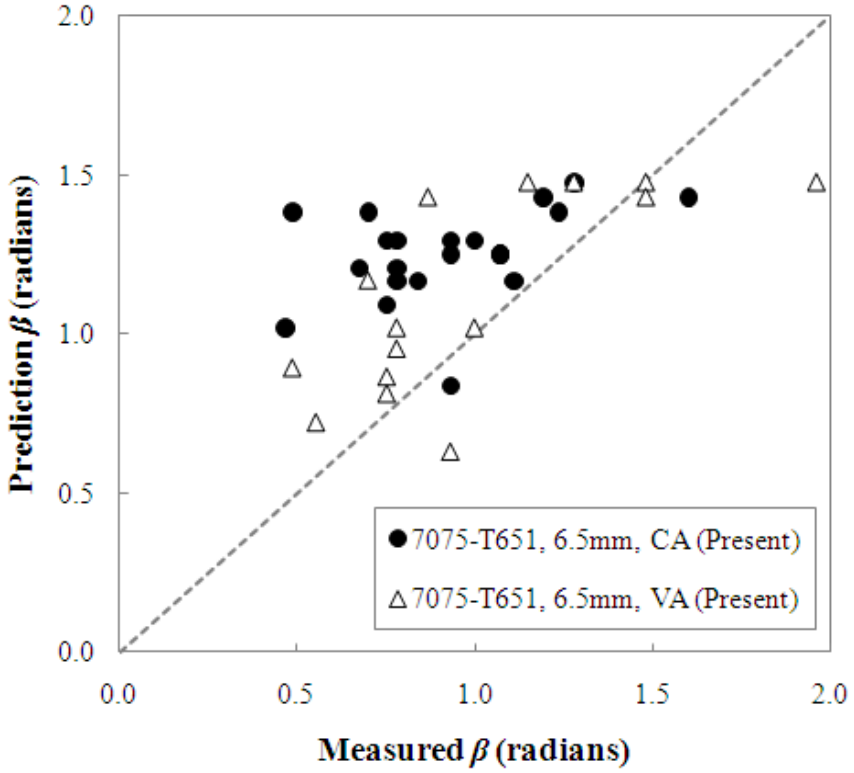

Figure 57. Comparison between the prediction and measured values of β for CA and VA tears produced in this study.

6.3. Analysis of empirical failure criteria

Due to the lack of a validated, unified fracture criterion, the numerical results of elastic-plastic conditions are used to investigate the use of continuum model for void nucleation. The two semi-empirical relationships have been mentioned by Anderson (2005) and the results are shown in Figure 58. This analysis suggests that there is no obvious empirical relationship.

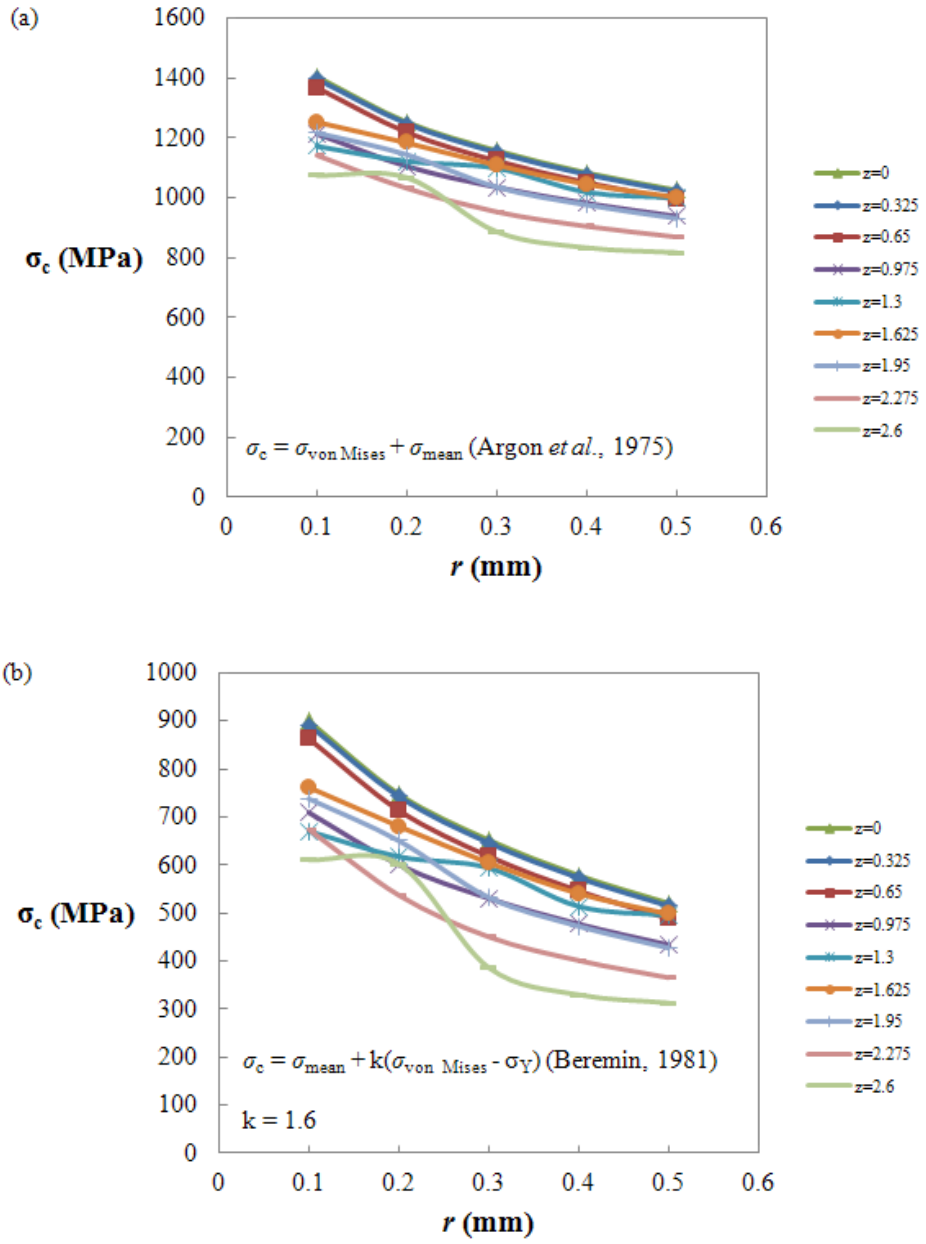

Figure 58. Numerical analysis based on the semi-empirical relationship for void nucleation. Details of references can be sought from Anderson (2005).

Chapter 7. Conclusions and Recommendations

7.1. Conclusions

7.2. Recommendations

7.1. Conclusions

Quantitative fractography of fatigue fracture surfaces is used extensively in aircraft accident investigation to correlate various progression markings, associated with the crack front position, with the load cycle history which was experienced by the failed component in service. This analysis is vital to estimate the crack growth history in the critical component. Matching the results of this analysis to the predicted fatigue crack growth, however, is often complicated by stable tearing crack growth. Bands of stable tearing are often observed on fracture surfaces in a range of structural metals but their growth are not incorporated into fatigue predictive models. Therefore, the presence of large stable tearing bands can greatly complicate the derivation of a crack growth history, especially in cases where the load history record is poor. Therefore, the main challenge in fracture surface analysis is to relate the multiple tears, of different extents, to the loads present in the load history. The main objective of this research was to develop improved analytical and prognostic models for predicting stable tearing jump length Δa in aluminium alloys. This research involves a series of tests which produced stable tearing in 7075 aircraft aluminium alloy under constant amplitude (CA) and variable amplitude (VA) loading.

Macroscopic and microscopic characteristics of CA and VA tearing were studied and the main conclusion relates to the notable differences between tearing under CA and VA loading. The tearing after VA usually appears duller than the CA tearing, but both types of tearing have similar fracture mechanism and are also comparable to the face of the final unstable failure. This study reveals that the stress intensity factor is one of the key controlling parameters in tearing onset and arrest. The CA and VA tearing can be characterized by the first onset stress intensity factor $K_{2D}(a_i)$ at which

these two tearing conditions occur. The magnitude of $K_{2D}(a_i)$ for VA tearing was found to be equivalent to the material's plane strain fracture toughness, K_{Ic}, but is slightly lower than the initiation *K*-value for CA tearing. The loading conditions also have been observed to impose different effects on the size of tearing. This study suggests that for similar *K*, the CA tearing at initiation has smaller tearing crack jump length Δa, than the VA tearing, but as the crack progresses, the size of Δa under VA conditions is markedly larger than that sustainable under CA conditions. The CA condition seems to confer apparent resistance to tearing, which results in smaller tearing crack jumps, than in VA loading conditions. This study also shows that stable tearing crack jump length Δa under CA and VA conditions can be associated with the plastic zone size, but their correlations with the plastic zone size are differed between the two loading conditions.

The static tearing curve was developed based on the standard K_R curve test method. This study shows that the *K*-value at which static tearing commences is approximately equivalent to the first onset stress intensity factor for VA tearing. This result supports the notion that the onset of stable tearing occurs at *K*-level of magnitude that is comparable with the static plane strain fracture toughness K_{Ic}. The K_R (*K*-value with plastic zone correction) is plotted against the effective crack length Δa_e and the fatigue tearing data from these tests is found to agree very well with the static *R*-curve. This result shows that the *R*-curve method can be used to estimate the Δa of both CA and VA tearing during fractographic analysis, but this technique requires the *R*-curve to be developed for particular configuration.

The complex crack front curvatures observed at tearing arrest distort simple estimates of stress intensity factor and hence a three-dimensional (3D) finite element

(FE) analysis has been undertaken to estimate the through thickness stress intensity factor K_{3D} variation. Generally, the K-value at mid-thickness region reduces, while the K-values at the sides of the specimen increase as the crack-front becomes more curved. Based on the parametric finite element analysis of the stress-intensity factor K_{3D} at the mid-thickness of three VA tearing, this study presents a new validated stable tearing model for predicting the crack jump length Δa during stable tearing. The main features of this new model are that the tongue-shaped of stable tearing is idealised as a trapezoidal shape and the average of areal ratio of tearing is approximately constant. Comparisons between the model predictions and experimental results indicate that this new model produces satisfactory prediction of stable tearing crack jump length Δa in aluminium alloys of different cross-sectional thickness.

The study provides advanced knowledge in predicting the stable tearing behaviour under fatigue conditions and improves the modelling capability for the phenomenon of stable tearing in aluminium alloys structural metals. The results of this study help in establishing confident and accurate durability assessment of aircraft structure, notably in assisting quantitative fractography during accident investigation and assessing physical validation to the fatigue crack growth prediction model. The usefulness of the knowledge can also be applied and extended to other engineering materials and structures.

7.2. Recommendations

This study uses the stress intensity factor K as the main controlling parameter, which has been shown to be valid since the occurrence of all stable tearing jumps are in compliance with the small-scale yielding conditions. The Irwin's correction factor

has been used to account for the plasticity effect. A more complex model such as the Dugdale model may be useful in improving the accuracy of the prediction results. The new validated stable tearing model is proposed based on the assumption that no crack growth occurs at the free surface, which is valid for small *K*-values. For high applied *K*, the crack branching occurs on the free surface, and the crack occurs on the slanted plane in the subsurface region. The current XFEM application is only limited to crack growth modelling that occurs on the same plane and hence further study is recommended to study the effect of crack branching during stable tearing formation and the effect of corner singularity at the intersection between the crack front and the free surface.

Future study should also investigate the effect of the sharp change in the crack front (corner) for the trapezoidal shape of the crack front and the capability of numerical modelling to predict the complete crack front shape of stable tearing under increasing load.

References

Abaqus, 2009, Version 6.9, Hibbit, Karlsson & Sorensen, Inc., Providence, Rhode Island, USA.

Abdelaziz, Y. & Hamouine, A. 2008. A survey of the extended finite element. *Computers and Structures* 86(11-12): 1141-1151.

Ab Rahman, M.F., Mohammed, R.D., Clark, G. 2010a. The influence of plastic zone size in stable tearing. In *Proceedings of the 21st Australasian Conference on the Mechanics of Structures and Materials*. Melbourne, Australia: Victoria University.

Ab Rahman, M.F., Mohammed, R.D., Yu, X., Liu, Q., Clark, G. 2010b. Assessment of stable tearing on fatigue fracture surfaces. *Engineering Failure Analysis* 17(6): 1313-1327.

Ab Rahman, M.F., Mohammed, R.D., Yu, X., Liu, Q., Clark, G. 2010c. Stable tearing in aircraft materials. In *Proceedings of the 27th International Congress of the Aeronautical Science*s. Nice, France: Optimage.

Ab Rahman, M.F., Mohammed, R.D., Yu, X., Liu, Q., Clark, G. 2010d. Prediction of stable tearing in fatigue crack growth. *Procedia Engineering* 2(1): 1515-1521.

Achon, P., Ehrstrom, J.C., Pineau, A. 1996. Modeling ductile fracture of Al alloys in relation with statistical distribution of second phase particles. *Journal de Physique* 6(6): 3-12.

Alizadeh, H., Hills, D.A., de Matos, P.F.P., Nowell, D., Pavier, M.J., Paynter, R.J., Smith, D.J., Simandjuntak, S. 2007. A comparison of two and three-dimensional analyses of fatigue crack closure. *International Journal of Fatigue* 29(2): 222-231.

Anderson, T.L. 2005. *Fracture mechanics: Fundamentals and applications*. 3rd ed. Florida, USA: CRC Press.

ASTM E 1823. 2008. Standard terminology relating to fatigue and fracture testing. In *Annual Book of ASTM Standards*, Section Three, Metals test methods and analytical procedures: 1118-1139. Philadelphia, USA: ASTM International.

ASTM E 399. 2008. Standard test method for linear-elastic plane-strain fracture toughness K_{Ic} of metallic materials. In *Annual Book of ASTM Standards*, Section Three, Metals test methods and analytical procedures: 498-529. Philadelphia, USA: ASTM International.

ASTM E 561. 2008. Standard test method for *K-R* curve determination. In *Annual Book of ASTM Standards*, Section Three, Metals test methods and analytical procedures: 593-611. Philadelphia, USA: ASTM International.

ASTM E 647. 2008. Standard test method for measurement of fatigue crack growth rates. In *Annual Book of ASTM Standards*, Section Three, Metals test methods and analytical procedures: 671-715. Philadelphia, USA: ASTM International.

Banerjee, S. 1981. Influence of specimen size and configuration on the plastic zone size, toughness and crack growth. *Engineering Fracture Mechanics* 15(3-4): 343-390.

Bao, R. & Zhang, X. 2010. Fatigue crack growth behaviour and life prediction for 2324-T39 and 7050-T7451 aluminium alloys under truncated load spectra. *International Journal of Fatigue* 32(7): 1180-1189.

Barenblatt, G.I. 1982a. Comment on the discreteness of fracture. *Strength of Materials* 14(5): 702.

Barenblatt, G.I. 1982b. The discreteness of fracture. *Strength of Materials* 14(5): 695-699.

Barenblatt, G.I. & Botvina, L.R. 1993. Self-oscillatory modes of fatigue fracture and the formation of self-similar structures at the fracture surface. In *Proceedings of the Mathematical and Physical Sciences* 442(1915): 489-494. London, UK: The Royal Society.

Barter, S.A., Clark, G., Goldsmith, N.T. 1993. Influence of initial defect conditions on structural fatigue in RAAF aircraft. In A.F. Blom (ed), *Durability and structural reliability of airframes*: 281-304. Warley, UK: Engineering Materials Advisory Services (EMAS).

Barter, S.A., Sharp, P.K., Clark, G. 1997. The identification of fatigue critical regions during fatigue testing of Macchi MB326H centre section lower booms. In *Proceedings of the 9th International Conference on Fracture*. Sydney, Australia: Elsevier.

Barter, S., Molent, L., Goldsmith, N., Jones, R. 2005. An experimental evaluation of fatigue crack growth. *Engineering Failure Analysis* 12(1): 99-128.

Bathias, C. & Vancon, M. 1978. Mechanisms of overload effect on fatigue crack propagation in aluminium alloys. *Engineering Fracture Mechanics* 10(2): 409-424.

Beden, S.M., Abdullah, S., Ariffin, A.K. 2009. Review of fatigue crack propagation models for metallic components. *European Journal of Scientific Research* 28(3): 364-397.

Belytschko, T. & Black, T. 1999. Elastic crack growth in finite elements with minimal remeshing. *International Journal for Numerical Methods in Engineering* 45(5): 602-620.

Bhaumik, S.K., Sujata, M., Venkataswamy, M.A. 2008. Fatigue failure of aircraft components. *Engineering Failure Analysis* 15(6): 675-694.

Bland, R.B. & Sandorff, P.E. 1943. The control of life expectancy in airplane structures. *Aeronautical Engineering Review* 2: 7-21.

Blom, A.F. 2001. Fatigue science and engineering – achievements and challenges. In J. Rouchon (ed), *Design for Durability in the Digital Age,* Proceedings of the 21st Symposium of the International Committee on Aeronautical Fatigue: 3-63. Toulouse, France: Cepadues.

Bolotin, V.V. 1999a. Analytical modelling of fatigue crack propagation. *Fatigue & Fracture of Engineering Materials & Structures* 22(11): 939-947.

Bolotin, V.V. 1999b. *Mechanics of fatigue*. Florida, USA: CRC Press.

Botvina, L.R. & Limar, L.V. 1985. Relationship of the spacing of the fatigue striations to the range in the stress intensity factor. *Materials Science* 21(2): 144-152.

Botvina, L.R., Yarema, S.Y., Grechko, V.V., Limar, L.V. 1981b. Kinetics of fatigue fracture of VT3-1 titanium alloy. *Materials Science* 17(6): 518-524.

Bowen, A.W. & Forsyth, P.J.E. 1977. The effect of frequency changes on fatigue crack growth in 7178-T6 aluminium alloy. In *Proceedings of the International Conference on Fracture*: 1217-1222. Waterloo, Canada: University of Waterloo Press.

Bowen, A.W. & Forsyth, P.J.E. 1978. The effect of frequency changes on fatigue crack growth in 7178-T6 aluminium alloy. In D.M.R. Taplin (ed), *Advances in research on the strength and fracture of materials*: 1217-1222. New York, USA: Pergamon Press.

Bowen, A.W. & Forsyth, P.J.E. 1981. On the mechanism of mixed fatigue-tensile crack growth. *Materials Science and Engineering* 49(2): 141-154.

Brocks, W., Anuschewski, P., Scheider, I. 2010. Ductile tearing resistance of metal sheets. *Engineering Failure Analysis* 17(3): 607-616.

Broek, D. 1986. *Elementary engineering fracture mechanics*. 4th ed. Dordrecht, Netherlands: Kluwer Academic Publishers.

Brown Jr., W.F. & Srawley, J.E. 1966. *Plane strain crack toughness testing of high strength metallic materials*, ASTM STP 410. Philadelphia, USA: American Society for Testing and Materials (ASTM).

Brown, R.D. & Weertman, J. 1978. Effects of tensile overloads on crack closure and crack propagation rates in 7050 aluminium. *Engineering Fracture Mechanics* 10(4): 867-878.

Bucci, R.J., Thakker, A.B., Sanders, T.H., Sawtell, R.R., Staley, J.T. 1980. Ranking 7XXX aluminium alloy fatigue crack growth resistance under constant amplitude and spectrum loading. In D.F. Bryan, J.M. Potter (eds), *Effect of load spectrum variables on fatigue crack initiation and propagation*, ASTM STP 714: 41-78. Philadelphia, USA: American Society for Testing and Materials (ASTM).

Burton, W.S., Sinclair, G.B., Solecki, J.S., Swedlow, J.L. 1984. On the implications for LEFM of the three-dimensional aspects in some crack/surface interaction problems. *International Journal of Fracture* 25(1): 3-32.

Byrnes, R., Sharp, P.K., Goldsmith, N.T., Clark, G. 1998. Empirical analysis of stable tearing on fracture surfaces. In *Proceedings of the Structural Integrity and Fracture Conference*. Melbourne, Australia.

Byrnes, R., Sharp, P.K., Goldsmith, N.T., Clark, G. 2000. *Modelling of stable tearing during fatigue of 7050 aluminium alloy*. Technical Report DSTO-TR-1032. Melbourne, Australia: Defence Science and Technology Organisation (DSTO).

Campbell, G.S. & Lahey, R. 1984. A survey of serious aircraft accidents involving fatigue fracture. *International Journal of Fatigue* 6(1): 25-30.

Campbell, G.S. 1981. A note on fatal aircraft accidents involving metal fatigue. *International Journal of Fatigue* 3(4): 181-185.

Celik, C.E., Vardar, O., Kalenderoglu, V. 2004. Comparison of retardation behaviour of 2024-T3 and 7075-T6 alloys. *Fatigue & Fracture of Engineering Materials & Structures* 27(8): 713-722.

Ciesielski, M., Kaniowski, J., Karlinski, W. 2009. Determination of the fatigue crack-growth rate from the fractographic analysis of a specimen representing the aircraft wing skin. *International Journal of Fatigue* 31(6): 1102-1109.

Chanani, G.R. & Mays, B.J. 1977. Observation of crack-closure behaviour after single overload cycles in 7075-T6 single-edge-notched specimens. *Engineering Fracture Mechanics* 9(1): 65-73.

Christensen, R.H. 1961. Cracking and fracture in metals and structures. In *Proceedings of the Crack Propagation Symposium*: 326-374. Cranfield, UK: Cranfield College of Aeronautics.

Clark, G. 1979. Significance of fatigue stress intensity in fracture toughness testing. *International Journal of Fracture* 15(5): R179-R181.

Clark, G., Jost, G.S., Young, G.D. 1997. Recovery of the RAAF Macchi MB326H – the tale of an ageing trainer fleet. In P. Pool (ed), *Fatigue in new and ageing aircraft*: 39-58. Warley, UK: Engineering Materials Advisory Services (EMAS).

Cotterell, B. 1970. On fracture path stability in the compact tension test. *International Journal of Fracture Mechanics* 6(2): 189-192.

Daneshpour, S., Kocak, M., Langlade, S., Horstmann, M. 2009. Effect of overload on fatigue crack retardation of aerospace Al-alloy laser welds using crack-tip plasticity analysis. *International Journal of Fatigue* 31(10): 1603-1612.

de Matos, P.F.P. & Nowell, D. 2008. The influence of the Poisson's ratio and corner point singularities in three-dimensional plasticity-induced fatigue crack closure: A numerical study. *International Journal of Fatigue* 30(10-11): 1930-1943.

Dixon, J.R. 1966. Effects of crack-front geometry and plate thickness on the stress distribution in cracked plate. In *Proceedings of the Physical Basis of Yield and Fracture Conference*: 6-16. Oxford, UK: Institute of Physics and the Physical Conference.

Dorward, R.C. & Pritchett, T.R. 1988. Advanced aluminium alloys for aircraft and aerospace applications. *Materials & Design* 9(2): 63-69.

Dougherty, D.J., de Koning, A.U., Hillberry, B.M. 1992. Modelling high crack growth rates under variable amplitude loading. In M.R. Mitchell (ed), *Advances in Fatigue Lifetime Predictive Techniques*, ASTM STP 1122: 214-233. Philadelphia, USA: American Society for Testing and Materials (ASTM).

Dowling, N.E. 2007. *Mechanical behaviour of materials – engineering methods for deformation, fracture, and fatigue*. 3rd ed. New Jersey, USA: Pearson Education.

Drar, H. 1995. Fractographic aspects of fatigue of sintered Ni-steels. *Materials Characterization* 34(2): 129-141.

Eastin. R.G. 2003. A critical review of strategies used to deal with fatigue. In *Proceedings of the 22th International Committee on Aeronautical Fatigue (ICAF) Symposium*: 163-187. Lucerne, Switzerland: Engineering Materials Advisory Services (EMAS).

Elber, W. 1970. Fatigue crack closure under cyclic tension. *Engineering Fracture Mechanics* 2(1): 37-45.

Fatemi, A. & Yang, L. 1998. Cumulative fatigue damage and life prediction theories: A survey of the state of the art for homogeneous materials. *International Journal of Fatigue* 20(1): 9-34.

Finlay, S.J. & Harrison, N.D. 2002. Why aircraft fail. *Materials Today* November: 18-25.

Flabel, J.C. 2005. *Practical stress analysis for design engineers*. Idaho, USA: Lake City Publishing Company.

Fleck, N.A. 1985. Fatigue crack growth due to periodic underloads and overloads. *Acta Metallurgica* 33(7): 1339-1354.

Forsyth, P.J.E. 1976. Some observations and measurements on mixed fatigue/tensile crack growth in aluminium alloys. *Scripta Metallurgica* 10(5): 383-386.

Forsyth, P.J.E. 1978. Causes of mixed fatigue-tensile-crack growth and significance of microscopic crack behaviour. *Metals Technology* 5(10): 351-357.

Forsyth, P.J.E. 1983. A unified description of micro and macroscopic fatigue crack behavior. *International Journal of Fatigue* 5(1): 3-14.

Forsyth, P.J.E. & Bowen, A.W. 1981. The relationship between fatigue crack behavior and microstructure in 7178 aluminum alloy. *International Journal of Fatigue* 3(1): 17-25.

Forsyth, P.J.E. & Ryder, D.A. 1960. Some results derived from the microscopic examination of crack surfaces. *Aircraft Engineering* 32(4): 96-99.

Forsyth, P.J.E. & Ryder, D.A. 1961. Some results of the examination of aluminium alloy specimen fracture surfaces. *Metallurgia* 63(377): 117-124.

Fries, T.P. & Belytschko, T. 2010. The extended/generalized finite element method: An overview of the method and its applications. *International Journal for Numerical Methods in Engineering* 84(3): 253-304.

Froes, F.H. 1989. Aerospace materials for the twenty-first century. *Materials and Design* 10(3): 110-120.

Frost, N.E. 1962. Effect of mean stress on the rate of growth of fatigue cracks in sheet materials. *Journal of Mechanical Engineering Sciences* 4(1): 22-35.

Frost, N.E., Holden, J., Phillips, C.E. 1961. Experimental studies into the behaviour of fatigue cracks. In *Proceedings of the Crack Propagation Symposium*: 166-187. Cranfield, UK: Cranfield College of Aeronautics.

Geary, W. 1992. A review of some aspects of fatigue crack growth under variable amplitude loading. *International Journal of Fatigue* 14(6): 377-386.

Glinka, G., Gmur, Z., Swiderski, Z. 1984. An examination of mixed fatigue-tensile surface crack growth in rails. *Engineering Fracture Mechanics* 20(1): 103-112.

Goldsmith, N.T. & Clark, G. 1989. Fractographic techniques for the assessment of aircraft component cracking. In A. Berkovits (ed), *Aeronautical fatigue in the*

electronic era: 199-214. Warley, UK: Engineering Materials Advisory Services (EMAS).

Goldsmith, N.T. & Clark, G. 1990. Analysis and interpretation of aircraft component defects using quantitative fractography. In B.M. Strauss, S.K. Putatunda (eds), *Quantitative methods in fractography*: 52-68. Philadelphia, USA: American Society for Testing and Materials (ASTM).

Goldsmith, N.T., Clark, G., Barter, S.A. 1996. A growth model for catastrophic cracking in an RAAF aircraft. *Engineering Failure Analysis* 3(3): 191-201.

Goranson, U.G. 1997. Fatigue issues in aircraft maintenance and repairs. *International Journal of Fatigue* 20(6): 413-431.

Guo, W. 1993. Elastoplastic three-dimensional crack border field – I. Singular structure of the field. *Engineering Fracture Mechanics* 46(1): 93-104.

Guo, W. 1995. Elastoplastic three-dimensional crack border field – III. Fracture parameters. *Engineering Fracture Mechanics* 51(1): 51-71.

Hardrath, H.F. 1973. Structural integrity in aircraft. *Journal of Testing and Evaluation* 1(1): 3-12.

Hardrath, H.F. & McEvily, A.J. 1962. Engineering aspects of fatigue crack propagation. In *Proceedings of the Crack Propagation Symposium*: 231-270. Cranfield, UK: Cranfield College of Aeronautics.

Heinz, A., Haszler, A., Keidel, C., Moldenhauer, S., Benedictus, R., Miller, W.S. 2000. Recent development in aluminium alloys for aerospace applications. *Materials Science and Engineering* 280(1): 102-107.

Hersman, D.A.P. & Higgins, K.O. 2007. *In-flight separation of right wing flying boat, Inc. (doing business as Chalk's Ocean Airways) Flight 101 Grumman Turbo Mallard (G-73T), N2969 Port of Miami, Florida, December 19, 2005*. Accident Report NTSB/AAR-07/04. Washington D.C., USA: National Transportation Safety Board.

Hertzberg, R.W. 1996. *Deformation and fracture mechanics of engineering materials*. 4th ed. New Jersey, USA: John Wiley & Sons.

Heyer, R.H. & McCabe, D.E. 1972. Crack growth resistance in plane-stress fracture testing. *Engineering Fracture Mechanics* 4(3): 413-430.

Hoeppner, D.W. 1996. Industrial significance of fatigue problems. In *ASM Handbook Volume 19, Fatigue and Fracture*: 3-4. Ohio, USA: ASM International.

Hoff, N.J. 1984. Innovation in aircraft structures – Fifty years ago and today. In *Proceedings of the 25th Structures, Structural Dynamics and Materials Conference*: 1-14. California, USA: American Institute of Aeronautics and Astronautics.

Hudson, C.M. & Hardrath, H.F. 1963. *Investigation of the effects of variable-amplitude loadings on fatigue crack propagation patterns*. Technical Note D-1803. Langley, USA: National Aeronautics and Space Administration (NASA).

Immarigeon, J.P., Holt, R.T., Koul, A.K., Zhao, L., Wallace, W., Beddoes, J.C. 1995. Lightweight materials for aircraft applications. *Materials Characterization* 35(1): 41-67.

Irwin, G.R. 1960. Plastic zone near a crack and fracture toughness. In C.T. Bethel, W.A. Bellingham (eds.), *Selected papers on Foundations of Linear Elastic Fracture Mechanics*, Vol. CP 1; SPIE Milestone Series: 267-279. Society for Experimental Mechanics/ Society of Photo-Optical Instrumentation Engineers.

Ivanova, V.S. 1982a. Comment on the article by G. I. Barenblatt "The discreteness of fracture". *Strength of Materials* 14(5): 699-701.

Ivanova, V.S. 1982b. Discreteness and self-similarity of failure in stable fatigue crack growth. *Strength of Materials* 14(5): 675-684.

Ivanova, V.S. 1982c. Reply to G. I. Barenblatt's comments. *Strength of Materials* 14(5): 703.

Ivanova, V.S., Kudryashov, V.G., Shtovba, Y.K., Kopeliovich, B.A. 1972. Fractographic investigation of the ductility of fracture in aluminium and titanium alloys. *Strength of Materials* 4(11): 1314-1319.

Jakab, P.L. 1999. Wood to metal: The structural origins of the modern airplane. *Journal of Aircraft* 36(6): 914-918.

Janssen, M., Zuidema, J., Wanhill, R.J.H. 2006. *Fracture mechanics*. 2nd ed. Delft, Netherlands: VSSD.

Johnson, F.A. & Radon, J.C. 1976. Fracture energy and crack tunnelling. *Journal of Testing and Evaluation* 4(3): 209-217.

Jones, M.H. & Brown Jr., W.F. 1970. The influence of crack length and thickness in plane strain fracture toughness tests. In W.F. Brown Jr. (ed), *Review of developments in plane strain fracture toughness testing*, ASTM STP 463: 63-101. Philadelphia, USA: American Society for Testing and Materials (ASTM).

Kaufman, J.G. 1970. Progress in fracture testing of metallic materials. In W.F. Brown Jr. (ed), *Review of developments in plane strain fracture toughness testing*, ASTM STP 463: 3-21. Philadelphia, USA: American Society for Testing and Materials (ASTM).

Kitsunai, Y. 1985. Fatigue crack growth behaviour in mild steel weldments at low temperatures. In R.I. Stephens (ed), *Fatigue at low temperatures*, ASTM STP 857: 274-292. Philadelphia, USA: American Society for Testing and Materials (ASTM).

Kitsunai, Y. 1986. Ductile-brittle transition behaviour of structural steel in fatigue crack growth under low temperature. *Bulletin of the Japan Society of Mechanical Engineers* 29(258): 3979-3985.

Knott, J.F. 1973. *Fundamentals of fracture mechanics*. London, UK: Butterworth.

Krafft, J.M., Sullivan, A.M., Boyle, R.W. 1961. Effect of dimensions on fast fracture instability of notched sheets. In *Proceedings of the Crack Propagation Symposium*: 8-28. Cranfield, UK: Cranfield College of Aeronautics.

Kuna, M. 1982. Three-dimensional elastic analysis of CT specimen with straight and curved crack fronts. *International Journal of Fracture* 19(3): R63-R67.

Kunz, J., Kovarik, O., Lauschmann, H., Siegl, J., Augustin, P. 2010. Fractographic reconstitution of fatigue crack growth in integrally stiffened panels. *Procedia Engineering* 2(1): 1711-1720.

Kwon, S.W. & Sun, C.T. 2000. Characteristics of three-dimensional stress fields in plates with a through-the-thickness crack. *International Journal of Fracture* 104(3): 291-315.

Laird, C. 1967. The influence of metallurgical structure on the mechanisms of fatigue crack propagation. In *Fatigue crack propagation*, ASTM STP 415: 131-180. Philadelphia, USA: American Society for Testing and Materials (ASTM).

Lancaster, J. 1997. *Engineering catastrophes – causes and effects of major accidents*. Cambridge, UK: Abington Publishing.

Lauschmann, H., Siegl, J., Sumbera, J., Siska, F., Nedbal, I. 2006. An unifying concept for fatigue: the reference crack growth rate. *Materials Characterization* 56(4-5): 257-265.

Lei, Y. 2008. Finite element crack closure analysis of a compact tension specimen. *International Journal of Fatigue* 30(1): 21-31.

Limar, L.V. 1987. Features of the fatigue failure of titanium alloys. *Metal Science and Heat Treatment* 29(10): 771-775.

Limar, L.V., Botvina, L.R., Yarema, S.Y. 1989. Structural aspects of fatigue crack growth in VT3-1 titanium alloy. *Materials Science* 25(1): 73-77.

Lindley, T.C. & Richards, C.E. 1974. The relevance of crack closure to fatigue crack propagation. *Materials Science and Engineering* 14(3): 281-293.

Liu, Q., Hamel, P., Hu, W., Sharp, P.K., Lahousse, A., Clark, G. 2005. *Modelling of stable tearing in aircraft structures*. Technical Report DSTO-TR-1657. Melbourne, Australia: Defence Science and Technology Organisation (DSTO).

Logsdon, W.A. 1976. Elastic plastic fracture toughness values: Their experimental determination and comparison with conventional linear elastic fracture toughness values for five materials. In J.R. Rice, P.C. Paris (eds), *Mechanics of crack growth*, ASTM STP 590: 43-60. Philadelphia, USA: American Society for Testing and Materials (ASTM).

Lynch, S.P. 2007. Progression markings, striations, and crack-arrest markings on fracture surfaces. *Journal of Materials Science and Engineering* 468-470: 74-80.

Lynch, S.P. & Moutsos, S. 2006. A brief history of fractography. *Journal of Failure Analysis and Prevention* 6(6): 54-69.

Lynch, S.P. & Wanhill, R.J.H. 2004. A tribute to Dr. Dennis Ryder (1926-2002): A pioneer in failure analysis, fractography, and fatigue. *Journal of Failure Analysis and Prevention* 4(2): 24-29.

Mann, J.Y. 1967. *Fatigue of materials – an introductory text*. Victoria, Australia: Melbourne University Press.

Mann, J.Y. 1983. Aircraft fatigue, with particular emphasis on Australian operations and research. In *Proceedings of the 12th International Committee on Aeronautical Fatigue (ICAF) Symposium*: 1-88. Toulouse, France: Centre d'Essais Aeronautique de Toulouse.

Margolin, B.Z. & Shvetsova, V.A. 1991. Effect of cyclic deformation on the resistance of a material to brittle failure. *Strength of Materials* 23(1): 14-23.

May, M.J. 1970. British experience with plane strain fracture toughness (K_{Ic}) testing. In W.F. Brown Jr. (ed), *Review of developments in plane strain fracture toughness testing*, ASTM STP 463: 42-62. Philadelphia, USA: American Society for Testing and Materials (ASTM).

McEvily, A.J. 2002. *Metal failures: mechanisms, analysis, prevention*. New York, USA: John Wiley & Sons.

McIntyre, D. 1975. Fractographic analysis of fatigue failures. *Journal of Engineering Materials and Technology* 97: 194-205.

Mills, W.J. & Hertzberg, R.W. 1975. The effect of sheet thickness on fatigue crack retardation in 2024-T3 aluminium alloy. *Engineering Fracture Mechanics* 7(4): 709-711.

Molent, L. 2010. Fatigue crack growth from flaws in combat aircraft. *International Journal of Fatigue* 32(4): 639-649.

Neale, B.K. 1976. The influence of crack shape on fracture toughness testing. *International Journal of Fracture* 12(3): 499-502.

Neale, B.K. 1978. An investigation into the effect of thickness on the fracture behaviour of compact tension specimens. *International Journal of Fracture* 14(2): 203-212.

Newman Jr., J.C. 1997. Prediction of crack growth under variable-amplitude loading in thin-sheet 2024-T3 aluminium alloys. In J.H. Beynon, M.W. Brown, R.A. Smith, T.C. Lindley, B. Tomkins (eds), *Proceedings of the International Conference on Engineering against Fatigue*: 261-268. Sheffield, UK: Taylor & Francis.

Nicoletto, G. 1989. Fatigue crack-tip mechanics in 7075-T6 aluminium alloy from high-sensitivity displacement field measurements. In A. Saxena, J.D. Landes, J.L. Bassani (eds), *Nonlinear fracture mechanics*, Volume 1: Time-dependent fracture: 415-432. Philadelphia, USA: ASTM International.

Ortiz, J.E., Mantic, V., Paris, F. 2006. A domain-independent integral for computation of stress intensity factors along three-dimensional crack fronts and edges by BEM. *International Journal of Solids and Structures* 43(18-19): 5593-5612.

Paris, P.C. & Erdogan, F. 1963. A critical analysis of crack propagation laws. *Journal of Basic Engineering* 85(4): 528-534.

Partl, O. & Schijve, J. 1990. Reconstitution of crack growth from fractographic observations after flight simulation loading. *International Journal of Fatigue* 12(3): 175-183.

Paul, D. & Pratt, D. 2004. History of flight vehicle structures 1903-1990. *Journal of Aircraft* 41(5): 969-977.

Pearson, S. 1968. *Fatigue crack propagation experiments on vacuum remelted FV 535 steel*. Technical Report 68232. Farnborough, UK: Royal Aircraft Establishment.

Pelloux, R.M.N. 1969. Review of theories and laws of fatigue crack propagation. In *Proceedings of the Air Force Conference on Fatigue and Fracture*: 409-416. Miami Beach, USA.

Petrak, G.J. 1972. A note on fatigue crack front straightness in K_{Ic} testing. *Engineering Fracture Mechanics* 4(2): 311-313.

Plumbridge, W.J. & Ryder, D.A. 1969. The influence of specimen geometry on the mode of fatigue crack growth in aluminium. *Acta Metallurgica* 17(12): 1449-1452.

Pook, L. 2007. *Metal fatigue: What is it, why it matters*. Dordrecht, Netherlands: Springer.

Powell, B.E. 1995. Fatigue crack growth behaviour of two contrasting titanium alloys. *International Journal of Fatigue* 170(3): 221-227.

Rhodes, D., Radon, J.C., Culver, L.E. 1980. Cyclic and monotonic crack propagation in a high toughness aluminium alloy. *International Journal of Fatigue* 2(2): 61-67.

Rungta, R., Rice, R.C., Buchheit, R.D., Broek, D. 1985. An investigation of shell and detail cracking in railroad rails. In *Corrosion, Microstructure and Metallography*: 383-406. Philadelphia, USA: American Society for Metals and International Metallographic Society.

Ryder, D.A., Davies, T.J., Brough, I., Hutchings, F.R. 1987. General practice in failure analysis. In *ASM Handbook Volume 12, Fractography*: 15-46. Ohio, USA: ASM International.

Sanford, R.J. 2003. *Principles of fracture mechanics*. New Jersey, USA: Prentice Hall.

Schijve, J. 1974. Fatigue damage accumulation and incompatible crack front orientation. *Engineering Fracture Mechanics* 6(2): 245-252.

Schijve, J. 1979. Four lectures on fatigue crack growth. *Engineering Fracture Mechanics* 11(1): 167-221.

Schijve, J. 1991. Predictions on fatigue. *JSME International Journal* 34(3): 269-280.

Schijve, J. 1994. Fatigue of aircraft materials and structures. *International Journal of Fatigue* 16(1): 21-32.

Schijve, J. 1996. Fatigue crack growth under variable-amplitude loading. In *ASM Handbook Volume 19, Fatigue and Fracture*: 110-133. Ohio, USA: American Society for Materials (ASM) International.

Schijve, J. 1998. Fatigue specimens for sheet and plate material. *Fatigue & Fracture of Engineering Materials & Structures* 21(3): 347-357.

Schijve, J. 1999. The significance of fractography for investigations of fatigue crack growth under variable-amplitude loading. *Fatigue & Fracture of Engineering Materials & Structures* 22(2): 87-99.

Schijve, J. 2009a. Fatigue damage in aircraft structures, not wanted, but tolerated? *International Journal of Fatigue* 31(6): 998-1011.

Schijve, J. 2009b. *Fatigue of structures and materials*. 2nd ed. Dordrecht, Netherlands: Springer.

Schijve, J. & de Rijk, P. 1965. *The crack propagation in two aluminium alloys in an indoor and an outdoor environment under random and programmed load sequences*. Technical Report M 2156. Amsterdam, Netherlands: National Aerospace Laboratory.

Schijve, J., Jacobs, F.A., Tromp, P.J. 1976. *Environmental effects on crack growth in flight-simulation tests on 2024-T3 and 7075-T6 material*. Technical Report 76104 U. Amsterdam: National Aerospace Laboratory.

Schijve, J., Skorupa, M., Skorupa, A., Machniewicz, T., Gruszczynski, P. 2004. Fatigue crack growth in the aluminum alloy D16 under constant and variable amplitude loading. *International Journal of Fatigue* 26(1): 1-15.

Schutz, W. 1979. The prediction of fatigue life in the crack initiation and propagation stages – a state of the art survey. *Engineering Fracture Mechanics* 11(2): 405-421.

Schutz, W. 1996. A history of fatigue. *Engineering Fracture Mechanics* 54(2): 263-300.

Schwalbe, K.H. 1977. Influence of stress state on static crack growth in AlZnMgCuO.5. *Engineering Fracture Mechanics* 9(3): 557-583.

Schwalbe, K.H. 1979. Some properties of stable crack growth. *Engineering Fracture Mechanics* 11(2): 331-342.

Schwalbe, K.H. & Setz, W. 1981. *R* curve and fracture toughness of thin sheet materials. *Journal of Testing and Evaluation* 9(4): 182-194.

Shanyavsky, A.A., Orlov, E.F., Koronov, M.Z. 1995. Fractographic analyses of fatigue crack growth in D16T alloy subjected to biaxial cyclic loads at various *R*-ratios. *Fatigue & Fracture of Engineering Materials & Structures* 18(11): 1263-1276.

Shen, H. & Guo, W. 2005. 3D constraint effect on 3D fatigue crack propagation. *International Journal of Fatigue* 27(6): 617-623.

Shi, J., Chopp, D., Lua, J., Sukumar, N., Belytschko, T. 2010. Abaqus implementation of extended finite element method using a level set representation for three-dimensional fatigue crack growth and life predictions. *Engineering Fracture Mechanics* 77(14): 2840-2863.

Shih, T.T. & Wei, R.P. 1974. A study of crack closure in fatigue. *Engineering Fracture Mechanics* 6(1): 19-32.

Siegl, J., Nedbal, I., Kunz, J. 2009. Fatigue crack growth history in damage tolerance design of aircraft structures. *International Journal of Fatigue* 31(6): 1062-1067.

Siegl, J., Schijve, J., Padmadinata, U.H. 1991. Fractographic observations and predictions on fatigue crack growth in an aluminium alloy under miniTWIST flight-simulation loading. *International Journal of Fatigue* 13(2): 139-147.

Sih, G.C. 1981. Experimental fracture mechanics: Strain energy density criterion. In G.C. Sih (ed), *Mechanics of fracture – experimental evaluation of stress concentration and intensity factors*: XVII-LVI. Dordrecht, Netherlands: Kluwer Academic Publishers.

Singh, K.D., Parry, M.R., Sinclair, I. 2011. Variable amplitude fatigue crack growth behavior – a short overview. *Journal of Mechanical Science and Technology* 25(3): 663-673.

Skorupa, M. 1998. Load interaction effects during fatigue crack growth under variable amplitude loading – a literature review, Part I: Empirical trends. *Fatigue & Fracture of Engineering Materials & Structures* 21(8): 987-1006.

Starke Jr., E.A. & Staley, J.T. 1996. Application of modern aluminium alloys to aircraft. *Progress in Aerospace Sciences* 32(2-3): 131-172.

Steigerwald, E.A. & Hanna, G.L. 1962. Initiation of slow crack propagation in high-strength materials. In *Proceedings of the Sixty-fifth Annual Meeting of the American Society of Testing Materials* 62: 885-913.

Stepanenko, V.A., Shtukaturova, A.S., Yasnyi, P.V. 1984. Stereofractographic investigation of the zone of static advance and the dynamic jump of a fatigue crack in casing steel. *Material Science* 19(6): 550-556.

Stephens, R.I., Fatemi, A., Stephens, R.R., Fuchs, H.O. 2001. *Metal fatigue in engineering*. 2nd ed. New York, USA: John Wiley & Sons.

Strawley, J.E. 1976. Wide range stress intensity factor expressions for ASTM E 399 standard fracture toughness specimens. *International Journal of Fracture* 12(3): 475-476.

Suresh, S. 1983. Micromechanisms of fatigue crack growth retardation following overloads. *Engineering Fracture Mechanics* 18(3): 577-593.

Suresh, S. 1998. *Fatigue of materials*. 2nd ed. Cambridge, UK: Cambridge University Press.

Swift, S. 1999. Gnats and camels. In J.L. Rudd (ed), *Structural Integrity for the Next Millenium*: 685-708. Warley, UK: Engineering Materials Advisory Services (EMAS).

Toor, P.M. 1973. A review of some damage tolerance design approaches for aircraft structures. *Engineering Fracture Mechanics* 5(4): 837-880.

Torres, Y., Gallardo, J.M., Dominguez, J., Jimenez, E.F.J. 2010. Brittle fracture of a crane hook. *Engineering Failure Analysis* 17(1): 38-47.

Troshchenko, V.T. 2003. Some peculiarities of fatigue crack growth at various stages of its development. *Strength of Materials* 35(6): 545-561.

Troshchenko, V.T. 2009. Fatigue fracture toughness of metals. *Fatigue & Fracture of Engineering Materials & Structures* 32(4): 287-291.

Troshchenko, V.T. & Pokrovskii, V.V. 1980. Influence of loading cycle on the crack resistance characteristics of steels. Report 2. *Strength of Materials* 12(12): 1477-1480.

Troshchenko V.T. & Pokrovskii, V.V. 1983a. Fracture toughness of structural alloys under cyclic loading. Communication 1. *Strength of Materials* 15(6): 735-742.

Troshchenko, V.T. & Pokrovskii, V.V. 1983b. Fracture toughness of structural alloys under cyclic loading. Communication 2. *Strength of Materials* 15(6): 743-750.

Troshchenko, V.T. & Pokrovskii, V.V. 2003a. Fatigue fracture toughness of metals and alloys. Part 1: Experimental procedures and materials and general principles. *Strength of Materials* 35(1): 1-13.

Troshchenko, V.T. & Pokrovskii, V.V. 2003b. Fatigue fracture toughness of metals and alloys. Part 2: Experimental procedures and materials and general principles. *Strength of Materials* 35(2): 105-113.

Troshchenko, V.T., Pokrovski, V.V., Kaplunenko, V.G., Timofeev, B.T. 1987. Effect of the dimensions of specimens and of cycle asymmetry on the regularities of unstable crack propagation under cyclic loading. *Strength of Materials* 19(3): 287-293.

Troshchenko, V.T., Pokrovskii, V.V., Skorenko, Y.S., Koshelev, V.M., Yasnii, P.V. 1980a. Effect of load cyclicity on the fracture toughness characteristics of steels. Report 1. *Strength of Materials* 12(11): 1341-1348.

Troshchenko, V.T., Pokrovsky, V.V., Kaplunenko, V.G., Karzov, G.P., Timofeyev, V.T., Dragunov, Y.G. 1992. The effect of metallurgical factors on crack resistance of pressure-vessel materials. *Nuclear Engineering and Design* 135(2): 225-237.

Troshchenko, V.T., Pokrovsky, V.V., Yasnii, P.V. 1994. Unstable fatigue crack propagation and fatigue fracture toughness of steels. *Fatigue & Fracture of Engineering Materials & Structures* 17(9): 991-1001.

Troshchenko, V.T., Prokopenko, A.V., Pokrovskii, V.V. 1978. Fracture toughness characteristics of metals in fatigue. Report No. 2. *Strength of Materials* 10(3): 255-260.

Troshchenko, V.T., Prokopenko, A.V., Pokrovsky, V.V. 1979. Cyclic loading and fracture toughness of steels. *Fatigue of Engineering Materials and Structures* 1(2): 247-266.

Troshchenko, V.T., Yasnii, P.V., Pokrovskii, V.V. 1980b. Laws of unstable crack growth under cyclic loading. *Strength of Materials* 12(6): 669-674.

Troshchenko, V.T., Yasnii, P.V., Pokrovskii, V.V. 1982. Calculation of fatigue and life of crack-bearing structural elements under cyclic load. *Strength of Materials* 14(11): 1434-1439.

Troshchenko, V.T., Yasnii, P.V., Pokrovskii, V.V. 1985, Prediction of the effect of the asymmetry of the load cycle on the cyclic fracture toughness of structural alloys. *Strength of Materials* 17(11): 1515-1520.

Troshchenko, V.T., Yasnii, P.V., Pokrovskii, V.V., Tkach, Y.V. 1988. Fatigue crack propagation: Report 1, relationships governing unstable propagation. *Strength of Materials* 20(10): 1281-1286.

Tuba, I.S. 1966. A method of elastic-plastic plane stress and strain analysis. *The Journal of Strain Analysis for Engineering Design* 1(2): 115-120.

Turan, D. & Karci, A. 2009. Failure analysis of an aircraft piston engine components. *Engineering Failure Analysis* 16(4): 1339-1345.

Vander Voort, G.F. 1992. Visual examination and light microscopy. In *ASM Handbook, Volume 12, Fractography*. Ohio, USA: ASM International.

Vardar, O. 1988. Effect of single overload in FCP. *Engineering Fracture Mechanics* 30(3): 329-335.

Vardar, O. & Yildirim, N. 1990. Crack growth retardation due to intermittent overloads. *International Journal of Fatigue* 12(4): 283-287.

Vasudevan, A.K., Sadananda, K., Glinka, G. 2001. Critical parameters for fatigue damage. *International Journal of Fatigue* 23(1): 39-53.

Vlasveld, J.A. & Schijve, J. 1979. *Tongue-shaped crack extension during fatigue of high strength aluminium alloys*. Report LR-279. Delft: Delft University of Technology.

Vlasveld, J.A. & Schijve, J. 1980. Tongue-shaped crack extension during fatigue of high strength aluminium alloys. *Fatigue of Engineering Materials and Structures* 3(2): 129-145.

Vlieger, H. 1988. Damage tolerance of stiffened-skin structures: Prediction and experimental verification. In T.A. Cruse (ed), *Fracture Mechanics: Nineteenth Symposium*: 169-219. Philadelphia, USA: American Society for Testing and Materials (ASTM).

Wanhill, R.J.H. 2002. *Milestone case histories in aircraft structural integrity*. NLR-TP-2002-521. Amsterdam, Netherlands: National Aerospace Laboratory (NLR).

Wanhill, R.J.H. 2003. *Failure of backstay rod connectors on a luxury yacht*. NLR-TP-2003-375. Amsterdam, Netherlands: National Aerospace Laboratory (NLR).

Wanhill, R.J.H., Bartelds, G., de Koning, A.U. 1982. Fatigue crack front shape. *International Journal of Fatigue* 4(1): 52-53.

Wanhill, R.J.H., 't Hart, W.G.J., Schra, L. 1979. Flight simulation fatigue crack propagation in 7010 and 7075 aluminium plate. *International Journal of Fatigue* 1(4): 205-209.

Ward-Close, C.M., Blom, A.F., Ritchie, R.O. 1989. Mechanisms associated with transient fatigue crack growth under variable-amplitude loading: An experimental and numerical study. *Engineering Fracture Mechanics* 32(4): 613-638.

Wei, R.P. 2010. *Fracture mechanics – integration of mechanics, materials science, and chemistry*. New York, USA: Cambridge University Press.

Weitzmann, R.H. & Finnie, I. 1972. Measuring fracture toughness – a simplified approach using controlled crack propagation. *Journal of Materials*, JMLSA 7(3): 294-298.

Williams, J.C. & Starke Jr., E.A. 2003. Progress in structural materials for aerospace systems. *Acta Materialia* 51(19): 5775-5799.

Withey, P.A. 1997. Fatigue failure of the de Havilland Comet I. *Engineering Failure Analysis* 4(2): 147-154.

Wood, H.A. 1975. Application of fracture mechanics to aircraft structural safety. *Engineering Fracture Mechanics* 7(3): 557-564.

Wu, Z. 2006. On the through-thickness crack with a curved front in center-cracked tension specimens. *Engineering Fracture Mechanics* 73(17): 2600-2613.

Xue, Y., El Kadiri, H., Horstemeyer, M.F., Jordon, J.B., Weiland, H. 2007. Micromechanisms of multistage fatigue crack growth in a high-strength aluminium alloy. *Acta Materialia* 55(6): 1975-1984.

Yasnii, P.V. 1981. Study of unstable crack propagation and arrest during cyclic loading. *Strength of Materials* 13(11): 1350-1355.

Yasnii, P.V. & Pyndus, Y.I. 2002. Effect of single overloading on the propagation of fatigue cracks in D16T alloy. *Materials Science* 38(2): 225-229.

Yasnii, P.V., Pokrovskii, V.V., Prokopenko, A.V. 1983. Relationship between fracture toughness characteristics for cyclic and dynamic loadings. *Strength of Materials* 15(8): 1058-1064.

Yildirim, N. & Vardar, O. 1990. Study of periodic overloads at a fixed overload-ratio. *Engineering Fracture Mechanics* 36(1): 71-76.

Yamamoto, Y., Sumi, Y., Shimoyama, T., Funada, T. 1987. On thumb-nail pattern of fatigue crack front observed in standard compact tension specimen. *International Journal of Fracture* 34(2): 149-157.

Yu, P., Guo, W., She, C., Zhao, J. 2008. The influence of Poisson's ratio on thickness-dependent stress concentration at elliptical holes in elastic plates. *International Journal of Fatigue* 30(1): 165-171.

Zapffe, C.A. & Worden, C.O. 1949. Fractography as a technique in crystal chemistry. *Acta Crystallographica* 2(6): 377-382.

Zhang, B. & Guo, W. 2007. Three-dimensional stress state around quarter-elliptical corner cracks plates subjected to uniform tension loading. *Engineering Fracture Mechanics* 74(3): 386-398.

Zhao, J., Guo, W., She, C. 2007. The in-plane and out-of-plane stress constraint factors and K-T-T_z description of stress field near the border of a semi-elliptical surface crack. *International Journal of Fatigue* 29(3): 435-443.

Zhao, T., Zhang, J., Jiang, Y. 2008. A study of fatigue crack growth of 7075-T651 aluminium alloy. *International Journal of Fatigue* 30(7): 1169-1180.

Zheng, X. 2001. On some basic problems of fatigue research in engineering. *International Journal of Fatigue* 23(9): 751-766.